MULTI-FREQUENCY DIGITAL COMMUNICATIONS IN UNDERWATER CHANNELS

MANORA KUMUDINIE CALDERA

MULTI-FREQUENCY DIGITAL COMMUNICATIONS IN UNDERWATER CHANNELS

by

Manora Kumudinie Caldera B.Sc. Eng. (Hons.)

 A thesis submitted to the School of Graduate Studies in partial fulfillment of the requirements for the degree of Master of Engineering

Faculty of Engineering and Applied Science.
Memorial University of Newfoundland

September 1986

St.John's Newfoundland Canada

ISBN 0-315-36971-X

ABSTRACT

Strong multipath conditions which exist particularly in a shallow water acoustic channel make conventional coherent transmission schemes ineffective. To this end many non-coherent detection schemes employing frequency diversity have been proposed to improve transmission reliability.

In this thesis, a novel transmission scheme based on the Sliding Discrete Fourier Transform (SDFT) is proposed for communicating in multipath acoustic channels and it's performance is evaluated analytically and by computer simulations. The system described uses constant envelope multi-frequency signals. Since the envelope of the received signal varies depending on the intensities of the direct path and multipath signals, it is assumed that an Automatic Gain Controller (AGC) stabilizes the received signal before carrying out the demodulation. Due to the non-linearity effect of the AGC process, the analytical evaluation is complicated for the case with AGC. Hence the analytical evaluation is carried out only for the case with no AGC at the receiver.

First, the variation of eye opening with Direct to Multipath Ratio (DMR) and the minimum DMR required for correct detection are determined. Then the effect of the synchronization error at the receiver on the eye opening is obtained. Finally, the error performance of the signal in the presence of Gaussian noise is evaluated for various DMR values.

A computer simulation is carried out for the case with an AGC at the receiver. By generating sequences of random data for transmission, the eye pat-

terns of the received signals are obtained. The variation of DMR with the distance between the transmitter and the receiver is also plotted for various transmitter-receiver locations and configurations.

Based on the results obtained, the proposed system is shown to be a reliable communication scheme in underwater channels.

ACKNOWLEDGMENTS

It is a pleasure to convey my sincere gratitude to Dr. A. Zielinski, now in the Faculty of Engineering, University of Victoria, B.C., for giving me the opportunity to pursue my Graduate studies under his supervision. Special thanks are due to Dr. N. Ekanayake, Faculty of Engineering and Applied Sciences, Memorial University of Newfoundland, for the valuable advice as my supervisor during the second year of my studies.

I am grateful to Dr. F.A. Aldrich, Dean of Graduate Studies, Dr. C.J. Michalski, Assistant Dean of Graduate Studies, Dr. G.R. Peters, Dean of Engineering and Dr. T.R. Chari, Associate Dean of Engineering, of Memorial University of Newfoundland, for granting me admission to the Graduate program and providing the necessary financial assistance.

My thanks are extended to the International Center for Ocean Development, Halifax., for awarding me a Fellowship during the second year of my studies.

I am indebted to University of Moratuwa, Srilanka., for granting study leave.

I would like to thank my husband Havindra, for his patience, understanding and encouragement throughout the course of my studies. Finally, I take this opportunity to thank all individuals who helped in many ways to make this thesis possible.

TABLE OF CONTENTS

LIST OF TABLES

LIST OF FIGURES

CHAPTER 1

INTRODUCTION

1.1 Underwater Communication Techniques

In line with the growing interest in ocean research and industrial offshore developments there is an increasing demand for efficient, reliable and high capacity underwater communication systems [1,5,9]. A communication link is required for diverse underwater operations such as communication with submersibles, telemetry and remote control of subsea oil production units, blow out preventers (BOP's), remote operated vehicles (ROV's), transmission of measurements from underwater sensors and others [14,21,34,35].

Since the end of first world war, research has been conducted on evaluating electromagnetic and acoustic waves for underwater communications [3]. Apart from that, in 1970's, Williscroft and Macleod [38] have investigated underwater communications by means of an Electric Current Field (ECF). The main drawback of ECF communication is it's limited range as the received signal strength is inversely proportional to the water conductivity and the range separating transmitter and receiver.

The major limitation in the use of electromagnetic radiation for underwater communications is the extremely high absorption of electromagnetic waves in sea water. As can be seen in Fig (1.1), the electromagnetic energy attenuation is extremely high except for the narrow band of optical frequencies. Even at optical frequencies, the attenuation is high if the water is not clear.

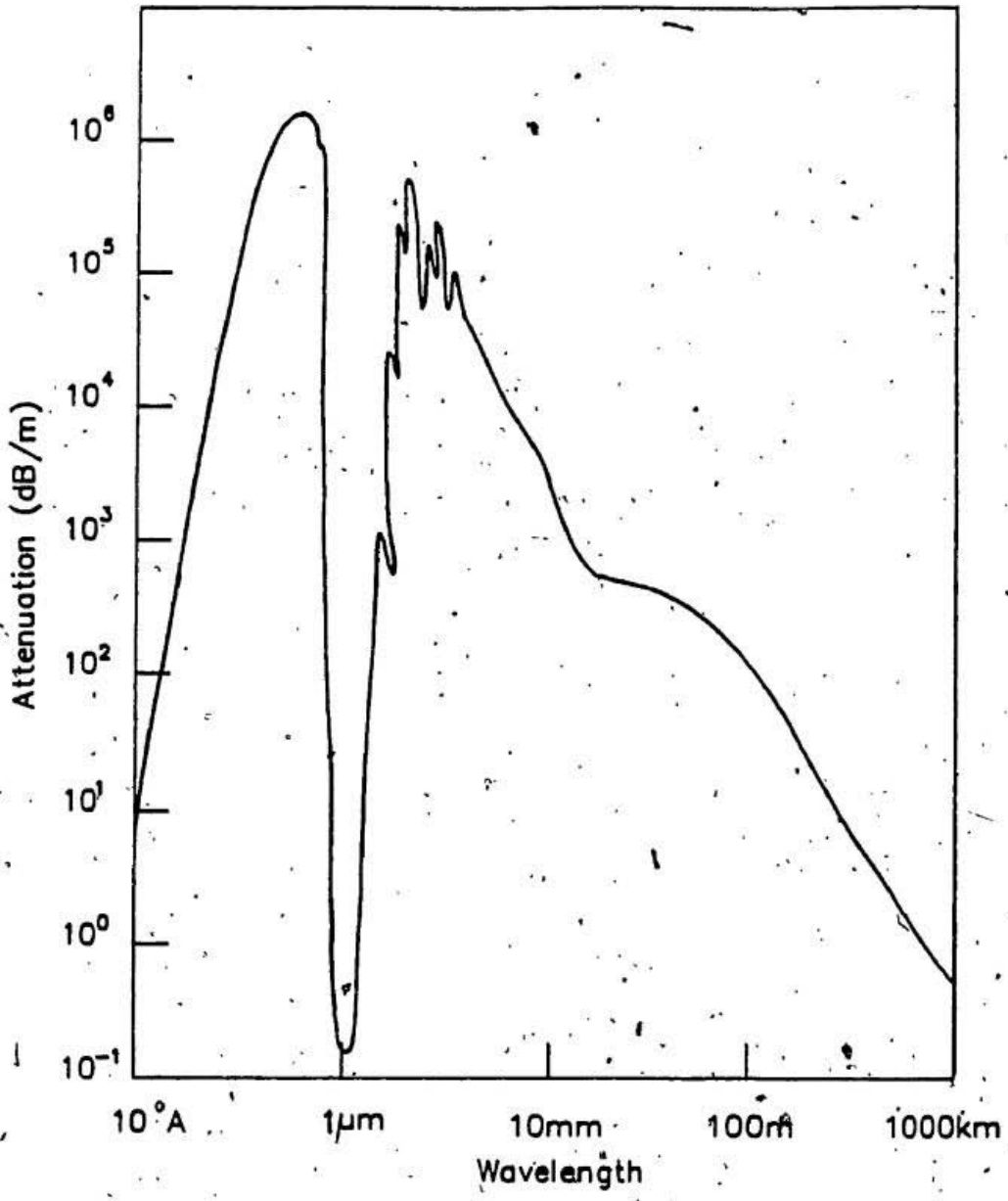

Fig. 1.1 Attenuation of electromagnetic signals in sea water.

In comparison to electromagnetic wave propagation, the absorption of acoustic energy in the sea water is several orders of magnitudes lesser. Due to this relatively low attenuation, acoustic transmission is the only viable communication link for underwater communications.

Underwater communication by means of acoustic waves, however, encounters several problems related to the characteristics of the acoustic channel such as ambient noise, Doppler shift, refraction, scattering and multipath [2,9]. With sufficient transmitting power to achieve an adequate received signal level, the principal obstacle against high speed, reliable transmission is believed to be multipath interference. This effect is particularly severe in shallow water transmission where strong surface and bottom reflections are encountered.

The multipath phenomenon affects acoustic communication in several ways such as time-smearing, frequency-smearing and fading of the received signal [39]. These effects adversely affect the receiver in signal decoding. To alleviate the effect of multipaths and for reliable underwater communications, the communication systems need to be designed by carefully selecting a proper modulation and signal processing technique. As such, various non-coherent systems employing frequency and spatial diversity have been proposed and tested, with varying degrees of success. In the following section, some of the important features of several underwater communication systems are briefly reviewed.

1.2 Literature Review

In the past literature, a considerable amount of research had been carried out on underwater acoustic communications. The main consideration in these research was based on the selection or specification of a modulation technique, as it determines the factors such as cost, complexity, reliability and performance of a communication system. Among the conventional modulation methods, binary Frequency Shift Keying (FSK) is the most attractive modulation technique for signal transmission at present, as it does not require a coherent channel for detection [13].

Out of the extensions of FSK modulation, Multilevel Frequency Shift Keying (MFSK) modulation technique is used in many reliable underwater acoustic communication systems [7,12,13,16,22,32,34,37]. MFSK modulation technique achieves a higher data rate by employing multiple tones for data transmission. Although communication systems which employ MFSK modulation had been costly to implement in the past due to hardware constraints imposed by multitone signal processing, the rapid advancement of solid state technology has made this technique more attractive in recent years.

The development of DATS (Digital Acoustic Telemetry System) [7], which is an untethered system that could be used in unmanned vehicles, is a good outcome of the application of MFSK modulation technique. DATS is capable of signal transmission at a rate of 400 bits/sec with an error probability of 3×10^{-3} in decoding. To improve the capabilities of this system in underwater telemetry,

further research work is being done at Massachusetts Institute of Technology and Woods Hole Oceanographic Institute [40].

A recently proposed free swimming submersible called the ARCS (Autonomous Remote-Controlled Submersible) [13] also employs MFSK modulation technique. This is an underwater acoustic telemetry system specially developed for long range, medium rate, full duplex digital transmission in shallow water, under ice covered environment. ARCS has the disadvantage of decrease in bit rate per channel with the system reliability.

Another underwater communication system which utilizes MFSK modulation was formed by combining conventional MFSK modulation with transducer arrays which produce directional beams [33]. The capability of radiating a narrow beam, with very low sidelobe levels of a parametric source is used to overcome the multipath problem in this method. The test results have revealed the possibility of data, voice and picture transmission at data rates of the order of kilobit/sec over short ranges. Achieving a higher data rate in long ranges, however, demands a large bandwidth due to the increase in absorption at high frequencies.

For the purpose of underwater vehicle tracking, in early 1980's Chase [12] introduced a new modulation technique called Space-FSK (SFSK). In this technique, the use of a time expanded version of FSK has been incorporated for signal transmission in order to reduce the multipath effect. This offers reliable signal identification and message validation at Signal to Noise Ratios above 7 dB. Although SFSK was developed for underwater tracking, it has been proved to be

adaptable to most of underwater communication applications.

A new idea of reducing multipath interference in underwater acoustic communication systems was introduced by Zielinski and Barbour [8,41,42]. This idea is based on the observation that the time separation between direct and multipath waveforms can be utilized to suppress the multipath interference. This system employs narrowband Amplitude Modulation (AM) and Frequency Modulation (FM) using a swept carrier for message transmission. In order to increase the data rate of this system, Howse [19] has considered a ramp waveform, instead of a sinusoidal sweep. The experimental results have indicated that both these techniques perform well in an underwater multipath environment. However, further refinements are needed to make the probability of error of the system to lie within acceptable limits.

In addition to the application of modulation techniques, channel diversity (frequency, space or time) is being used to communicate in multipath environments. Among these, frequency diversity is attractive to assure a reliable communication channel [39]. Moreover, the reliability of data transmission is improved in most cases, using error correcting or detecting codes [13,30].

Apart from these, many other techniques for combating the effect of multipath in underwater communication systems have been discussed in the literature [4,11,17,21,29-31]. As each of these solutions has it's own limitations in different situations, further research directed towards counteracting the multipath effect has become vital and essential. This thesis is focused on finding a better

way of performing the underwater acoustic communication in multipath environment.

1.3 Organization of the Thesis

This thesis is primarily concerned with the development of a reliable underwater acoustic communication system under strong multipath environments. The proposed system uses a modulation technique based on Continuous Phase Frequency Shift Keying (CPFSK) for digital signal transmission. The received signal is demodulated using a new demodulation method conceptualized on Sliding Discrete Fourier Transform (SDFT) algorithm. The prime reason behind the selection of SDFT demodulation technique is the attractiveness of this technique in remotely operated vehicles due to less power and space requirements, and the simplicity in implementation with commercially available integrated circuits.

As outlined in the preyious section, sound propagation in underwater is influenced by reflection from the sea surface and bottom, refraction due to velocity gradients, and attenuation due to absorption and spreading losses. It is also distorted by multipath arrivals arising from reflection. Chapter 2 outlines a brief description of these factors and the development of a simple model representing the ocean.

Some of the important fundamentals of Discrete Fourier Transform (DFT) and Fourier Transform (FT) applied in different forms of time domain signals are reviewed in Chapter 3. The development and implementation of SDFT algorithm which is used in demodulating the received signal are also explained in the same.

Chapter 4 describes the signal design and the modulation technique used for signal transmission. The information is transmitted in blocks of bits using a selected set of frequencies depending on the binary state 'one' or 'zero'. These frequencies are chosen so as to avoid Inter Symbol Interference (ISI). Since the effect of multipath is to cause ISI, the frequency selection scheme also overcomes the distortion caused by multipath signals. Operation of the receiver is also described in chapter 4.

The performance of the system is analytically evaluated in Chapter 5. The variation of eye pattern of the received signal with Direct to Multipath Ratio (DMR) is obtained in different transmitter-receiver configurations, in the presence and absence of synchronization error at the receiver. The error performance of the system in these configurations are also evaluated in the presence of Gaussian noise.

In order to test the transmission scheme described in Chapter 4, a digital computer simulation is performed. The simulation technique and the results are presented in Chapter 6. Finally Chapter 7 summerizes the conclusions of the research.

The analytical and simulated results obtained in the thesis reveal that this SDFT scheme is a reliable means for communication in multipath underwater channel.

CHAPTER 2

MULTIPATH MODELING OF THE OCEAN

2.1 Introduction

As discussed in Chapter 1, the major limitation to reliable, high rate underwater acoustic communication arises from the presence of multipath. Hence to design a communication system, specially to combat the multipath effect, it is essential to develop a simple model for multipath prediction.

The purpose of this chapter is to develop a simple multipath model for acoustic communication. In addition, the background information on underwater acoustic propagation, and the calculation of intensities and the time delays of multipaths are also described.

2.2 Multipath Distortion

The direction of wave propagation is changed by reflections at surface and bottom of the sea and also by refraction or bending as the wave moves through regions of different characteristic velocities. Therefore the received signal at a certain time consists of signals which are refracted, reflected from the surface, reflected from the bottom or any combination of these as shown in Fig (2.1).

Hence a single short burst of acoustic energy is received as a train of pulses, each of different delay, duration and amplitude. In Fig (2.2), the first pulse represents energy propagated along the direct refraction path; subsequent pulses represent energy arrivals from reflected paths. When a continuous signal is

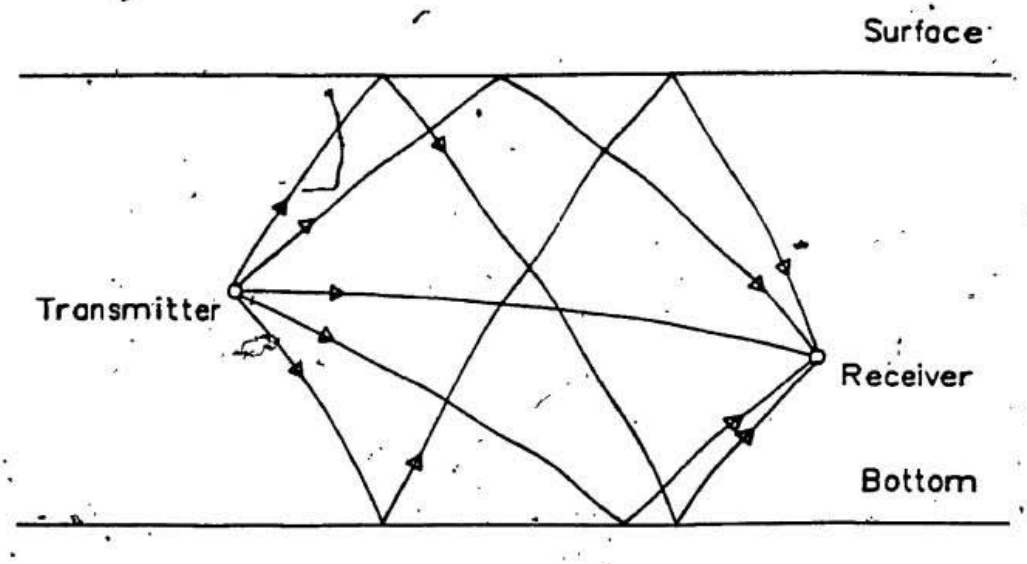

Fig. 2.1 Ray paths of an acoustic signal in sea water.

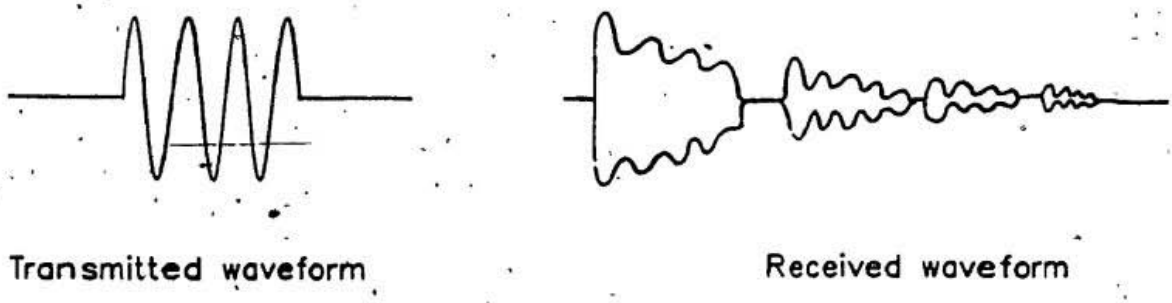

Fig. 2.2 Transmitted and received waveforms of a single short burst transmitted.

Fig. 2.3 Transmitted and received waveforms of a continuous signal transmitted.

transmitted, it also propagates according to the same way as for a single short burst as illustrated in Fig (2.3). This causes the received pulse to be distorted by multipath and fading distortions.

Therefore, to design a reliable acoustic communication system in the presence of multipaths it is essential to obtain a multipath model of the ocean. This could be achieved by considering the effects of reflection and refraction of an acoustic signal. The following section briefly explains the above effects of a sound wave.

2.3 Refraction and Reflection of Sound Waves

The refraction of sound in the ocean is resulted from the spatial variations in sound speed. The sound speed in sea water can be given by [25],

$$C = 1449.2 + 4.6T - 0.055T^2 + 0.00029T^3 + (1.34 - 0.01T)(S-35) + 0.016Z \qquad (2.1)$$

where C = sound speed in m/sec

T = temperature in ^{0}C.

S = salinity in ppt.

Z = depth in m.

This shows that an acoustic wave changes its velocity when it enters a region with different temperature, salinity and depth. Also Snell's law states that the sound waves bend towards the region of lower velocity according to the equation

$$\frac{\cos\theta_1}{C_1} = \frac{\cos\theta_2}{C_2} \qquad (2.2)$$

where θ_1 and θ_2 are the grazing angles for layers 1 and 2, C_1 and C_2 are the characteristic velocities of layers 1 and 2.

Therefore the directions of the signal as it propagates from medium 1 to 2, or 2 to 3 and so on in a continuously stratified medium could be given by

$$\frac{\cos\theta_1}{C_1} = \frac{\cos\theta_2}{C_2} = \cdots = \frac{\cos\theta_n}{C_n} \tag{2.3}$$

where θ_n and C_n are the grazing angle and the characteristic velocity of layer n, respectively.

This effect is illustrated in Fig (2.4) considering the ocean layer thicknesses infinitesimal with different characteristic velocities.

In shallow water, the variation of sound velocity with depth is completely unknown. Therefore in this thesis, the velocity of sound in water is assumed to be constant, neglecting the refraction effect. Consequently, the ray paths are considered as straight.

The direction of an acoustic wave in the ocean changes not only by refraction, but also by reflection from the bottom and the surface of the ocean. The direction of reflected acoustic signal could be obtained using the model given in Fig (2.5). Here the sound wave incident on a boundary is reflected at the same grazing angle and in the same plane. Hence it can be seen that a surface reflection introduces a 180^0 phase shift and a certain power loss to the incident wave. The loss in power is dependent on the surface roughness and it will be explained in Sec (2.5) in detail.

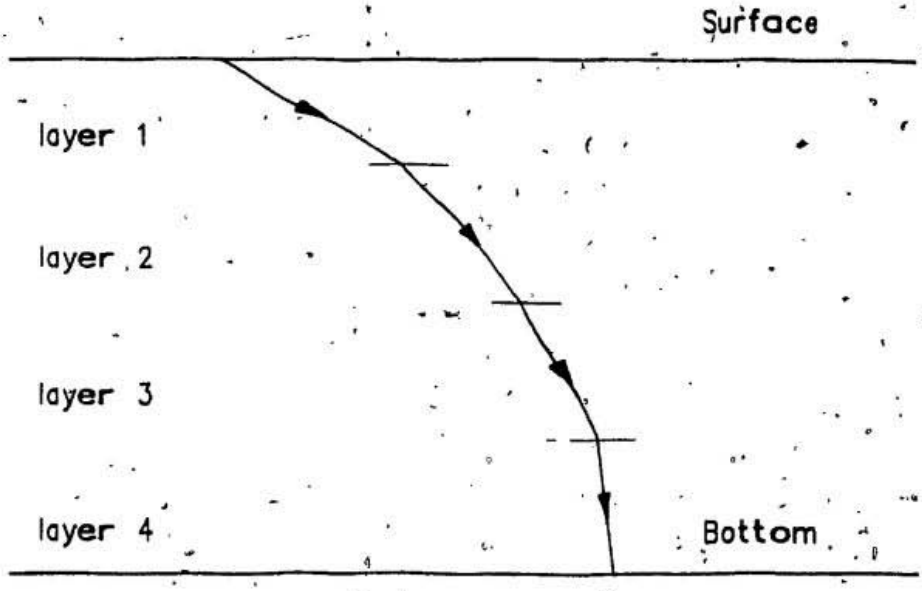

Fig. 2.4 Ray bending in a horizontally stratified medium with different characteristic velocities.

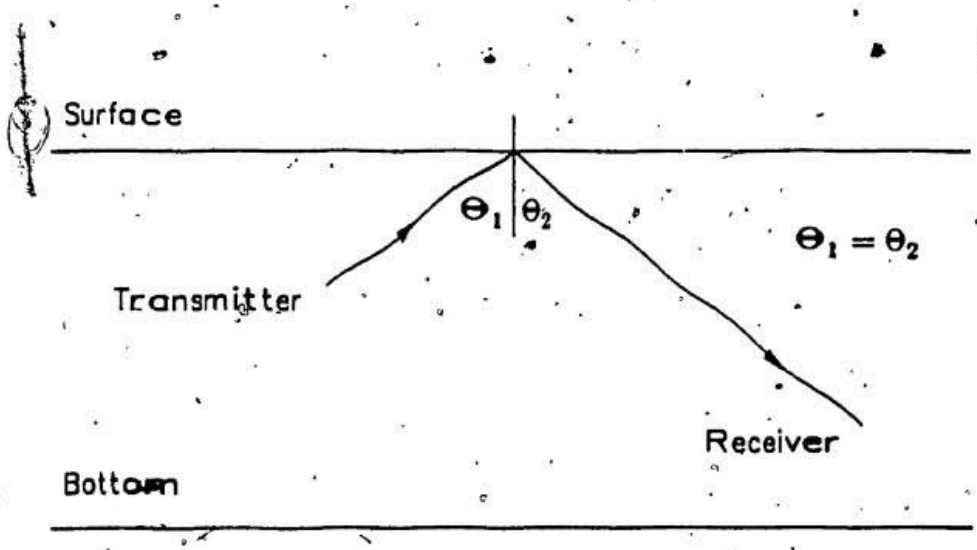

Fig. 2.5 Surface reflection model of an acoustic signal.

Hence the above discussed behaviors of sound waves can be used to develop a multipath model for the transmitter-receiver configuration illustrated in Fig (2.6).

A signal is transmitted from a transmitter located at depth y_T to a receiver at depth y_R separated from the transmitter by a horizontal distance x_R. The signal at the receiver consists of a direct path and an infinite number of reflected paths which arises from surface and bottom reflections, each with different time delay and intensity. The intensities and the time delays of these multipaths have been obtained categorizing the multipaths into the following major groups.

(a) Paths with equal number of bottom and surface reflections given that the first reflection is from the surface.

(b) Same as (a) except the first reflection is from the bottom.

(c) Paths with unequal number of surface and bottom reflections given that the first reflection is from the surface.

(d) Same as (c) except the first reflection is from the bottom.

If t_n is the time taken by a pulse to travel along the n^{th} path, then it follows that

$$t_n = \frac{l_n}{C} \tag{2.4}$$

where C = Velocity of sound in sea water.
and l_n = distance traveled by the pulse.

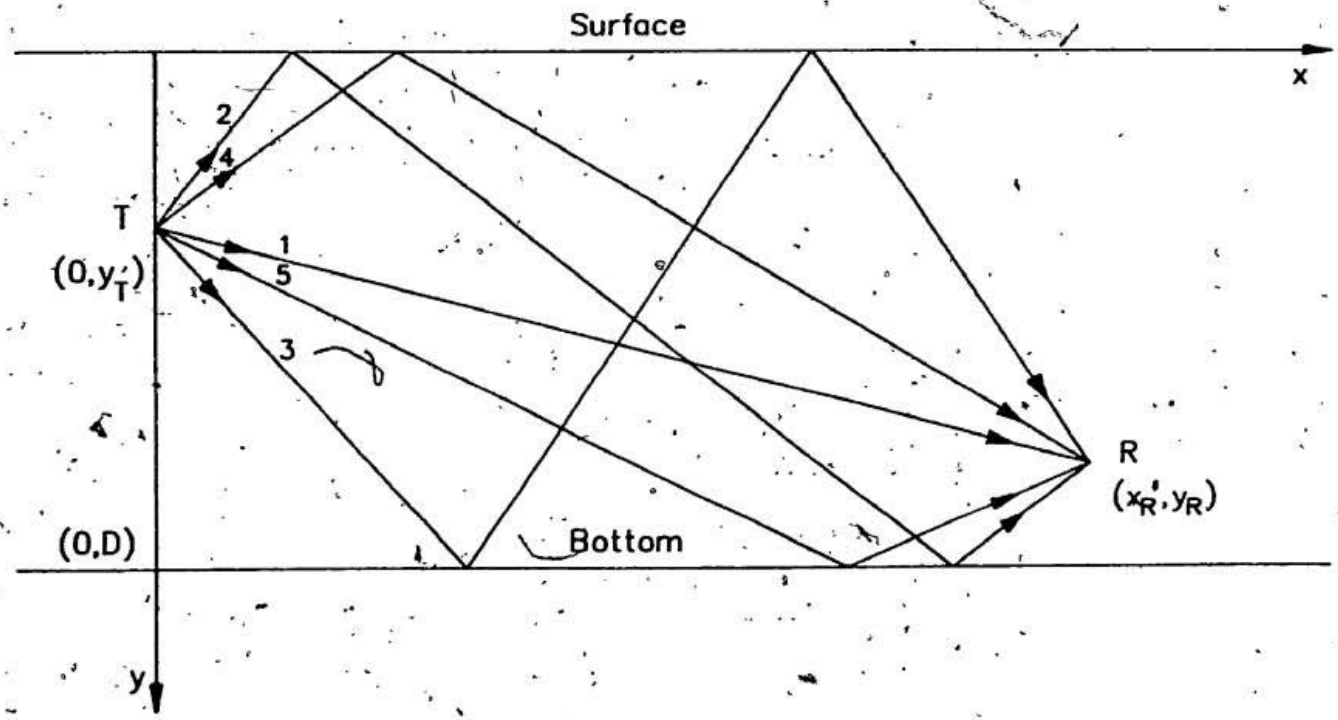

Fig. 2.6 Structure of a multipath acoustic channel.

The intensity of the n^{th} multipath at the receiver in logarithmic scale is given by [20],

$$I_n = TSL - SL - AL - s.SRL - b.BRL \quad (2.5)$$

where,

TSL = Source level of the ominidirectional transmitter in dB.
SL = Spreading loss in dB.
AL = Absorption loss in dB.
s = Number of surfac reflections.
b = Number of bottom reflections.
SRL = Surface reflection loss in dB.
BRL = Bottom reflection loss in dB.

It is clear from Equation (2.5), that the intensity of each of the multipaths depends on the source level of the transmitter and the losses involved. Hence to obtain the multipath model of the ocean as shown in Fig (2.7), it is essential to have a good knowledge of the above losses, and these losses will be discussed in the following sections.

2.4 Transmission Losses

When an acoustic signal travels through the sea, it becomes delayed, distorted and weakened, The weakening of the transmitted signal at the receiver is described as the transmission loss. This loss is considered to be the sum of the loss due to spreading, which is simply a geometrical loss, and the loss due to absorption, which is a true loss of energy to the medium.

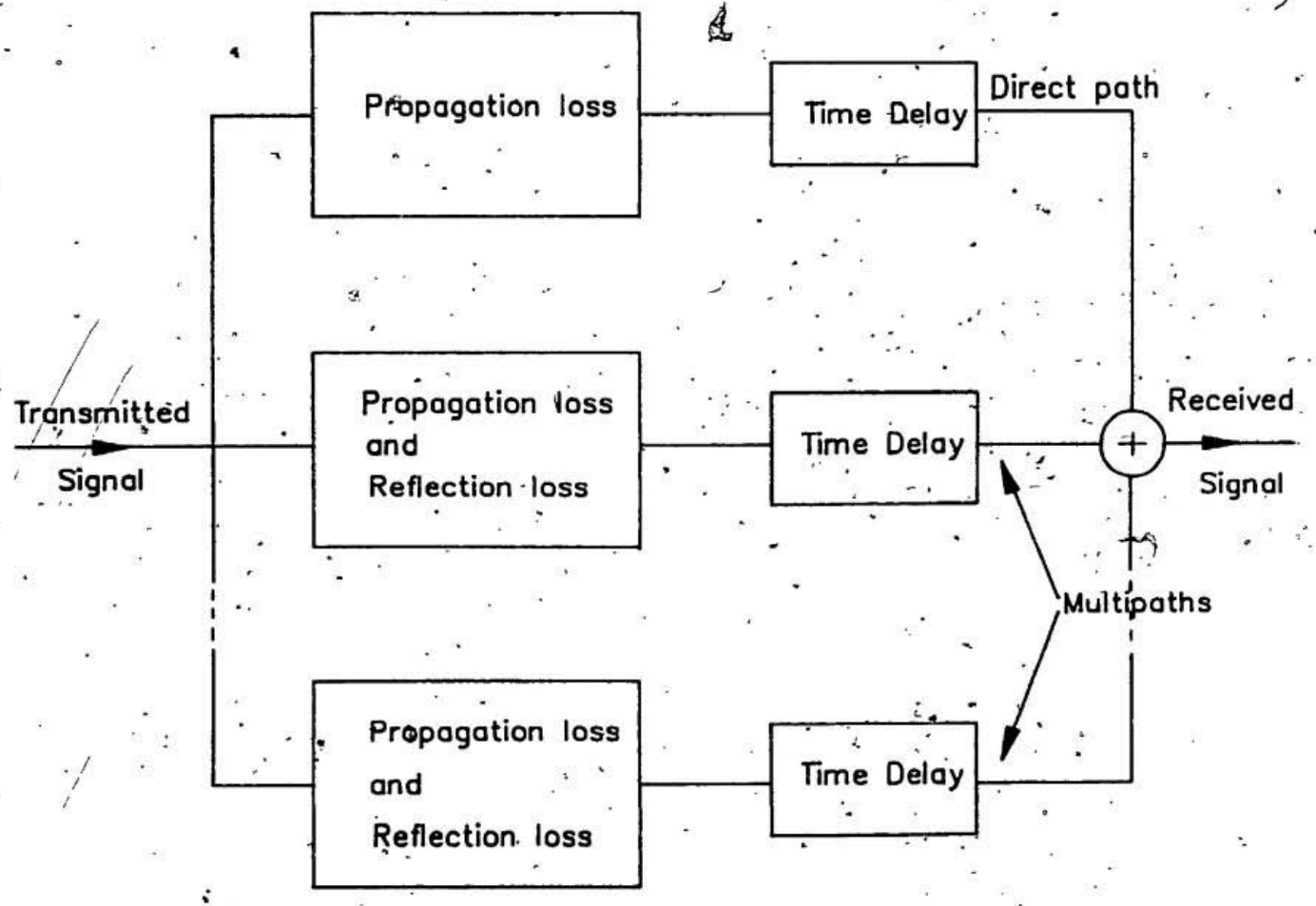

Fig. 2.7 Multipath model of ocean.

2.4.1 Spreading Loss

Spreading loss is a geometrical effect representing the regular weakening of a sound signal as it spreads outward from the source.

Spreading is modeled either with a free-space spherical geometry or with a horizontally stratified geometry. At short ranges the spherical model is more appropriate and at longer ranges the cylindrical model is more appropriate.

In spherical spreading, the power generated by a source of sound located in an unbounded medium is radiated equally in all directions so as to equally distribute over the surface of a sphere surrounding the source. Thus when an acoustic wave travels through an unbounded medium, it undergoes a spherical spreading loss which is given by

$$SL = 20 \log r \tag{2.6}$$

where SL = Spherical spreading loss in dB.

r = distance in m.

When the medium has plane-parallel upper and lower bounds or when the medium is bounded, the spreading is no longer spherical due to the reason that sound cannot cross the bounding planes. In this situation, the spreading is said to be cylindrical. The cylindrical spreading loss is also given by

$$SL = 10 \log r \tag{2.7}$$

where r is the distance traveled in m and SL is the cylindrical spreading loss in dB.

In most locations the actual spreading is observed to be somewhere between those two extremes indicated. Hence in the absence of specific information for a particular location, spherical spreading may be assumed. Due to this reason, spherical spreading has been considered in this thesis to calculate the spreading loss.

2.4.2 Absorption Loss

The other cause of transmission loss is the actual absorption of sound energy by sea water. The exact nature of this process is a complex function of frequency, temperature, pressure and salinity, and is not completely understood.

The absorption of sound in the sea water is high, compared with that in pure water [36]. At frequencies between 5 and 10 kHz, it has been found that the absorption in sea water is about 30 times that in distilled water. This excess absorption has been explained in the literature using chemical reactions that occur in sea water. Fig (2.8) shows the variation of absorption coefficient in sea water and distilled water with frequency.

The absorption of sound in water is caused by shear and volume viscosities of the medium and this loss depends on the frequency. The resulting expression for total absorption in water becomes

$$\alpha = \frac{\omega^2 \left(\frac{4\eta_s}{3} + \eta_v \right)}{2\rho_0 c^3} \tag{2.8}$$

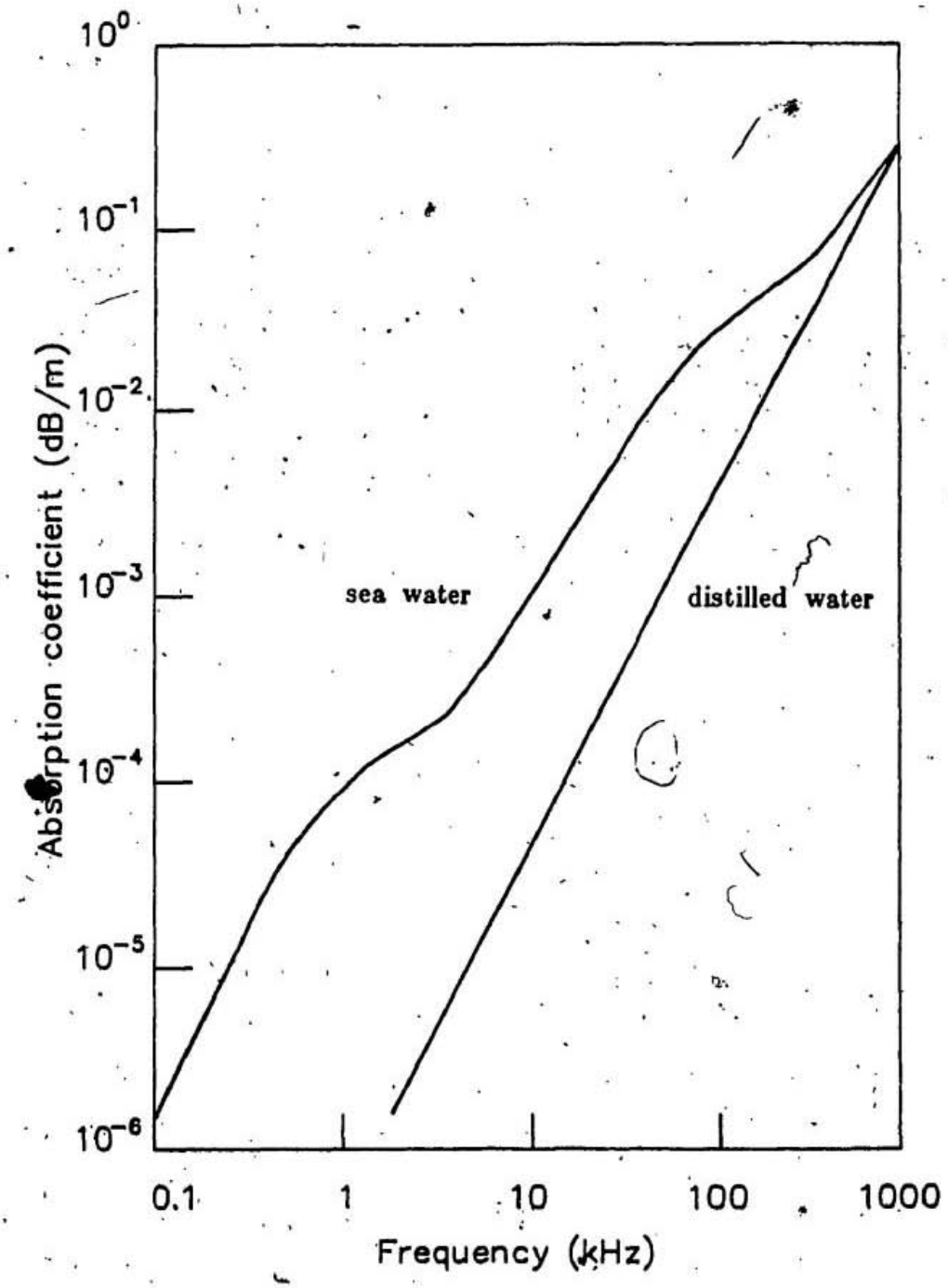

Fig. 2.8 Variation of absorption coefficient in sea water and in distilled water with frequency.

where

α = absorption coefficient in dB/m.

ω = frequency in rad/sec.

c = velocity of sound in water in m/sec.

ρ_0 = density of water in Kg/m^3.

η_s = shear viscosity.

η_v = volume viscosity.

Direct measurement of the coefficient of volume viscosity by Libermann [26] indicates that η_v in water is approximately three times the coefficient of shear viscosity η_s.

It has been found that the dominant cause of absorption in sea water when the frequency is in the range 1 kHz to 100 kHz, is due to ionic relaxation of the dissolved $MgSO_4$ molecules in sea water [24]. Further absorption at frequencies below 1 kHz is assumed to be due to a chemical relaxation involving boric acid.

Hence with these two chemical relaxation mechanisms involved in sea water, in addition to the absorption mechanism active in fresh water, the absorption coefficient in sea water could be expressed by [23],

$$\alpha = \frac{A f_1 f^2}{(f_1)^2 + f^2} + \frac{B f_2 f^2}{(f_2)^2 + f^2} + C f^2 \qquad (2.9a)$$

$$= \alpha\,(\text{boric acid}) + \alpha\,(MgSO_4) + \alpha\,(H_2O) \qquad (2.9b)$$

where f_1 and f_2 are the relaxation frequencies associated with the boric acid and $MgSO_4$ relaxations respectively and are temperature dependent. The constants A, B and C depend on the temperature and on the hydrostatic pressure. In addition, the values of A and B become zero for freshwater.

The variation of the relaxation frequencies f_1 and f_2 with temperature, was first obtained by Fisher and Simmons [15] as

$$f_1 = 1.32 \times 10^3 (T + 273) \exp [-1700 / (T + 273)] \quad (2.10a)$$

and

$$f_2 = 1.55 \times 10^7 (T + 273) \exp [-3052 / (T + 273)] \quad (2.10b)$$

where T is in ^0C, f_1 and f_2 are in Hz.

The expressions for A, B and C of Equation (2.9a), are rather complicated but can be simplified. Combining these results the frequency dependent absorption coefficient α at 4^0C is given by [27],

$$\alpha = 0.0011 \left[\frac{0.1 f^2}{1 + f^2} + \frac{40 f^2}{4100 + f^2} + 2.75 \times 10^{-4} f^2 \right] \quad (2.11)$$

where f is the frequency in kHz. The three terms within the brackets in this expression refer to the contribution of boric acid relaxation, $MgSO_4$ relaxation and viscous absorption respectively.

Now the loss due to absorption can be calculated as

$$AL = \alpha r \quad (2.12)$$

where

AL = absorption loss in dB.
α = frequency dependent absorption coefficient in dB/m given in Equation (2.11).
r = distance traveled by the sound wave in m.

Hence, using Equations (2.6) and (2.12), the total transmission loss TL could be

expressed as,

$$TL = 20 \log r + \alpha r \qquad (2.13)$$

2.5. Reflection Loss

When an acoustic wave meets a plane boundary, a portion of the acoustic energy is transmitted across the boundary, while the rest is reflected back introducing a power loss to the incident wave. This power loss is referred to as the Reflection loss and is given by,

$$RL = 10 \log \frac{I_i}{I_r} \qquad (2.14)$$

where I_r and I_i are the reflected and incident intensities of an incident plane wave.

If the boundary is perfectly smooth, it forms an almost perfect reflector of sound. Then the intensity of sound reflected from the smooth boundary will be nearly equal to that incident upon it. Hence, from Equation (2.14), it can be seen that the RL of a smooth surface will be closely equal to zero decibels.

The ocean surface and bottom provide discontinuities in the propagation medium with the result that the sound waves are reflected back from both of these boundaries. These two boundaries differ in some of their characteristics and are similar in others.

The bottom may range from soft mud to hard rock and from flat to mountainous. Generally, hard smooth bottoms are good reflectors, causing a bottom reflection loss (BRL) of about one to three dB per reflection at low grazing angles

(10^0) and at medium frequencies (10 kHz). Mud bottoms will cause an attenuation of approximately 15 dB under the same circumstances.

Relatively, the air-water interface at the surface of the ocean is a greater discontinuity, and if the surface is smooth, it acts almost like a perfect mirror with zero dB loss per reflection. However, the loss associated with a reflection from the surface is related to the surface roughness parameter [36] by,

$$g = \frac{8\,\pi\,\sigma\,f\sin\theta}{3} \tag{2.15}$$

where

g = surface rougness parameter.
σ = rms surface wave height in m.
θ = grazing angle in deg.

The surface reflection loss in the specular direction can then be approximated by [27],

$$SRL = \begin{cases} -10\log(1 - 0.57g) & \text{for } g < 1.4 \\ 7 & \text{for } g \geq 1.4 \end{cases} \tag{2.16}$$

where SRL is the surface reflection loss in dB. This loss for low grazing angles and medium frequencies is about 3 dB [36].

With the knowledge of transmission and reflection losses, the intensities of each eigenray in Fig (2.6) could be obtained.

2.6 Calculation of Intensity and the Propagation Delay of each Eigen-ray.

Recalling the Equation (2.5) in Sec (2.3) it can be seen that the intensity of the direct path I_D in dB can be expressed as

$$I_D = TSL - SL - AL \tag{2.17}$$

For the direct path, the length l_n is given by

$$l_n = \left[x_R^2 + (y_R - y_T)^2\right]^{\frac{1}{2}} \tag{2.18}$$

Hence using Equations (2.4) and (2.17), the time taken by a pulse to travel along the direct path and the intensity of the direct path I_D can be obtained.

The ray path 2 in Fig (2.6) comes under the category (a) in Sec (2.3) as the number of surface reflections is equal to the number of bottom reflections and the first reflection is from the sea surface. The length of the sound ray in this instant can be written as

$$l_{ns=b} = \left[x_R^2 + [\, y_T + (s + b)\, D - y_R \,]^2\right]^{\frac{1}{2}} \tag{2.19}$$

where D is the depth in m. and $l_{ns=b}$ denotes the length of the n^{th} multipath with equal number of surface and bottom reflections, given the first reflection is from the surface.

Hence for the path 3 in Fig (2.6), we can denote the length by $l_{nb=s}$ and is given by

$$l_{nb=s} = \left[x_R^2 + [\,(D - y_T) + (s + B)\, D - (D - y_R)\,]^2\right]^{\frac{1}{2}} \tag{2.20}$$

Similarly the ray paths 4 and 5 in Fig (2.6) come under the categories (c) and (d). The length of these are denoted by $l_{ns\neq b}$ and $l_{nb\neq s}$ and are given by

$$l_{ns\neq b} = \left[x_R^2 + [\, y_T + (\, s + b - 1\,)\, D + y_R\,]^2\right]^{\frac{1}{2}} \tag{2.21}$$

and

$$l_{nb\neq s} = \left[x_R^2 + [\,(\, D - y_T\,) + (\, s + b - 1\,)\, D + (\, D - y_R\,)\,]^2\right]^{\frac{1}{2}} \tag{2.22}$$

Using these values in Equation (2.4) and (2.5), the travel time and the intensity of each of the multipaths can be obtained.

Since the intensities of the multipaths add at the receiver, the ratio of direct path intensity to multipath intensity is given by [20]

$$\text{DMR} = 10 \log \left[\frac{10^{\frac{I_D}{10}}}{\sum \frac{10^{I_n}}{10}} \right] \tag{2.23}$$

where DMR = Direct to Multipath Ratio in dB

and the phase of each multipath with respect to the direct path is included in I_n itself.

CHAPTER 3

SLIDING DISCRETE FOURIER TRANSFORM

3.1 Introduction

Since the demodulation scheme devised in this thesis relies on the operation of Sliding Discrete Fourier Transform (SDFT) algorithm, the development and the properties of SDFT algorithm are discussed in this chapter. SDFT could be considered as an extension of the conventional Discrete Fourier Transform (DFT). Hence the basic properties of DFT, Fourier Transform and inverse transform of different forms of signals are described first and then the properties of SDFT are introduced.

3.2 Various Forms of Fourier Transform

In describing the properties of Fourier transform and inverse transform, it is quite convenient to use the concepts of time and frequency. It is very instructive to see the variety of forms that the transform takes, when the time and frequency variables assume combinations of continuous and discrete forms.

Here it is considered four possible forms that could be used in representing Fourier transform and inverse transform functions which correspond to the four combinations. These combinations are obtained from successively assuming the continuous and discrete, time and frequency variables.

3.2.1 Continuous - time and Continuous - frequency

The Fourier transform X(f) of a continuous time function x(t) could be expressed as

$$X(f) = \int_{-\infty}^{+\infty} x(t) \exp(-j2\pi ft) \, dt \qquad (3.1)$$

The inverse transform is

$$x(t) = \int_{-\infty}^{+\infty} X(f) \exp(j2\pi ft) \, df \qquad (3.2)$$

The forms of the time function and the transform function are illustrated in Fig (3.1), which shows that a nonperiodic continuous-time function corresponds to a non-periodic continuous-frequency transform function.

3.2.2. Continuous-time and Discrete-frequency

This is the form of the Fourier transform that is most often referred to as Fourier series.

Let x(t) represents a periodic continuous-time function with period t_p. The Fourier transform of x(t) is a discrete-frequency function denoted by X(mF). The transform pair is then given by

$$X(mF) = \frac{1}{t_p} \int_0^{t_p} x(t) \exp(-j2\pi mFt) \, dt \qquad (3.3)$$

$$\text{and } x(t) = \sum_{-\infty}^{+\infty} X(mF) \exp(j2\pi mFt) \qquad (3.4)$$

The integral in Equation (3.3) is evaluated over one period of x(t).

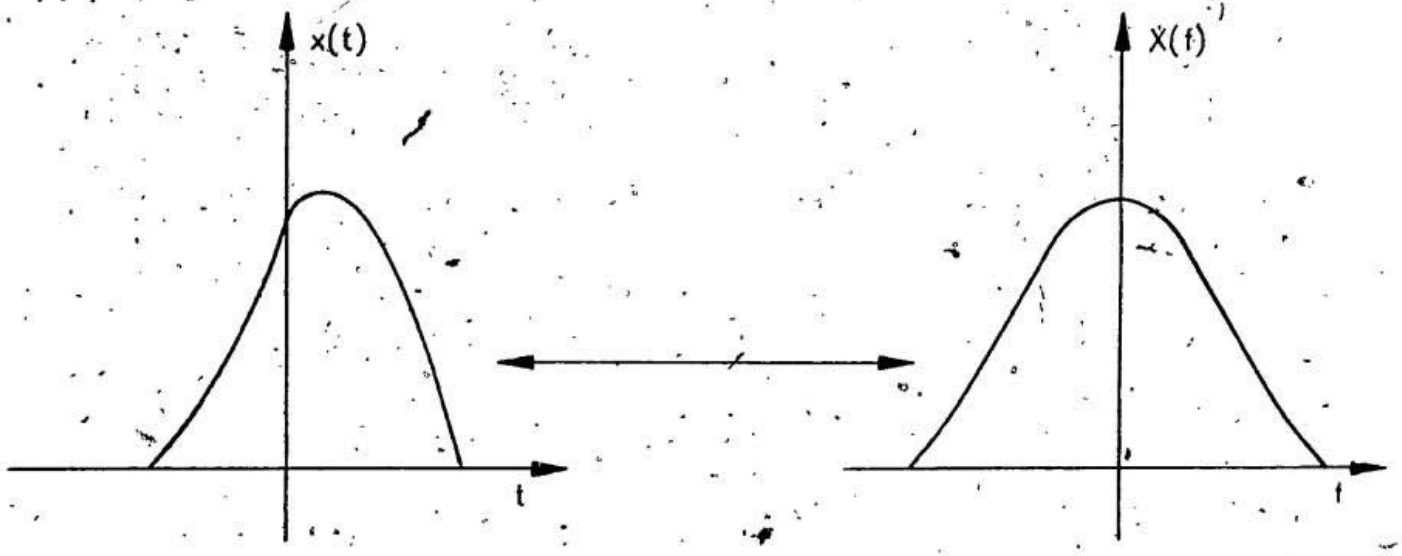

Fig. 3.1 Non-periodic continuous-time function and it's Fourier transform, which is a non-periodic continuous-frequency function.

The properties of these functions are illustrated in Fig (3.2). The frequency increment F between successive spectral components are related to the time period t_p by

$$F = \frac{1}{t_p} \tag{3.5}$$

Here it can be concluded that a periodic continuous-time function corresponds to a non-periodic discrete-frequency transform function.

3.2.3 Discrete-time and Continuous-frequency.

The Fourier transform X(f) of the discrete-time signal x(nT) is given by

$$X(f) = \sum_{0}^{\infty} x(nT) \exp(-j2\pi nfT) \tag{3.6}$$

and it's inverse by

$$\overline{x(nT)} = \frac{1}{f_s} \int_{0}^{f_s} X(f) \exp(j2\pi nft) \, df \tag{3.7}$$

The integral in Equation (3.7) is evaluated over one period of X(f).

Some of the properties of these functions are illustrated in Fig (3.3). The period of the frequency function is simply the sampling rate f_s and is related to the sample time T by

$$f_s = \frac{1}{T} \tag{3.8}$$

Here the conclusion is that a non-periodic discrete-time function corresponds to a periodic continuous-frequency transform function.

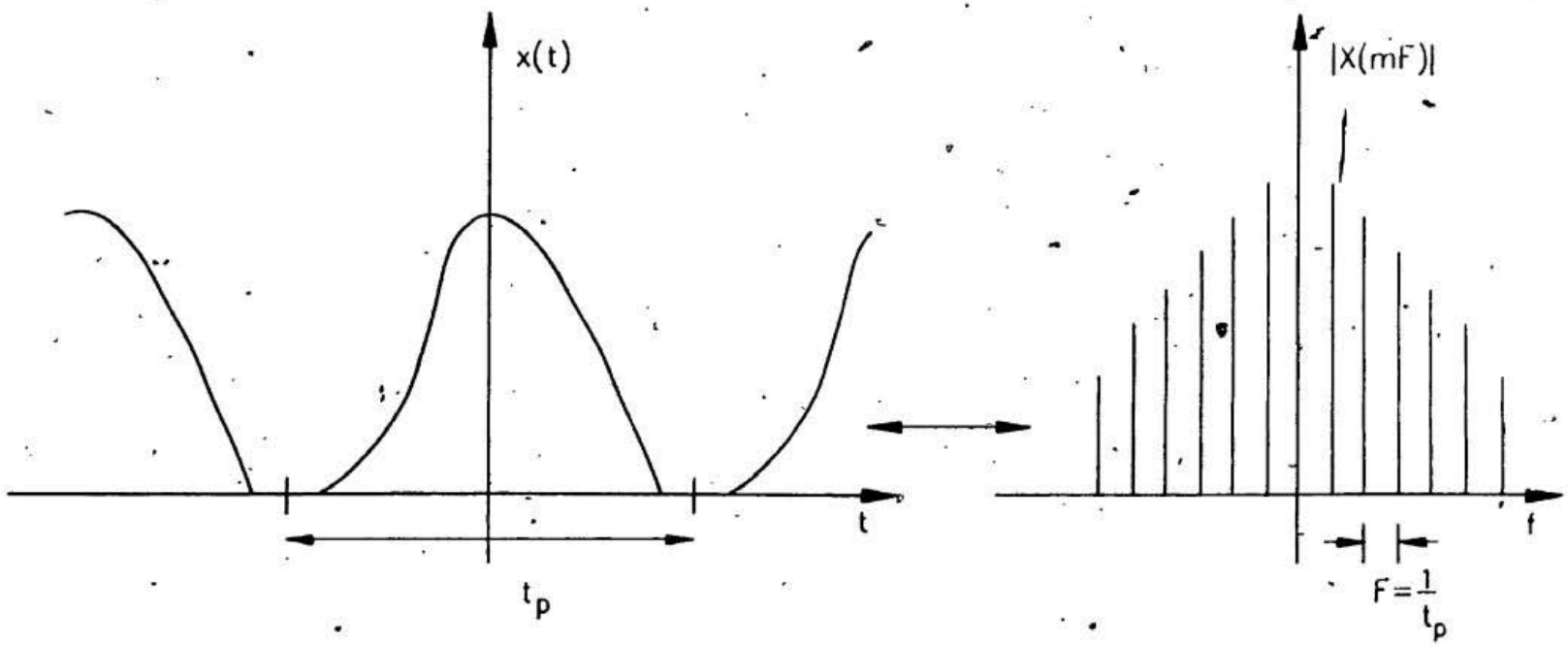

Fig. 3.2 Periodic continuous-time function and it's Fourier transform, which is a non-periodic discrete-frequency function.

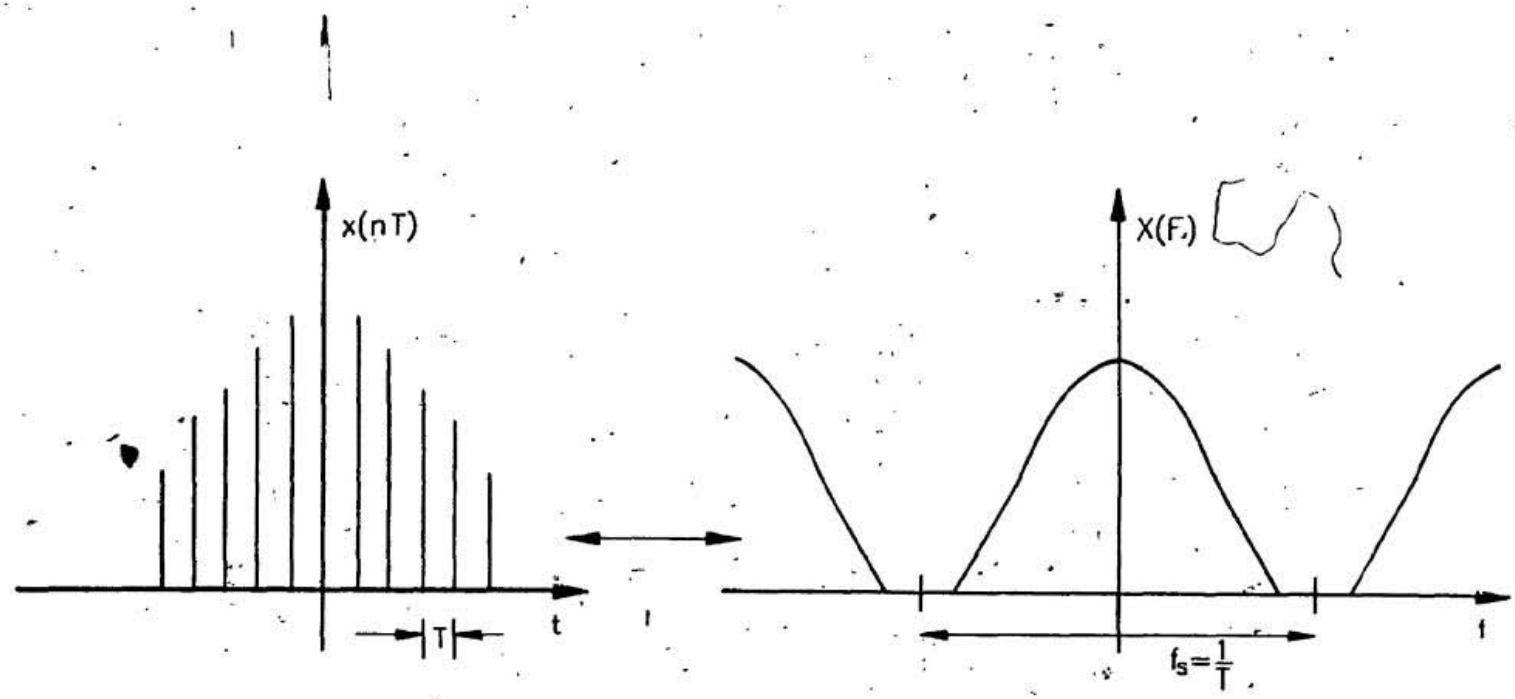

Fig. 3.3 Non-periodic discrete-time function and it's Fourier transform, which is a periodic continuous-frequency function.

3.2.4 Discrete-time and Discrete-frequency

For a periodic discrete-time signal x(nT), the Fourier transform X(mF) is given by

$$X(mF) = \sum_{n} x(nT) \exp(-j2\pi mnFT) \tag{3.9}$$

and it's inverse transform is given by

$$x(nT) = \frac{1}{N} \sum_{m} X(mF) \exp(j2\pi mnFT) \tag{3.10}$$

Both these summations are evaluated over one period of x(nT) and X(mF) respectively.

Equations (3.9) and (3.10) describe one form of the Discrete Fourier Transform (DFT) pair which will be explained in the next section.

The basic properties of the time and frequency functions are illustrated in Fig (3.4). Since the time function is sampled, the frequency function is periodic with period f_s as

$$f_s = \frac{1}{T} \tag{3.11}$$

On the other hand, since the frequency function is sampled, the time function is periodic with a period t_p given by

$$t_p = \frac{1}{F} \tag{3.12}$$

It can be seen, that a periodic discrete-time signal corresponds to a periodic discrete-frequency transform function.

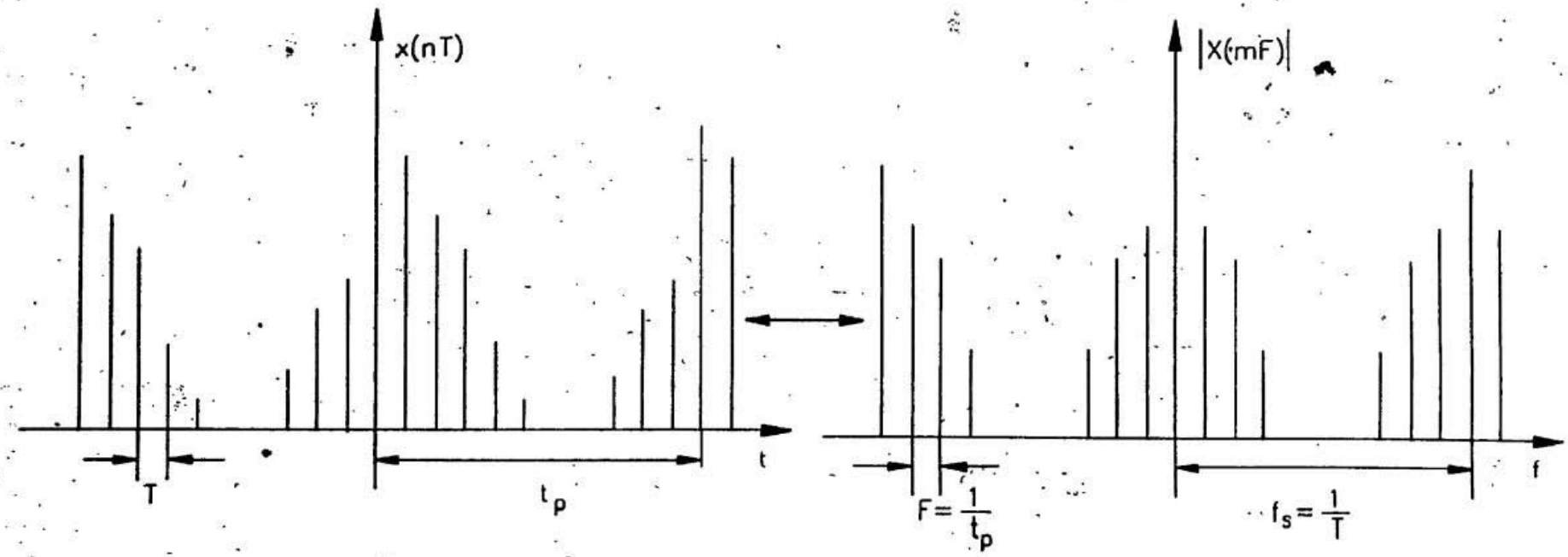

Fig. 3.4 Periodic discrete-time function and it's Fourier transform, which is a periodic discrete-frequency function.

By reviewing the preceding steps, several general conclusions can be made. If a function in one domain (either time or frequency) is periodic, then the corresponding transform in the other domain is a sampled form, which means it is a function of a discrete variable. Conversely, if a function in one domain is sampled, then the function in the other domain becomes periodic. The period in one domain is always the reciprocal of the increment between samples in the other domain. These properties are summarized in Table (3,1).

Table (3.1) Comparison of several forms of Fourier transform pairs.

Time Function	Frequency Function
(1) Non-periodic and continuous	Non-periodic and continuous
(2) Periodic and continuous	Non-periodic and discrete
(3) Non-periodic and discrete	Periodic and continuous
(4) Periodic and discrete	Periodic and discrete

When a function is evaluated by numerical procedures, it is always necessary to sample it in some fashion. This means that in order to fully evaluate a Fourier transform or inverse transform with digital operations, it is necessary that both the time and frequency functions be eventually sampled in one form or another. Thus, the last of the four possible Fourier pairs, (DFT), is the one that is of primary interest in digital computation.

3.3.1 Discrete Fourier Transform (DFT)

The N-point Discrete Fourier Transform (DFT) of a N-point sequence x(nT) derived by sampling a continuous signal x(t) with sampling period T (or sampling frequency $f_s = \frac{1}{T}$) is defined by

$$X(k\Omega) = \sum_{n=0}^{N-1} x(nT) \exp\left(\frac{-j2\pi nk}{N}\right) ; \qquad k = 0, 1 \ldots\ldots, N-1 \qquad (3.13)$$

where $\Omega = \frac{1}{NT} = \frac{f_s}{N}$

is the interval between adjacent discrete frequency components or the frequency resolution. The spectral components $X(k\Omega)$ are directly related to the Fourier Transform $X_w(f)$ of the windowed signal $x_w(t)$ defined as

$$x_w(t) = \begin{cases} x(t) & \text{for } 0 \le t \le T_0 = NT, \\ 0 & \text{otherwise} \end{cases} \qquad (3.14)$$

by the following equations

$$X(k\Omega) = X_R(k\Omega) \qquad (3.15a)$$

where

$$X_R(f) = \sum_{-\infty}^{+\infty} X_w(f - nf_s) \qquad (3.15b)$$

It follows from Equations (3.15a) and (3.15b) and the properties of the Fourier Transform, that for real signals, spectrum $X_R(f)$ is repetitive with period f_s and it's magnitude is symmetric with respect to $f_s/2$.

If the signal x(t) and the window function w(t) are considered as

$$x(t) = A \cos (\omega_c t + \Phi) \tag{3.16a}$$

and

$$w(t) = \begin{cases} 1 & \text{for } |t| \leq \tau/2 \\ 0 & \text{for } |t| > \tau/2 \end{cases} \tag{3.16b}$$

then

$$x_w(t) = \begin{cases} A \cos (\omega_c t + \Phi) & \text{for } |t| \leq \tau/2 \\ 0 & \text{for } |t| > \tau/2 \end{cases} \tag{3.16c}$$

The Fourier Transform of the signal in Equation (3.16c) is given by

$$X_w(f) = 1/2\, A \left[\exp(j\Phi) \, \delta (f - f_c) * W(f) + \exp(-j\Phi) \, \delta (f + f_c) * W(f) \right] \tag{3.17a}$$

$$= 1/2\, A \left[\exp(j\Phi) \, W (f - f_c) + \exp(-j\Phi) \, W (f + f_c) \right]$$

where the Fourier Transform W(f) of the pulse w(t) is given by

$$W(f) = \frac{\tau \sin \pi f \tau}{\pi f \tau} \tag{3.17b}$$

Fig (3.5) shows the magnitude of the spectrum of $X_w(f)$.

Hence according to Equations (3.15a) and (3.15b) the DFT of a windowed sinusoidal signal of frequency f_c will have spectral peaks at frequency f_c and at image frequency $f_c' = f_s - f_c$ as shown in Fig (3.6). Spectral peaks occur at the same positions for an input frequency f_c', leading to ambiguity in determination of input frequencies.

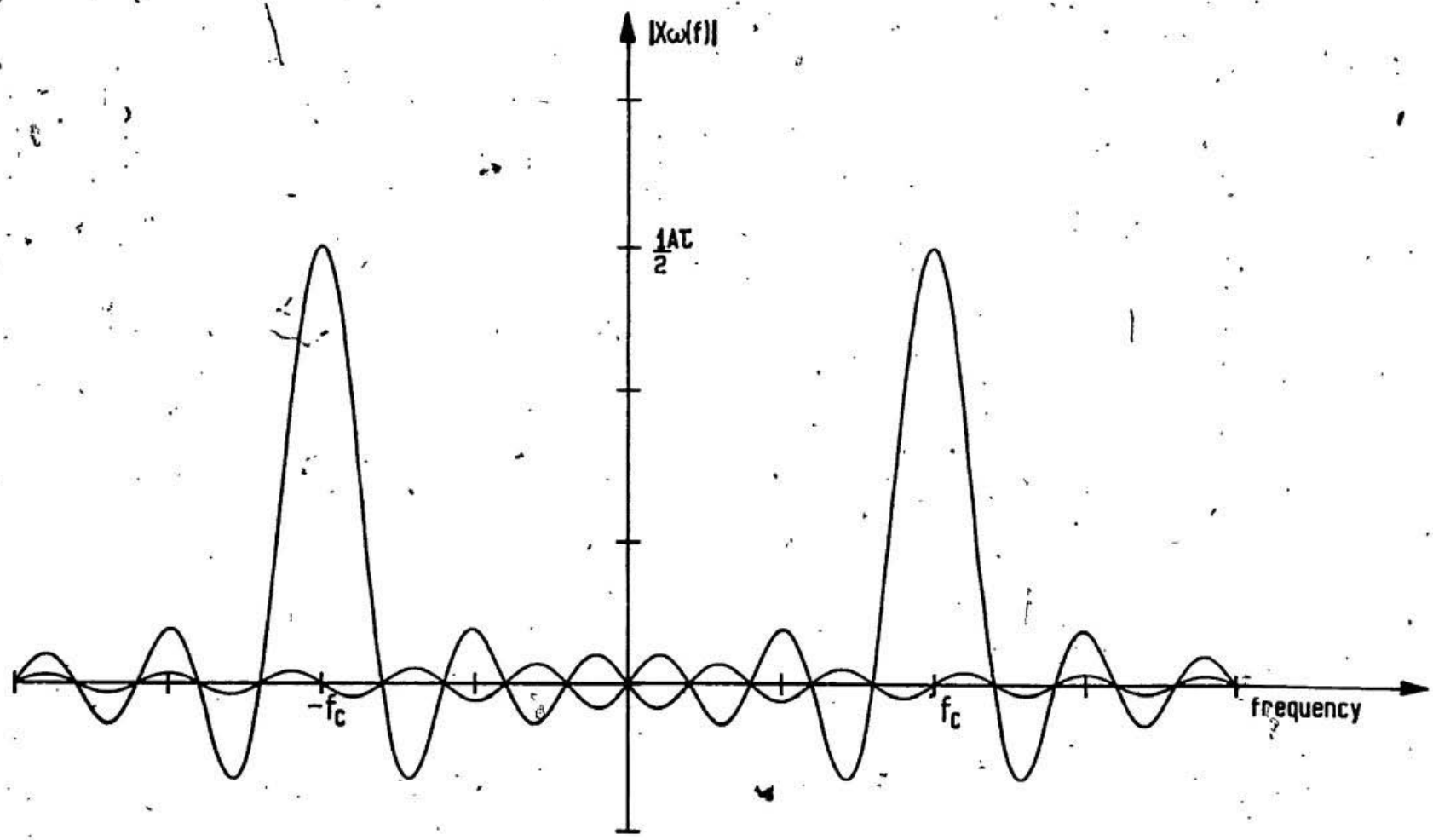

Fig. 3.5 The spectrum of the windowed-sinusoidal signal of frequency f_c.

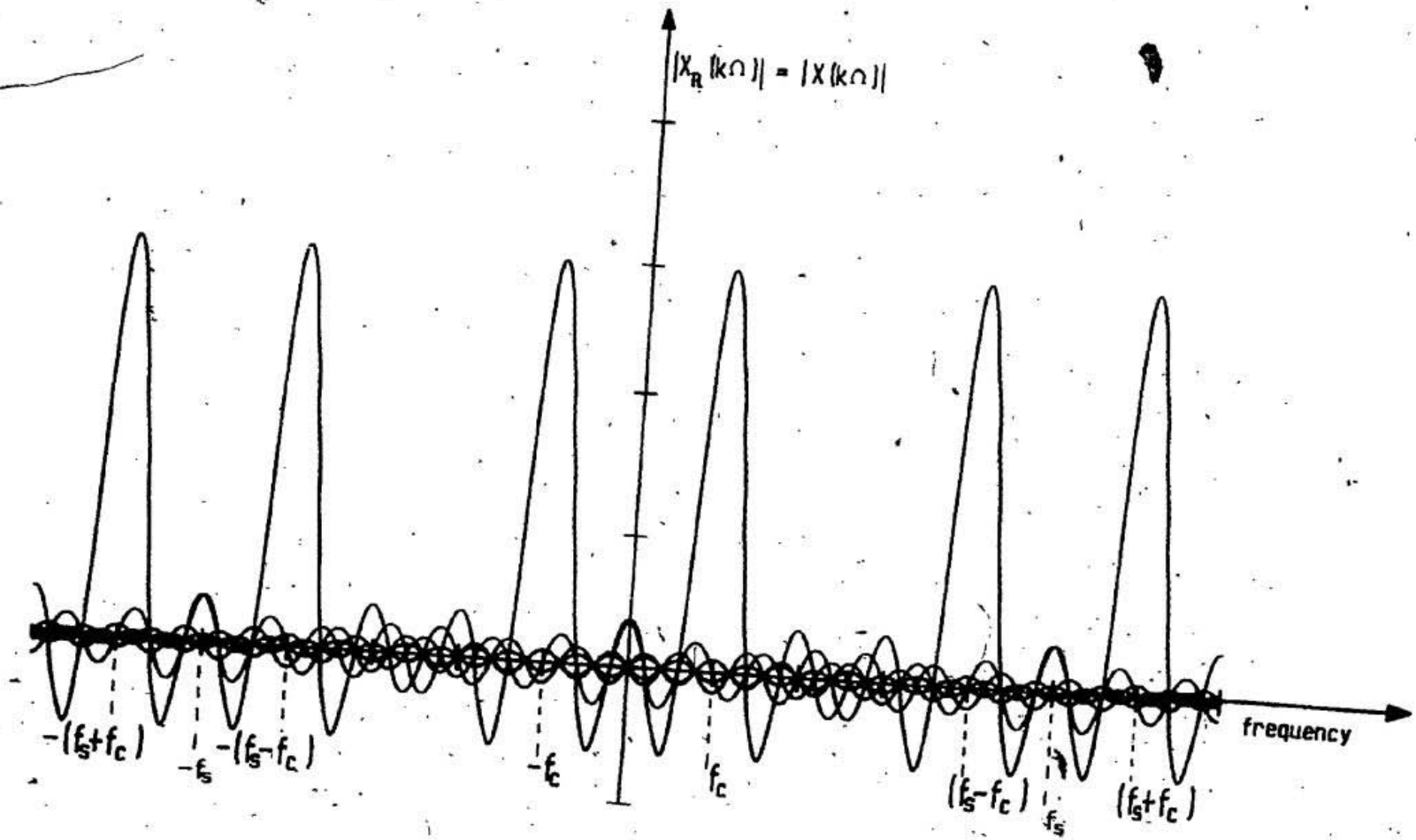

Fig. 3.6 DFT of a windowed sinusoidal signal.

3.3.2 DFT Implementation by Filtering Method

The factor 2nk in Equation (3.13) can be replaced by [6]

$$2nk = n^2 + k^2 - (k - n)^2 \tag{3.18}$$

This substitution changes Equation (3.13) to Equation (3.19) below.

$$X(k\Omega) = \sum_{n=0}^{N-1} x(nT) \exp\left(-j[n^2 + k^2 - (k-n)^2]\right)\frac{\pi}{N} \tag{3.19a}$$

$$= \exp\left(\frac{-j\pi k^2}{N}\right) \sum_{n=0}^{N-1} x(nT) \exp\left(\frac{-j\pi n^2}{N}\right) \exp\left(\frac{j\pi(k-n^2)}{N}\right) \tag{3.19b}$$

Equation (3.19b) indicates three operations as follows.

1. The multiplication of each term of input discrete time series x(nT) by the complex factor $\exp\left(-\frac{j\pi n^2}{N}\right)$. Let the resultant complex sequence be denoted by g_n

$$g_n = x(nT) \exp\left(-\frac{j\pi n^2}{n}\right)$$

$$= x(nT)\left[\cos\frac{\pi n^2}{N} - j \sin\frac{\pi n^2}{N}\right]. \tag{3.19c}$$

2. The performance of a discrete convolution between the sequence g_n and the sequence $\exp\left(\frac{j\pi k^2}{N}\right)$. This convolution is performed within the summation.

3. Multiplication of the resulting output sequence by the final factor $\exp\left(\frac{-j\pi k^2}{N}\right)$ for each point of $X(k\Omega)$.

Now, $X(k\Omega)$ can be simplified to

$$X(k\Omega) = \exp\left(\frac{-j\pi k^2}{N}\right)\left\{ g_k * \exp\left(\frac{j\pi k^2}{N}\right)\right\}$$

Where * indicates the convolution operation.

$$\text{Hence } \left|X(k\Omega)\right| = \left|\left(\frac{-j\pi k^2}{N}\right)\right|^2 \left|g_k * \exp\left(\frac{j\pi k^2}{N}\right)\right|^2 \qquad (3.20)$$

$$|X(k\Omega)| = |g_k * \exp\left(\frac{j\pi k^2}{N}\right)|$$

since $\exp\left(\frac{-j\pi k^2}{N}\right)$ has unit magnitude. The above operations are illustrated in Fig (3.7).

Equation (3.20) can be implemented with filters which have 2N-1 stages. During the first N-1 clock periods the filter is loaded with the pre-multiplied data, and during the succeeding N clock periods the convolution and squaring operations sequentially yield the magnitude squared of the Fourier coefficients. This approach has the disadvantage of requiring filters of length 2N for an N-point transform and is also inefficient in the use of the filters since only half of each filter contains useful information at any point in time.

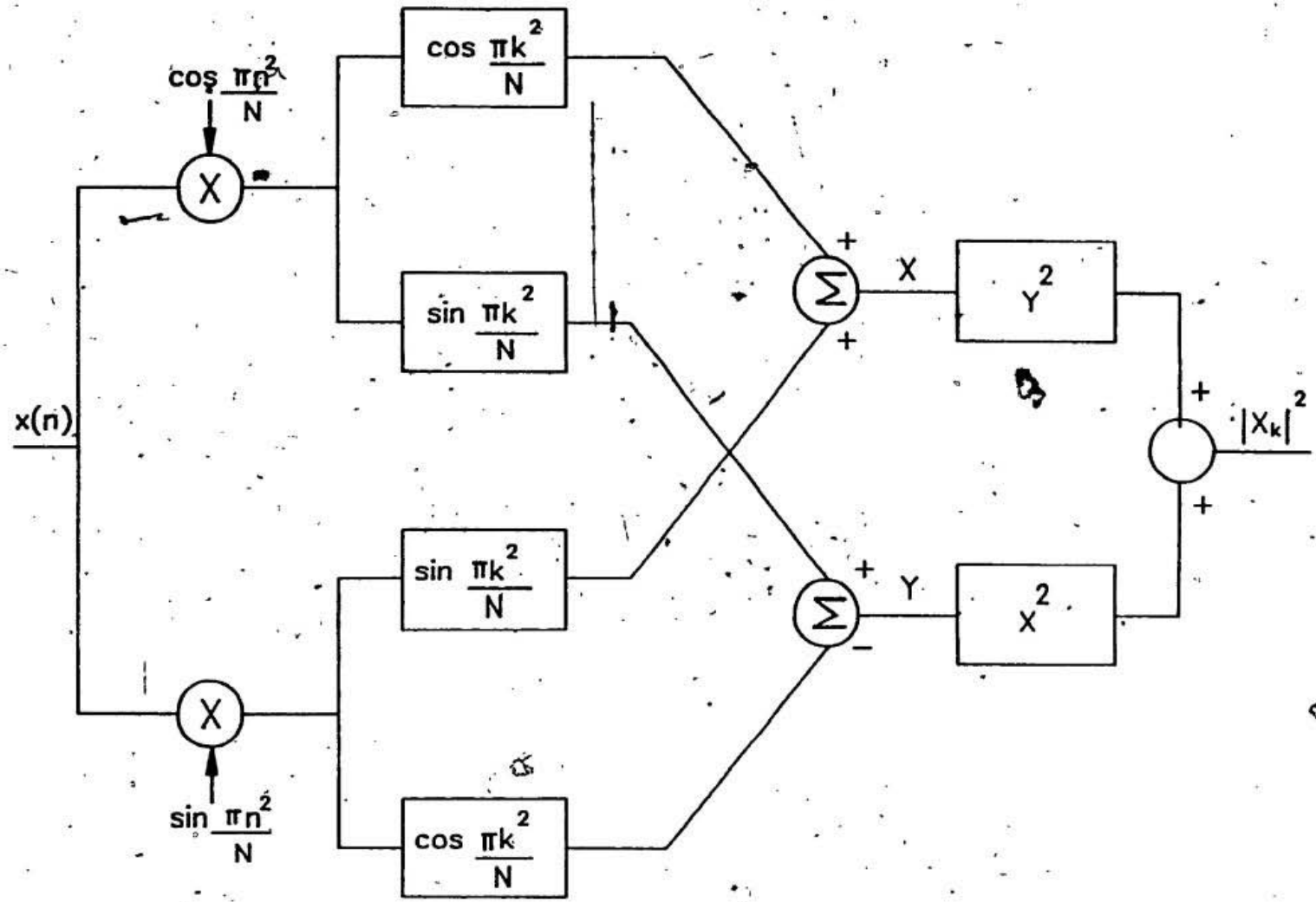

Fig. 3.7 Block diagram for implementation of DFT.

3.4.1 Sliding Discrete Fourier Transform (SDFT)

The Sliding Discrete Fourier Transform (SDFT) is defined by

$$X_s(\,k\Omega\,) = \sum_{n=k}^{N-1+k} x(nT)\exp\left(\frac{-j2\pi nk}{N}\right) \tag{3.21}$$

Here the input data is shifted by one sample each time a spectral component $X_s(\,K\Omega\,)$ is calculated. Unlike the conventional DFT algorithm SDFT can operate continuously in real time but only one spectral component is available at a given instant. Such operation resembles a scanning band-pass filter. This sliding observation window effects only spectrum phase but proper timing considerations are necessary if SDFT is to be used for spectral analysis.

To calculate the power spectrum using the sliding DFT, the substitution of (3.18) is used with (3.21) to obtain the following equation

$$|\,X_s(\,k\Omega\,)\,| = \left[\sum_{n=0}^{N-1} x[(\,n+k\,)\,T]\exp\left(\frac{-j\pi n^2}{N}\right)\exp\left(\frac{j\pi(k-n)^2}{2}\right)\right]^2 \tag{3.22}$$

Fig (3.8) gives a pictorial comparison [10] between the conventional DFT and Sliding DFT for the case of a 3-point transform. With the conventional DFT all three Fourier coefficients X(1), X(2), X(3) are calculated using the first three time samples x(1), x(2), x(3). These three coefficients are calculated by the filter during the next three clock periods, so that the time samples x(4), x(5), x(6) must be blanked. Then the cycle repeats as shown in Fig (3.8). Using the SDFT $X_s(1)$ is calculated on the sample record x(1), x(2), x(3) as before, but $X_s(2)$ is calculated on the sample record x(2), x(3), x(4). $X_s(3)$ on the record x(3), x(4), x(5) and

$$X(k) = \sum_{n=0}^{N-1} x(n) \exp\left[\frac{-j2\pi nk}{N}\right]$$

$$X_s(k) = \sum_{n=k}^{N-1+k} x(n) \exp\left[\frac{-j2\pi nk}{N}\right]$$

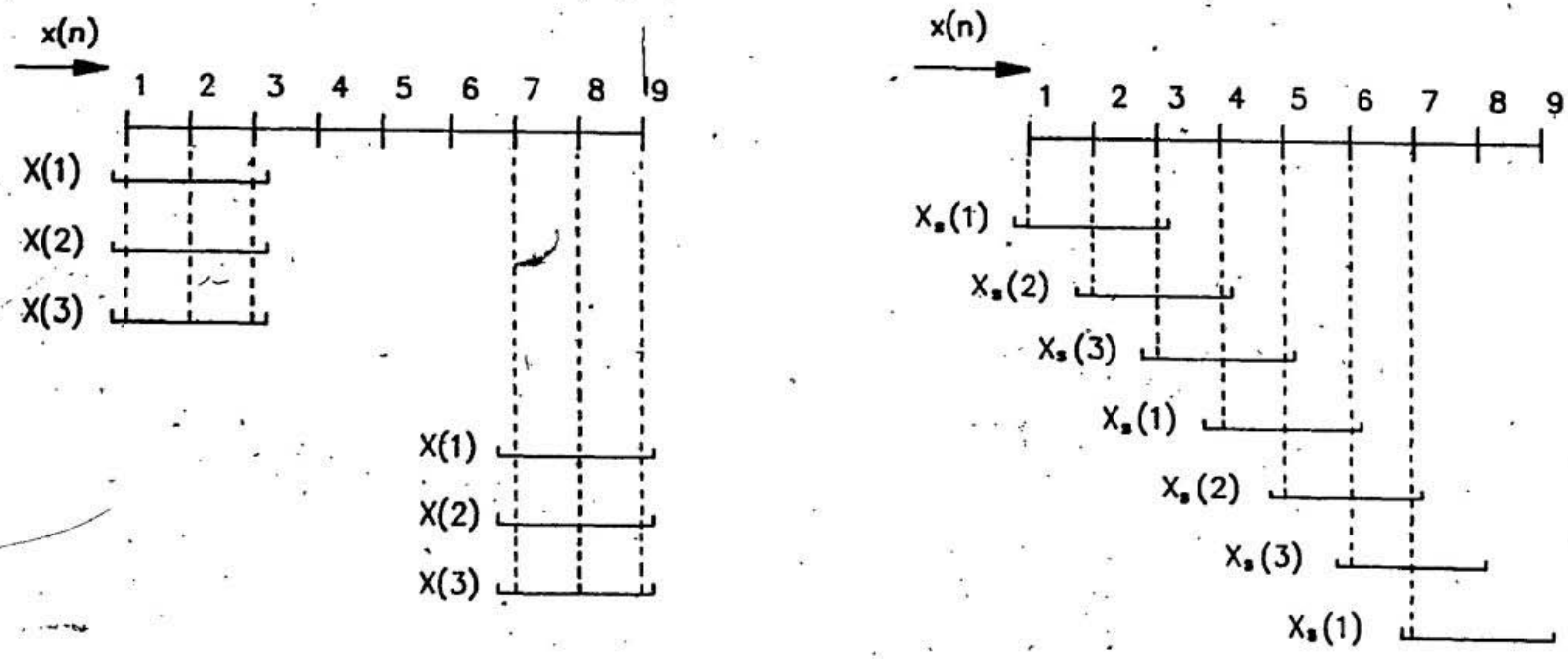

Fig. 3.8 Pictorial comparison between conventional DFT and SDFT.

the next $X_s(1)$ computation is made on the sample record x(4), x(5), x(6). The sample record is continually updated by replacing the oldest sample with a new one. This description shows that N Fourier coefficients are obtained for n time samples or the duty cycle is 100%.

3.4.2 Sliding DFT Implementation

The implementation of SDFT is very similar to the conventional DFT as shown in Fig (3.7). But the required number of filter stages here is reduced by half since no signal blanking is required.

This system can be conveniently implemented using charge-coupled transversal filters with chirp impulse response such as Recticon R5601A quad filter which uses 512 time domain samples for calculation of each spectral component and can operate for sampling frequencies from 4 kHz to 2 MHz [6].

With this knowledge the spectrum of the signal used in the transmission scheme explain in the next section is obtained using the SDFT algorithm.

CHAPTER 4

SDFT TRANSMISSION SCHEME

4.1 Introduction

In this chapter, a novel transmission scheme which exploits the advantages of the Sliding Discrete Fourier Transform (SDFT) described in Chapter 3 is developed. The new system uses constant envelope multifrequency signals and can tolerate large Doppler frequency shifts and strong multipath conditions. With the availability of VLSI circuits to implement the SDFT algorithm, the proposed system is particularly suitable for untethered remotely controlled submersibles where power and space conservation are of prime importance.

The remaining sections of this chapter address the design of signal waveforms and the selection of frequencies for transmission. A sample design of the system is introduced in order to illustrate the design methodology. Finally, the operation of the receiver is explained.

4.2 Signal Design

Consider a signal $x(t)$ formed by a sequence of M adjacent sinusoidal pulses of duration τ, each of different frequency f_i, phase Φ_i and amplitude A_i, which can be mathematically expressed as

$$x(t) = \sum_{i=1}^{M} w(t - \Delta_i)\, A_i \cos\left[2\pi f_i (t - \Delta_i) + \Phi_i \right] \qquad (4.1a)$$

where

$$w(t) = \begin{cases} 1 & \text{for } |t| \leq \tau/2 \\ 0 & \text{for } |t| > \frac{\tau}{2} \end{cases} \tag{4.1b}$$

$$\Delta_i = i\tau - \frac{\tau}{2} \tag{4.1c}$$

and i is a positive integer. The Fourier Transform of signal (4.1a) is given by

$$X(f) = \frac{1}{2} \sum_{i=1}^{M} A_i \left[e^{j\Phi_i} W(f - f_i) + e^{-j\Phi_i} W(f + f_i) \right] e^{-j\Delta_i} \tag{4.2a}$$

where W(f) is the Fourier Transform of the pulse w(t) which can be expressed as

$$W(f) = \tau \frac{\sin(\pi f \tau)}{\pi f \tau} \tag{4.2b}$$

It follows from Equations (4.2a) and (4.2b) that if the frequencies f_i are separated by an integer multiple of ΔF so as to avoid Inter Symbol Interference (ISI) where

$$\Delta F = \frac{1}{\tau} \tag{4.3}$$

then the magnitude of spectrum given by equation (4.2a) at frequencies f_i reduces to,

$$|X(f_i)| = \frac{1}{2} \tau A_i \tag{4.4}$$

f_i is related to ΔF and i as,

$$f_i = i\,(r\,\Delta F) \tag{4.5}$$

where r is an integer number. This is the basis for the detection scheme treated in this thesis where spectrum X(f) is obtained by using the Sliding Discrete

Fourier Transform algorithm. In Section (3.4.1), the SDFT is defined as

$$X_s(k\Omega) = \sum_{n=k}^{N-1+k} x(nT) \exp\left[-\frac{j2\pi kn}{N}\right] \tag{4.6}$$

In the proposed transmission scheme, a waveform as given in equation (4.1a) is utilized for transmission of digital data. The amplitudes A_i of all the signals are equal and phases Φ_i are adjusted to assure continuity between adjacent signaling elements each of duration τ.

The binary information is transmitted in blocks of M bits as shown in Fig (4.1). The frequencies f_i are selected from a set of M frequencies which satisfy the conditions (4.3) and (4.5). It is assumed that these frequencies are separated by B,

$$B = f_{i+1} - f_i = \tau \Delta F \tag{4.7}$$

The signaling rate R is given by,

$$R = \frac{1}{M\tau} \quad \text{Blocks/sec} \tag{4.8}$$

and the information rate can be written as,

$$I = \frac{1}{M\tau} M = \frac{1}{\tau} \quad \text{bits/sec} \tag{4.9}$$

If each block of signals is sampled to yield N discrete samples using a sampling frequency f_s, then it follows that

$$\frac{1}{f_s} N = M\tau$$

$$\text{and} \quad f_s = \frac{N}{M\tau} = \frac{NI}{M} \tag{4.10}$$

The frequency resolution Ω, and the number of spectral components N_F within the mainlobe of each signaling element are related to other parameters by

$$\Omega = \frac{f_s}{N} \tag{4.11}$$

$$\text{and} \quad N_F = 2\frac{\Delta F}{\Omega} = 2\frac{\Delta FN}{f_s} = 2M$$

The factors N_F and Ω play an important role if additional system functions, such as correction for Doppler shifts, are to be considered.

The demodulation of the signals designed with the above requirements is accomplished by the SDFT algorithm within the sliding observation window positioned initially as shown in Fig (4.1).

As the window advances to the right, the magnitudes of the spectral components $X_s(k\Omega)$ corresponding to frequencies f_i are used to determine whether a 'one' or a 'zero' was transmitted. A frequency $f_{i+1} > f_i$ is assigned to each of the time slots in the block. The assigned frequency is transmitted to represent the binary 'one' at the corresponding time slot. If the magnitudes of the spectral components corresponding to these frequencies exceed a certain threshold, the received signal is detected as an 'one' and a 'zero' otherwise. Therefore, a 'zero' can be represented by any frequency which has zero crossings at all the frequencies f_i in the frequency domain. However, $\frac{f_s}{2}$ has been selected to represent binary 'zero', as it has the minimal effect on the frequency spectrum under all possible conditions, due to the fact that the samples of this signal in time domain are zero. The selection of frequencies according to the above requirements avoids

the Inter Symbol Interference (ISI). Since the effect of multipaths is to cause ISI, the frequency selection scheme overcomes the distortion caused by the multipath signals.

According to this coding method, a sequence of M = 8 binary symbols: 1, 1, 0, 1, 1, 0, 1, 1 is represented by sequence of frequencies: f_1, f_2, $f_s/2$, f_4, f_5, $f_s/2$, f_7, f_8. Here, the first frequency f_1 is selected such that the image frequencies $f'_i = f_s - f_i$ are separated by B/2 from the signaling frequencies. This requirement can be written as

$$f_1 = \frac{\left(f_s + \frac{B}{2} - (m-1)B\right)}{2} \qquad (4.12)$$

When the frequencies f_i are selected with the above requirement, the image frequencies f_i' also have their zero crossings at all the frequencies f_i concerned.

The following is a sample design of the system assuming,

M=8, N=512, B=1000 Hz., and τ =8 msec.

Then the following parameters could be derived as,

$$\Delta F = \frac{1}{\tau} = 125 \text{ Hz.}$$

$$I = \frac{1}{8} = 125 \text{ bits/sec}$$

$$f_s = \frac{NI}{M} = \frac{512 \times 125}{8} = 8 \text{ kHz.}$$

$$N_F = 2M = 16 \quad \text{and}$$

$$\frac{f_s}{N} = \frac{8000}{512} = 15.62 \text{ Hz.}$$

from equation (4.12), f_1=750 Hz.

Then the other frequencies could be obtained as,

$f_i = 750 + 1000\,(i-1)$ Hz and

$f'_i = 7250 - 1000\,(i-1)$ Hz; $i = 1, 2, 3, \ldots, 8$

According to this signal design, the spectral components $X_s(k_1\Omega)$; $k_1 = 48 + 64\,(i-1)$ represent the frequencies $f_i = 750 + 1000\,(i-1)$ for i=1, 2, ..., 8. The digital data transmitted are detected using the technique described in the following section.

4.3 Operation of the Receiver

Transmission requirements and characteristics of an acoustic transducer require a different set of signaling frequencies from that selected from the the point of view of demodulation. Since the ocean rapidly weakens the acoustic energy of the signal when the frequency of the signal increases, relatively low frequencies are desirable for long range communications. But at very low frequencies, the required transducer size is impractically large and the achievable data rates are low. As a tradeoff, according to several recent studies on different sea states, the desired frequency range for most underwater acoustic communications has been established as 8 to 50 kHz. Therefore in the proposed scheme, the frequencies are selected within a narrow transmission bandwidth of 1 kHz positioned around a central frequency of 10 kHz. However, these transmitted frequencies F_i can be converted to the selected set f_i for the SDFT demodulation scheme with the use of a suitable mixer at the receiver.

A block diagram of a receiver is shown in Fig (4.2). The received signal x(t) is first band-limited by the bandpass filter (BPF) to remove undesired out of band noise. Then the amplitude of the received signal is stabilized using an Automatic Gain Controller (AGC). The block synchronization is established by BS and used to initialize proper sequencing of mixer frequencies generated by a frequency synthesizer FS. The resultant signal is low-pass filtered by a LPF having cut-off frequency f_s and subjected to SDFT analysis as discussed in Section (4.2). The SDFT processor can be implemented using Charged Coupled chirp Z transversal filter as explained in Section (3.4.2). The decoder D generates digital data DD based on the magnitudes of frequency components $X_s(k_1\Omega)$.

The position of spectral peaks can be used to detect a Doppler frequency shift and to correct it by a proper adjustment of the synthesizer frequency. Since each of the transmitted frequencies produce two distinct spectral peaks, these peaks also can be used in the detection process to increase probability of correct transmission.

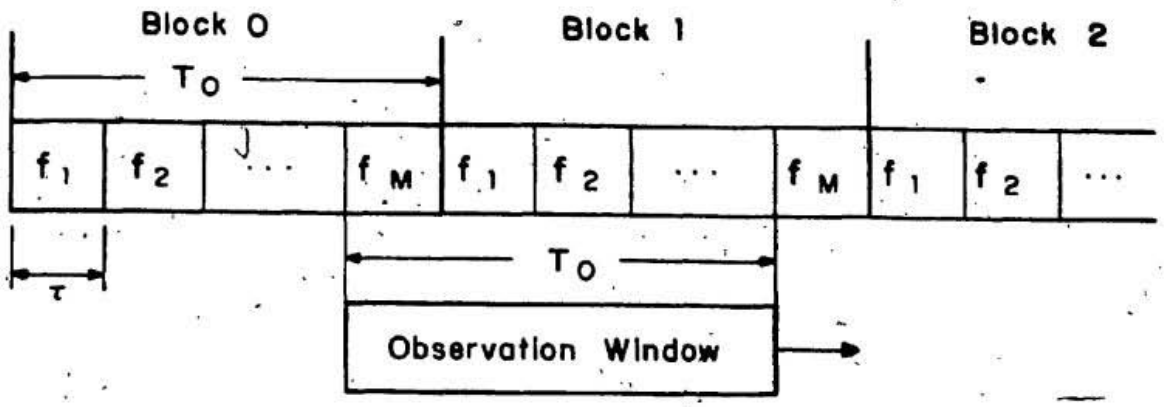

Fig. 4.1 Signal structure at the demodulator.

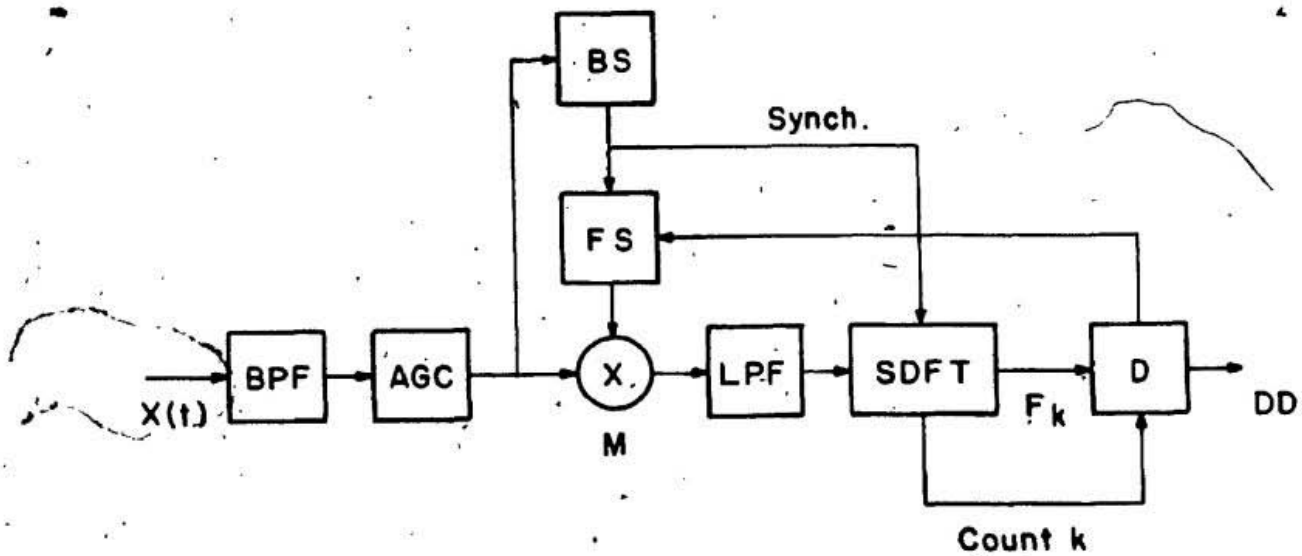

Fig. 4.2 Block diagram of the receiver.

CHAPTER 5

EVALUATION OF RECEIVER PERFORMANCE

5.1 Introduction

The objective of this chapter is to analytically evaluate the performance of the transmission scheme explained in the previous chapter. If AGC is used to stabilize the received signal, the analysis becomes complicated and untractable. In order to overcome this difficulty, a computer simulation has been carried out for the case with AGC, and it's results are presented in Chapter 6.

This chapter focuses on the evaluation of receiver performance for the case when no AGC is involved. The variation of eye opening with DMR is analyzed and the minimum DMR required for correct detection is obtained. Then the minimum DMR required for correct detection in the presence of synchronization errors is determined. Finally, the error performance of the system in the presence of Gaussian noise is evaluated.

5.2 Analysis of Spectral Components without Multipaths

The spectral components $X_s(k\Omega)$ of the received signal x(n) are obtained using the SDFT algorithm given by

$$X_s(k\Omega) = \sum_{n=k}^{N-1+k} x(n)\, W^{-kn} \qquad (5.1)$$

where $W = \exp\left(\frac{-j2\pi}{N}\right)$, $\Omega = \frac{f_s}{N}$,

f_s = sampling frequency and $N = 512$

According to the signaling scheme explained in Section (4.2), the spectral components of the frequencies $f_i = 750 + 1000\,(i-1)$ where i=1, 2,....8, are represented by $X_s(k_1\Omega)$, where $k_1 = 48 + 64(i-1)$. Depending on the magnitudes of these components, the receiver decides whether a 'one' or a 'zero' was transmitted.

Since $X_s(k_1\Omega)$ for all k_1 behave in the same manner, the analysis is carried out for $k_1 = 48$ only. Therefore, the spectral component for this case is,

$$X_s(48\Omega) = \sum_{n=48}^{512-1+48} x(n)\, W^{-48n} \tag{5.2}$$

where $X_s(48\Omega)$ is the spectral component corresponding to the frequency $f_1 = 750$Hz. At the time instant $X_s(48\Omega)$ is obtained, the position of the sliding window is as shown in Fig (5.1). If the effect of multipaths is neglected, the Equation (5.2) could be written as,

$$X_s(48\Omega) = \sum_{n=48}^{511+48} x(n)W^{-48n} \tag{5.3a}$$

$$\begin{aligned} &= \sum_{n=48}^{63} \sin 2\pi f_8 nT\, W^{-48n} + \sum_{n=64}^{127} \sin 2\pi f_1 nT\, W^{-48n} \\ &+ \sum_{n=128}^{191} \sin 2\pi f_2 nT\, W^{-48n} + \sum_{n=192}^{255} \sin 2\pi f_3 nT\, W^{-48n} \\ &+ \sum_{n=256}^{319} \sin 2\pi f_4 nT\, W^{-48n} + \sum_{n=320}^{383} \sin 2\pi f_5 nT\, W^{-48n} \\ &+ \sum_{n=384}^{447} \sin 2\pi f_6 nT\, W^{-48n} + \sum_{n=448}^{511} \sin 2\pi f_7 nT\, W^{-48n} \\ &+ \sum_{n=512}^{512+47} \sin 2\pi f_8 nT\, W^{-48n} \end{aligned} \tag{5.3b}$$

where $f_i = \begin{cases} (i-1)1000 + 750 \text{ Hz} & \text{when 'one' is transmitted.} \\ \dfrac{f_s}{2} = 4000 \text{ Hz} & \text{when 'zero' is transmitted.} \end{cases}$

and $i = 1, 2, \ldots, 8$

The value of T, which is the time spacing between two samples, is

$$T = \frac{1}{f_s} = \frac{1}{8000} = \frac{1}{8} \text{ mSec.}$$

To simplify the Equation (5.3b), each term is considered separately as follows:

The summation, $\sum_{n=64}^{127} \sin 2\pi f_1 nT\, W^{-48n}$ could be simplified as,

$$\begin{aligned}
\sum_{n=64}^{127} \sin 2\pi f_1 nT\, W^{-48n} &= \sum_{n=0}^{63} \sin 2\pi f_1 (n+64)T\, W^{-48(n+64)} \\
&= W^{-48\times 64} \sum_{n=0}^{63} \sin 2\pi f_1 (n+64)T\, W^{-48n} \\
&= \exp\left(\frac{-j2\pi 48\times 64}{512}\right) \sum_{n=0}^{63} \sin 2\pi f_1 (n+64)T\, W^{-48n} \\
&= \sum_{n=0}^{63} \sin 2\pi f_1 (n+64)T\, W^{-48n} \\
&= \sum_{n=0}^{63} \sin 2\pi f_1 nT\, W^{-48n} \qquad (5.4a)
\end{aligned}$$

Similarly it can be shown that,

$$\sum_{n=128}^{191} \sin 2\pi f_2 nT\, W^{-48n} = \sum_{n=0}^{63} \sin 2\pi f_2 nT\, W^{-48n} \qquad (5.4b)$$

$$\sum_{n=192}^{255} \sin 2\pi f_3 nT\, W^{-48n} = \sum_{n=0}^{63} \sin 2\pi f_3 nT\, W^{-48n} \qquad (5.4c)$$

$$\sum_{n=256}^{319} \sin 2\pi f_4 nT\, W^{-48n} = \sum_{n=0}^{63} \sin 2\pi f_4 nT\, W^{-48n} \qquad (5.4d)$$

$$\sum_{n=320}^{383} \sin 2\pi f_5 nT\, W^{-48n} = \sum_{n=0}^{63} \sin 2\pi f_5 nT\, W^{-48n} \qquad (5.4e)$$

$$\sum_{n=384}^{447} \sin 2\pi f_6 nT\, W^{-48n} = \sum_{n=0}^{63} \sin 2\pi f_6 nT\, W^{-48n} \qquad (5.4f)$$

$$\sum_{n=448}^{511} \sin 2\pi f_7 nT\, W^{-48n} = \sum_{n=0}^{63} \sin 2\pi f_7 nT\, W^{-48n} \qquad (5.4g)$$

The first summation in Equation (5.3b) can be simplified as

$$\sum_{n=48}^{63} \sin 2\pi f_8 nT\, W^{-48n} = \sum_{n=0}^{(63-48)} \sin 2\pi f_8 (n+48)T\, W^{-48(n+48)}$$

$$= W^{-48\times 48} \sum_{n=0}^{15} \sin 2\pi f_8 (n+48)T\, W^{-48n}$$

$$= \sum_{n=0}^{15} \sin 2\pi f_8 (n+48)T\, W^{-48n}$$

This expression can be further simplified as shown in Appendix A as

$$\sum_{n=48}^{63} \sin 2\pi f_8 nT\, W^{-48n} = 0, \quad f_8 = 7750 \text{ Hz} \text{ or } 4000 \text{ Hz}. \tag{5.5}$$

Similarly, the last summation in Equation (5.3b) is simplified in Appendix A as

$$\sum_{n=512}^{(512+47)} \sin 2\pi f_8 nT\, W^{-48n} = 0, \quad f_8 = 7750 \text{ Hz} \text{ or } 4000 \text{ Hz}. \tag{5.6}$$

Combining the above results the expression (5.3b) can be written as

$$X_s(48\Omega) = \sum_{i=1}^{7} \sum_{n=0}^{63} \sin 2\pi f_i nT\, W^{-48n} \tag{5.7}$$

The frequency f_i for transmitting 'zero' is selected such that it does not make any effect on the magnitude of $X_s(48\Omega)$. Therefore, only the values of f_i representing 'one' is considered in the following analysis. Now the Equation (5.7) can be written as

$$X_s(48\Omega) = \sum_{i=1}^{7} \sum_{n=0}^{63} \sin 2\pi \frac{[(i-1)1000 + 750]n}{8000} \left[\cos \frac{3\pi n}{16} - j \sin \frac{3\pi n}{16}\right]$$

Considering real and imaginary parts of $X_s(48\Omega)$ separately,

$$\text{Re}\left\{X_s(48\Omega)\right\} = \sum_{i=1}^{7} \sum_{n=0}^{63} \sin 2\pi \frac{[(i-1)1000 + 750]n}{8000} \cos \frac{3\pi n}{16} \tag{5.8a}$$

$$\text{Re}\left\{X_s(48\Omega)\right\} = \frac{1}{2}\sum_{i=1}^{7}\sum_{n=0}^{63}\left\{\sin\left[2\pi\frac{[(i-1)1000+750]n}{8000}+\frac{3\pi n}{16}\right]\right.$$
$$\left.+\sin\left[2\pi\frac{[(i-1)1000+750]n}{8000}-\frac{3\pi n}{16}\right]\right\}$$
$$= \frac{1}{2}\sum_{i=1}^{7}\sum_{n=0}^{63}\left\{\sin\left[\frac{2\pi(i-1)n}{8}+\frac{6\pi n}{16}\right]+\sin\frac{2\pi(i-1)n}{8}\right\}$$

Using Equation (A.3) in Appendix A, it can be readily shown that

$$\text{Re}\left\{X_s(48\Omega)\right\} = \frac{1}{2}\sum_{i=1}^{7}\left\{\sin\frac{63}{2}\left[\frac{2\pi(i-1)}{8}+\frac{3\pi}{8}\right]\sin\frac{64}{2}\left[\frac{2\pi(i-1)}{8}+\frac{3\pi}{8}\right]\right.$$
$$\text{cosec}\,\frac{1}{2}\left[\frac{2\pi(i-1)}{8}+\frac{3\pi}{8}\right]$$
$$\left.+\sin\frac{63}{2}\left[\frac{2\pi(i-1)}{8}\right]\sin\frac{64}{2}\left[\frac{2\pi(i-1)}{8}\right]\text{cosec}\,\frac{1}{2}\left[\frac{2\pi(i-1)}{8}\right]\right\}$$
$$= \frac{1}{2}\sum_{i=1}^{7}\left\{\sin\frac{63}{2}\left[\frac{\pi(i-1)}{4}+\frac{3\pi}{8}\right]\sin[8\pi i+4\pi]\,\text{cosec}\left[\frac{2\pi(i-1)+3\pi}{16}\right]\right.$$
$$\left.+\sin\frac{63}{2}\left[\frac{2\pi(i-1)}{8}\right]\sin[8\pi(i-1)]\,\text{cosec}\left[\frac{2\pi(i-1)}{16}\right]\right\}$$
$$= 0$$

The imaginary part of $X_s(48\Omega)$ can be simplified as,

$$\text{Im}\left\{X_s(48\Omega)\right\} = -\sum_{i=1}^{7}\sum_{n=0}^{63}\sin\left[\frac{2\pi[(i-1)1000+750]n}{8000}\right]\sin\frac{3\pi n}{16}$$
$$= -\sum_{n=0}^{63}\sin\frac{2\pi x750n}{8000}\sin\frac{3\pi n}{16}$$
$$-\sum_{i=2}^{7}\sum_{n=0}^{63}\sin\left[\frac{2\pi[(i-1)1000+750]n}{8000}\right]\sin\frac{3\pi n}{16}$$
$$= -\sum_{n=0}^{63}\sin^2\frac{3\pi n}{16}$$
$$-\sum_{i=2}^{7}\sum_{n=0}^{63}\sin\left[\frac{2\pi[(i-1)1000+750]n}{8000}\right]\sin\frac{3\pi n}{16}$$

$$\text{Im}\left\{X_s(48\Omega)\right\} = -\sum_{n=0}^{63} \sin^2\frac{3\pi n}{16}$$

$$-\frac{1}{2}\sum_{i=1}^{7}\sum_{n=0}^{63}\left\{\cos\left[\frac{2\pi(i-1)\,n}{8}+\frac{3\pi n}{16}-\frac{3\pi n}{16}\right]\right.$$

$$\left.-\cos\left[\frac{2\pi(i-1)\,n}{8}+\frac{3\pi n}{16}+\frac{3\pi n}{16}\right]\right\}$$

$$= -\sum_{n=0}^{63}\sin^2\frac{3\pi n}{16}$$

$$-\frac{1}{2}\sum_{i=2}^{7}\sum_{n=0}^{63}\left\{\cos\frac{\pi(i-1)n}{4}-\cos\left[\frac{\pi(i-1)n}{4}+\frac{3\pi n}{8}\right]\right\} \qquad (5.8b)$$

As shown in Appendix A the summation in Equation (5.8b) can be simplified as

$$\text{Im}\left\{X_s(48\Omega)\right\} = -\sum_{n=0}^{63}\sin^2\frac{3\pi n}{16}$$

$$= \text{Im}\left\{\sum_{n=0}^{63}\sin 2\pi f_1 nT\, W^{-48n}\right\}$$

$$= -32 \qquad (5.9)$$

Combining the values of real and imaginary parts, the desired result for the spectral component is obtained as

$$X_s(48\Omega) = 0 - j\,32 = \sum_{n=0}^{63}\sin 2\pi f_1 nT\, W^{-48n} \qquad (5.10a)$$

From Equation (5.10a), it is observed that the contribution from frequencies f_i where i=2, 3,..., 8, to $X_s(48\Omega)$ is zero. The magnitude of the spectral component $X_s(48\Omega)$ is

$$|\,X_s(48\Omega)\,| = 32 = \left|\sum_{n=0}^{63}\sin 2\pi f_1 nT\, W^{-48n}\right| \qquad (5.10b)$$

Hence it can be concluded that there is no effect on the magnitude of $X_s(k_1\Omega)$ from other frequencies in the same frame in the absence of multipath effects.

5.3 Analysis of Spectral Components with Multipaths and Evaluation of Minimum Eye Opening

When the multipath signals overlap with the direct path signal, the envelope of the received signal varies according to the intensities of direct path and multipath signals. Since the signaling scheme explained in Chapter 4 uses a constant envelope signal, the amplitude of the received signal needs to be stabilized by an AGC. When signal waveforms of different frequencies overlap together, theoretical analysis becomes complicated due to non-linearity effect of the AGC process. Therefore a computer simulation has been carried out to obtain the variation of the eye pattern with DMR for the case when AGC is used and the results are presented in the next chapter. The theoretical analysis without AGC, but with multipaths is given in this section for two transmitter-receiver configurations. The minimum eye opening is obtained for the two transmitter-receiver configurations by obtaining the minimum value of $|X_s(48\Omega)|$ when 'one' is transmitted and the maximum value of $|X_s(48\Omega)|$ when 'zero' is transmitted.

5.3.1 Configuration A : Transmitter at the surface

The transmitter-receiver configuration for this case is illustrated in Fig 5.2. The signal is transmitted from the transmitter located at the surface to the receiver located at depth y_R from the surface. The separation between the

transmitter and the receiver is x and the depth of the ocean is D.

In this situation, only two multipaths cause significant distortion and all the other multipaths can be neglected because they have negligible strength in comparison to the direct path signal. The two multipaths which cause distortions are,

(a) The multipath that has one bottom reflection and no surface reflections.

(b) The multipath that has one bottom and one surface reflection.

For convenience it is assumed that the first multipath signal arrives $(64a_1+l_1)$ samples delayed with respect to the direct path signal. Its strength is assumed to be α_1 measured with relative to the direct path signal. The second multipath is assumed to be delayed by $(64a_2+l_2)$ samples with respect to the direct path and its strength is assumed to be α_2 with respect to the direct path. Here, l_1, l_2, a_1 and a_2 are positive integers. Since the surface reflection introduces a 180^0 phase shift, the second multipath is 180^0 out of phase with the direct path.

The calculation becomes tedious with the multipath signals in the time slots at the two ends of the window. However, the effect of these multipaths on the spectrum is negligible. Hence neglecting the effect of the multipath signals at the two ends of the window, $X_s(48\Omega)$ has been obtained as follows. As shown in the previous section there is no effect on $X_s(48\Omega)$ from the frequencies f_i, i=2, 3,..., 8. Therefore, assuming that the frequency of the multipaths and the direct path is f_1=750 Hz, $X_s(48\Omega)$ could be approximated as,

$$X_s(48\Omega) \approx \sum_{n=64}^{127} \sin 2\pi f_1 nT\, W^{-48n} + \alpha_1 \sum_{n=(64a_1+l_1)}^{(64a_1+63+l_1)} \sin 2\pi f_1 nT\, W^{-48n} - \alpha_2 \sum_{n=(64a_2+l_2)}^{(64a_2+63+l_2)} \sin 2\pi f_1 nT\, W^{-48n}$$

$$X_s(48\Omega) \approx W^{-48\times64}\sum_{n=0}^{63}\sin 2\pi f_1 nT\, W^{-48n} + \alpha_1 W^{-48(64a_1+l_1)}\sum_{n=0}^{63}\sin 2\pi f_1 nT\, W^{-48n} - \alpha_2 W^{-48(64a_2+l_2)}\sum_{n=0}^{63}\sin 2\pi f_1 nT\, W^{-48n}$$

$$\approx \left[\sum_{n=0}^{63}\sin 2\pi f_1 nT\, W^{-48n}\right]\left[1+\alpha_1 W^{-48l_1}-\alpha_2 W^{-48l_2}\right]$$

$$\approx X_1\left[1+\alpha_1 W^{-48l_1}-\alpha_2 W^{-48l_2}\right] \qquad (5.11)$$

where $X_1 = \sum_{n=0}^{63}\sin 2\pi f_1 nT\, W^{-48n}$

Then substituting for W in Equation (5.11), the value of $X_s(48\Omega)$ can be written as

$$X_s(48\Omega) = X_1\left[1+\alpha_1\cos\frac{2\pi\times48l_1}{512} - j\,\alpha_1\sin\frac{2\pi\times48l_1}{512} - \alpha_2\cos\frac{2\pi\times48l_2}{512} + j\,\alpha_2\sin\frac{2\pi\times48l_2}{512}\right]$$

$$= X_1\left[\left(1+\alpha_1\cos\frac{3\pi l_1}{16}-\alpha_2\cos\frac{3\pi l_2}{16}\right) - j\left(\alpha_1\sin\frac{3\pi l_1}{16}-\alpha_2\sin\frac{3\pi l_2}{16}\right)\right]$$

The squared magnitude of $X_s(48\Omega)$ takes the form

$$|X_s(48\Omega)|^2 = |X_1|^2\left[\left(1+\alpha_1\cos\frac{3\pi l_1}{16}-\alpha_2\cos\frac{3\pi l_2}{16}\right)^2 + \left(\alpha_1\sin\frac{3\pi l_1}{16}-\alpha_2\sin\frac{3\pi l_2}{16}\right)^2\right]$$

$$= |X_1|^2\left[1+\alpha_1^2+\alpha_2^2+2\alpha_1\cos\frac{3\pi l_1}{16}-2\alpha_2\cos\frac{3\pi l_2}{16} - 2\alpha_1\alpha_2\cos\frac{3\pi l_1}{16}\cos\frac{3\pi l_2}{16} - 2\alpha_1\alpha_2\sin\frac{3\pi l_1}{16}\sin\frac{3\pi l_2}{16}\right]$$

$$| X_s(48\Omega) |^2 = | X_1 |^2 \left[1 + \alpha_1^2 + \alpha_2^2 + 2\alpha_1 \cos \frac{3\pi l_1}{16} - 2\alpha_2 \cos \frac{3\pi l_2}{16} - 2\alpha_1 \alpha_2 \cos \frac{3\pi(l_1 - l_2)}{16} \right] \quad (5.12)$$

It follows that the minimum value of $| X_s(48\Omega) |$ in Equation (5.12) occurs when,

$$\cos \frac{3\pi l_1}{16} = -1 \quad (5.13a)$$

$$\cos \frac{3\pi l_2}{16} = +1 \quad (5.13b)$$

$$\cos \frac{3\pi(l_1 - l_2)}{16} = +1 \quad (5.13c)$$

The values of l_1 and l_2 which satisfy the conditions given in Equations (5.13a) and (5.13b) are

$$l_1 = \frac{16}{3} [(2n_1 + 1)] \quad \text{and} \quad l_2 = \frac{16}{3} 2n_2$$

where n_1 and n_2 are positive integers. Using these values for l_1 and l_2 it can be shown that,

$$\cos \frac{3\pi(l_1 - l_2)}{16} = -1 \quad (5.13d)$$

First noting that $2\alpha_1\alpha_2 \cos \frac{3\pi(l_1 - l_2)}{16}$ has the least effect on $| X_s(48\Omega) |$ since $\alpha_1 > \alpha_2 > \alpha_1\alpha_2$, the restriction imposed in Equation (5.13c) is omitted. Then substituting the expressions in Equations (5.13a), (5.13b) and (5.13d) in Equation (5.12), the minimum value of $| X_s(48\Omega) |$ when 'one' is transmitted could be obtained as,

$$| X_s(48\Omega) |_{min} = | X_1 | \left(1 + \alpha_1^2 + \alpha_2^2 - 2\alpha_1 - 2\alpha_2 + 2\alpha_1\alpha_2\right)^{\frac{1}{2}}$$

$$= | X_1 | \left(1 - (\alpha_1 + \alpha_2)\right) \qquad (5.14)$$

If there are no multipaths, that is $\alpha_1 = \alpha_2 = 0$, the value of the spectral component becomes $| X_1 |$. Hence the threshold is $| X_1 | /2$ and if the magnitude of the corresponding spectral component is larger than $| X_1 | /2$, a 'one' is detected and vice-versa.

Therefore for correct detection,

$$| X_s(48\Omega) |_{min} > \frac{| X_1 |}{2}$$

$$| X_1 | \left(1 - (\alpha_1 + \alpha_2)\right) > \frac{| X_1 |}{2}$$

$$\text{i.e.} \quad (\alpha_1 + \alpha_2) < \frac{1}{2} \qquad (5.15)$$

The DMR at the receiver is given by,

$$\text{DMR} = 10 \log \left(\frac{1}{\alpha_1 + \alpha_2}\right)$$

and it has to be greater than 3 dB for correct detection according to Equation (5.15). Thus it can be concluded that the system works for all the situations when DMR $>$ 3 dB and no noise is present.

It is important to find the maximum value of $| X_s(48\Omega) |$ when 'zero' is transmitted in order to obtain the minimum eye opening. The maximum value of $| X_s(48\Omega) |$ when 'zero' is transmitted is obtained as follows.

If the transmitted digit is 'zero', the worst case occurs when the two multipaths are of the same frequency, $f_1 = 750$ Hz. The spectral component for this case is given as

$$X_s(48\Omega) \approx \sum_{64}^{127} \sin 2\pi \frac{f_s}{2} nT\, W^{-48n} + \alpha_1 \sum_{64a_1+l_1}^{64a_1+63+l_1} \sin 2\pi f_1 nT\, W^{-48n}$$
$$- \alpha_2 \sum_{64a_2+l_2}^{64a_2+63+l_2} \sin 2\pi f_1 nT\, W^{-48n}$$
$$\approx \alpha_1 W^{-48(64a_1+l_1)} \sum_{0}^{63} \sin 2\pi f_1 nT\, W^{-48n}$$
$$- \alpha_2 W^{-48(64a_2+l_2)} \sum_{0}^{63} \sin 2\pi f_1 nT\, W^{-48n}$$
$$\approx X_1 \left[\alpha_1 W^{-48l_1} - \alpha_2 W^{-48l_2}\right]$$

and its squared magnitude is given as

$$| X_s(48\Omega) |^2 = | X_1 |^2 \left[\alpha_1^2 + \alpha_2^2 - 2\alpha_1\alpha_2 \cos \frac{3\pi(l_1 - l_2)}{16}\right]$$

where $X_1 = \sum_{0}^{63} \sin 2\pi f_1 nT\, W^{-48n}$

To obtain the minimum eye opening, it is necessary to find the maximum of $| X_s(48\Omega) |$ when 'zero' is transmitted under the same conditions used to obtain the minimum $| X_s(48\Omega) |$ when 'one' is transmitted. Under the constraints in Equations (5.13a), (5.13b) and (5.13d),

$$| X_s(48\Omega) |_{max} = | X_1 | (\alpha_1 + \alpha_2) \quad \text{when 'zero is transmitted} \tag{5.16}$$

From Equations (5.14) and (5.16), the minimum eye opening (EO), can therefore be written as

$$EO = | X_1 | \left(1 - (\alpha_1 + \alpha_2)\right) - | X_1 | (\alpha_1 + \alpha_2) \tag{5.17}$$

5.3.2. Configuration B : Transmitter and Receiver in Water

Fig (5.3) shows the transmitter-receiver configuration for the above case. A signal is transmitted from the transmitter located at depth y_T from the surface to the receiver located at depth y_R from the surface. The transmitter and receiver are separated by x. The depth of the ocean is assumed to be D. In this case, four multipaths cause significant distortions, namely,

(a) One surface reflection with a 180^0 phase shift and an intensity α_3,

(b) One bottom reflection with an intensity α_4,

(c) One surface and one bottom reflection given that the first reflection is from the surface with a 180^0 phase shift and an intensity α_5,

(d) One surface and one bottom reflection given that the first reflection is from the bottom with a 180^0 phase shift and an intensity α_6.

It has been assumed that the above four multipaths arrive $(64a_3+l_3)$, $(64a_4+l_4)$, $(64a_5+l_5)$ and $(64a_6+l_6)$ samples delayed relative to the direct path where l_3, l_4, l_5, l_6, a_3, a_4, a_5 and a_6 are positive integers. The effect of multipath signals at the two ends of the window on $X_s(48\Omega)$ is neglected as before. Assuming that the multipath and direct path signals have the same frequency $f_1 = 750\text{Hz}$, $X_s(48\Omega)$ could be approximated as

$$X_s(48\Omega) \approx \sum_{n=64}^{127} \sin 2\pi f_1 nT\, W^{-48n} - \alpha_3 \sum_{n=(64a_3+l_3)}^{(64a_3+63+l_3)} \sin 2\pi f_1 nT\, W^{-48n}$$
$$+\alpha_4 \sum_{n=(64a_4+l_4)}^{(64a_4+63l_4)} \sin 2\pi f_1 nT\, W^{-48n} - \alpha_5 \sum_{n=(64a_5+l_5)}^{(64a_5+63+l_5)} \sin 2\pi f_1 nT\, W^{-48n}$$
$$-\alpha_6 \sum_{n=(64a_6+l_6)}^{(64a_6+63+l_6)} \sin 2\pi f_1 nT\, W^{-48n} \qquad (5.18)$$

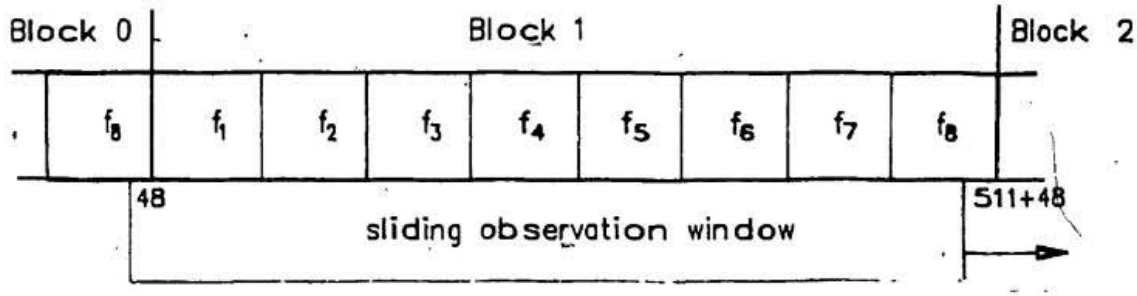

Fig. 5.1 Position of the sliding window when $X_s(48\Omega)$ is calculated.

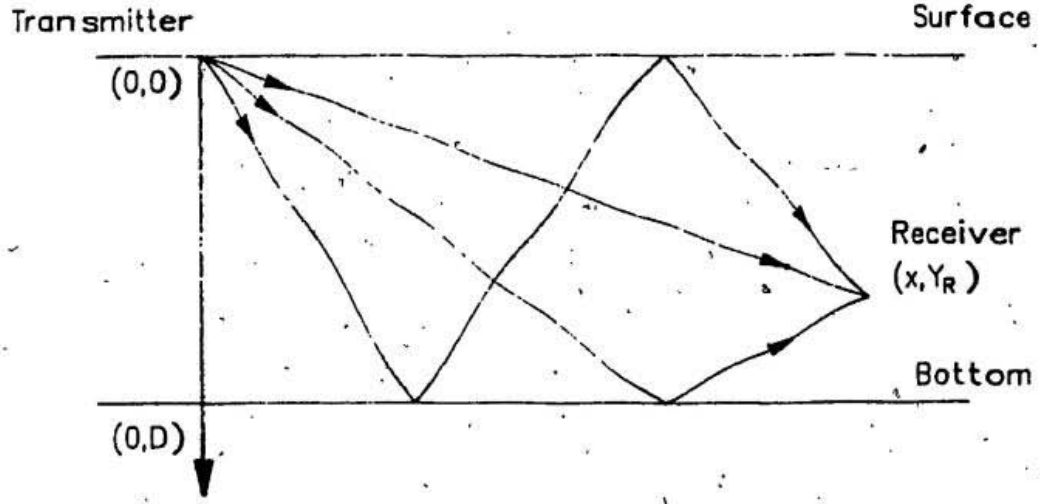

Fig. 5.2 Transmitter-receiver configuration for Configuration A.

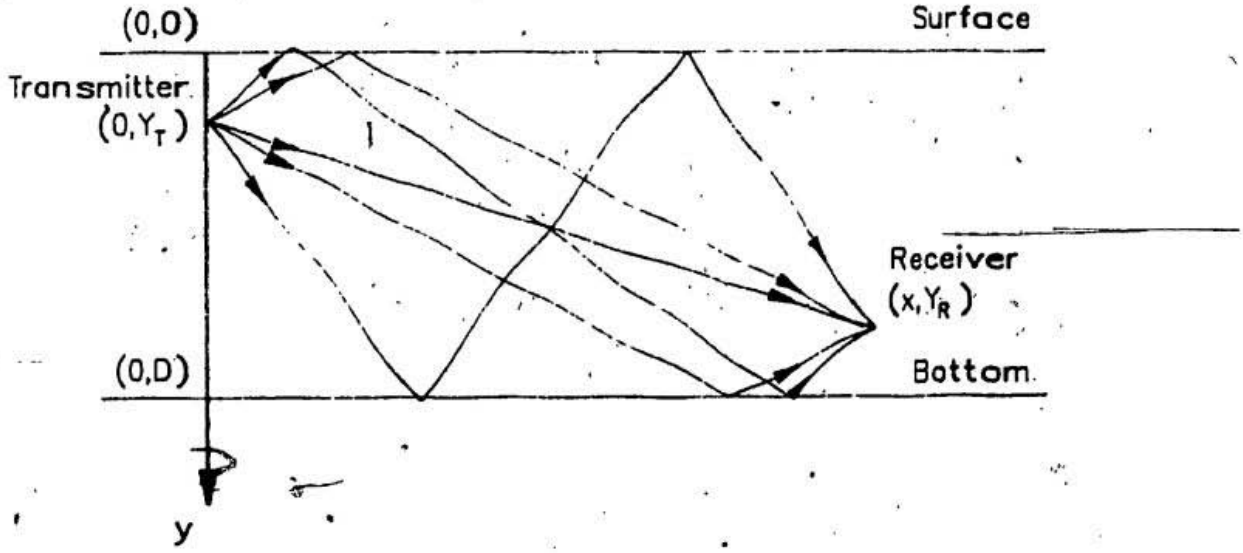

Fig. 5.3 Transmitter-receiver configuration for Configuration B.

As shown in Appendix B, the minimum value of $|X_s(48\Omega)|$ when 'one' is transmitted could be written as

$$|X_s(48\Omega)|_{min} = |X_1|\,[1-(\alpha_3+\alpha_4+\alpha_5+\alpha_6)] \tag{5.19}$$

where $X_1 = \sum_{n=0}^{63} \sin 2\pi f_1 nT\, W^{-48n}$ and $f_1 = 750$ Hz.

The maximum value of $|X_s(48\Omega)|$ when 'zero' is transmitted is obtained as explained in the previous section. Then,

$$|X_s(48\Omega)|_{max} = |X_1|\,[\alpha_3+\alpha_4+\alpha_5+\alpha_6] \text{ when 'zero is transmitted.} \tag{5.20}$$

Hence for correct detection,

$$|X_1|\,[\alpha_3+\alpha_4+\alpha_5+\alpha_6] < \frac{|X_1|}{2}$$

$$\alpha_3+\alpha_4+\alpha_5+\alpha_6 < \frac{1}{2} \tag{5.21}$$

and the corresponding value of DMR should satisfy the condition

$$\text{DMR} = 10 \log \left\{ \frac{1}{\alpha_3+\alpha_4+\alpha_5+\alpha_6} \right\} > 3\text{dB}.$$

As in the case of Configuration A, the system works in all the situations when the DMR > 3dB. The minimum eye opening for this case is given by

$$EO = |X_1|\,[1-(\alpha_3+\alpha_4+\alpha_5+\alpha_6)] - |X_1|\,(\alpha_3+\alpha_4+\alpha_5+\alpha_6) \tag{5.22}$$

5.4 Variation of Eye Opening with DMR

Varying the values of α_1, α_2, α_3, α_4, α_5 and α_6 in Equations (5.17) and (5.22), the eye opening for various DMR values can be obtained.

The minimum eye opening for a given Surface Reflection Loss (SRL) and Bottom Reflection Loss (BRL) depends on the transmitter-receiver location. These locations that correspond to the minimum eye opening will be found out in the following sections for the two configurations explained previously.

5.4.1 Transmitter-Receiver Locations for Minimum Eye opening for Configuration A

It has been shown in Section (5.3.1) in Equations (5.13a) and (5.13b) that the minimum eye opening is obtained when

$$\cos\frac{3\pi l_1}{16} = -1 \qquad \text{and} \qquad \cos\frac{3\pi l_2}{16} = +1$$

$$\text{i.e.} \quad l_1 = \frac{16}{3}(2n_1 + 1) \quad \text{and} \quad l_2 = \frac{16}{3}(2n_2)$$

If t_1 and t_2 are the arrival delays of first and the second multipaths with respect to the direct path, then,

$$t_1 = (64a_1 + l_1)\,T \qquad \text{and} \qquad t_2 = (64a_2 + l_2)\,T$$

where $T = \frac{1}{f_s} = \frac{1}{8}$ mSec is the time spacing between two samples.

As the distance x between the transmitter and the receiver increases, the time delays t_1 and t_2 of the first and the second multipaths increase. With the

increase of these time delays t_1 and t_2, the signal strength of the multipaths decreases. But as explained in the previous sections, in order to obtain the minimum eye opening the direct path cannot be overlapped with the multipaths of the same signal. Therefore, to obtain the minimum EO, not only t_1 and t_2 have to be made minimum but also the multipaths of the preceding signals have to be overlapped with the direct path signal. That is, by selecting $a_1=a_2=8$, $l_1=16$ and $l_2=32$,

$$t_1 = 64 + \frac{16}{8} = 66 \text{ mSec} \quad \text{and} \quad t_2 = 64 + \frac{32}{8} = 68\text{msec}$$

are the best suited values for t_1 and t_2 in order to obtain the minimum eye opening. With these time delays it can be shown that the effect of multipath signals at the two ends of the window on $X_s(48\Omega)$ is zero.

As explained in Section (2.6), the distance traveled by the direct path signal is

$$d_0 = \left[x^2 + y_R{}^2\right]^{\frac{1}{2}} \tag{5.23}$$

The distance traveled by the first multipath signal is

$$d_1 = \left[x^2 + (2D - y_R)^2\right]^{\frac{1}{2}} \tag{5.24}$$

and the distance traveled by the second multipath signal is

$$d_2 = \left[x^2 + (2D + y_R)^2\right]^{\frac{1}{2}} \tag{5.25}$$

Consequently, the time delays t_1 and t_2 are obtained as

$$t_1 = \frac{d_1 - d_0}{c} \tag{5.26a}$$

$$t_2 = \frac{d_2 - d_0}{c} \tag{5.26b}$$

where c = velocity of sound in water
= 1500 m/Sec.

Substituting the above selected values of t_1 and t_2 in Equations (5.26a) and (5.26b),

$$66\times10^{-3} = \frac{\left[x^2 + (2D - y_R)^2\right]^{\frac{1}{2}} - \left[x^2 + y_R{}^2\right]^{\frac{1}{2}}}{1500} \tag{5.27a}$$

$$68\times10^{-3} = \frac{\left[x^2 + (2D + y_R)^2\right]^{\frac{1}{2}} - \left[x^2 + y_R{}^2\right]^{\frac{1}{2}}}{1500} \tag{5.27b}$$

Solutions to these two equations were obtained by fixing the depth D as follows.

D = 350 m.	D = 300 m.
y_R = 5.33 m.	y_R = 4.59 m.
x = 2387.54 m.	x = 1740.76 m.

For the above two transmitter-receiver locations the intensities α_1 and α_2 of the two multipaths and the value of DMR at the receiver are obtained using Equations (2.5), (2.17) and (2.23). It is observed that the system works at these locations when SRL=3 dB and BRL>4.3 dB as the DMR exceeds 3 dB.

The variation of eye opening with DMR for this configuration is plotted by varying the BRL as shown in Fig (5.4).

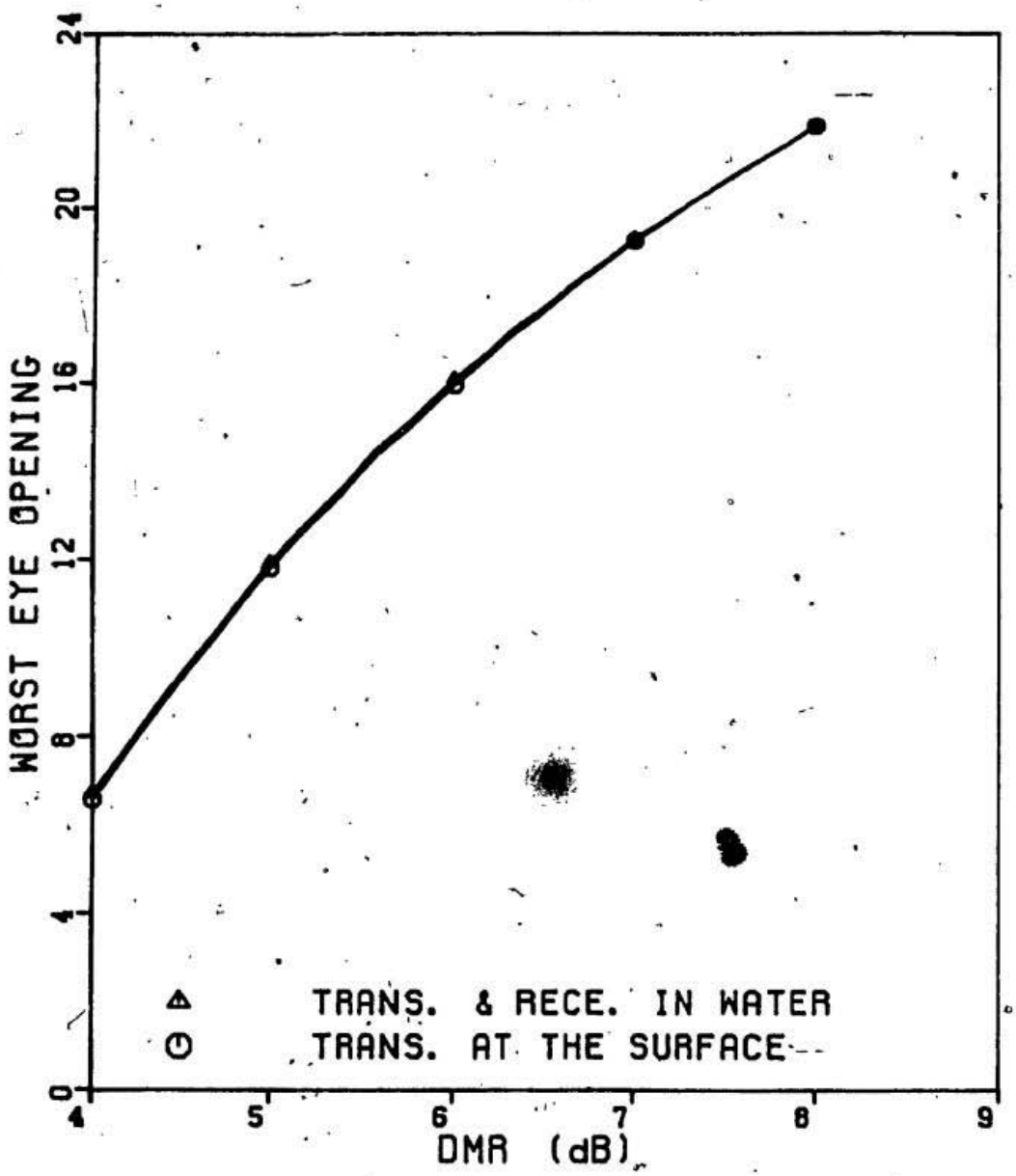

Fig. 5.4 Variation of Eye opening with DMR.

5.4.2 Transmitter-Receiver Locations for Minimum Eye Opening for Configuration B

As shown in Appendix B, the minimum eye opening is obtained when

$$l_3 = \frac{16}{3} 2n_3$$

$$l_4 = \frac{16}{3} (2n_4 + 1)$$

$$l_5 = \frac{16}{3} 2n_5$$

and $$l_6 = \frac{16}{3} 2n_6$$

n_3, n_4, n_5 and n_6 are positive integers. The suitable values for l_3, l_4, l_5, and l_6 are,

$$l_3 = 64, \quad l_4 = 48, \quad l_5 = 64, \quad \text{and} \quad l_6 = 64$$

as they are selected to be positive integers. Hence the time delays t_3, t_4, t_5, and t_6 of the first, second, third and fourth multipaths with respect to the direct path are

$$t_3 = (64a_3 + l_3)\, T \tag{5.28a}$$

$$t_4 = (64a_4 + l_4)\, T \tag{5.28b}$$

$$t_5 = (64a_5 + l_5)\, T \tag{5.28c}$$

$$t_6 = (64a_6 + l_6)\, T \tag{5.28d}$$

where $T = \frac{1}{8}$ mSec.

With these time delays the effect from the signals at the two ends of the window on $X_s(48\Omega)$ can be shown to be zero. In this situation, the distances traveled by the direct path, first, second, third and the fourth multipaths are obtained as explained in Section (2.6) as,

$$t_3 = \frac{d_3 - d'_0}{c} \tag{5.29a}$$

$$t_4 = \frac{d_4 - d'_0}{c} \tag{5.29b}$$

$$t_5 = \frac{d_5 - d'_0}{c} \tag{5.29c}$$

$$t_6 = \frac{d_6 - d'_0}{c} \tag{5.29d}$$

where,

$$d'_0 = \left[x^2 + (y_R - y_T)^2\right]^{\frac{1}{2}} \tag{5.30}$$

$$d_3 = \left[x^2 + (y_R + y_T)^2\right]^{\frac{1}{2}} \tag{5.31}$$

$$d_4 = \left[x^2 + (2D - y_R - y_T)^2\right]^{\frac{1}{2}} \tag{5.32}$$

$$d_5 = \left[x^2 + (2D - y_R + y_T)^2\right]^{\frac{1}{2}} \tag{5.33}$$

$$d_6 = \left[x^2 + (2D + y_R - y_T)^2\right]^{\frac{1}{2}} \tag{5.34}$$

By selecting t_3, t_4, t_5 and t_6 values which satisfy the set of Equations (5.28), the set of Equations (5.29) is solved for x, D, y_R and y_T. Then it is found that the worst eye opening is obtained when

t_3=68 msec, t_4=70 msec, t_5=184 msec, t_6=180 msec

$y_T = 92.82$ m, $y_R = 89.69$ m, $x = 112.21$ m, $D = 184.27$ m

The variation of eye opening with DMR for this case is plotted in Fig (5.4).

5.5 The Variation of Eye Opening in the Presence of Synchronisation Errors

For optimum demodulation of the received signal, the sampling operation in the receiver must be synchronized with the incoming signal or otherwise there will be a synchronization error at the receiver. Due to this synchronization error at the receiver, the sampling of the received signal starts at an incorrect position causing a change in magnitude of the spectrum. In this section the effect of synchronization error on the spectrum is analyzed.

A synchronization error occurs if the samples are counted starting from $(48\pm m)$ instead of the 48^{th} sample when calculating the 48^{th} spectral component $X_s(48\Omega)$ where m is a positive integer. In this case $X_s(48\Omega)$ becomes

$$X_s(48\Omega) = \sum_{n=48}^{511+48} x(n\pm m)\, W^{-48n} \qquad (5.35a)$$

$$= \sum_{x=48\pm m}^{511+(48\pm m)} x(n) W^{-48(n\mp m)} \qquad (5.35b)$$

First the synchronization effect is analyzed only for the case with no multipaths. Next the analysis is extended to the case with multipaths.

5.5.1 Synchronisation Error Without Multipaths

Here, only the direct path signal is considered. Equation (5.35a) is evaluated by considering only x(n+m). Thus

$$X_s(48\Omega) = \sum_{n=48}^{511+48} x(n+m)\, W^{-48n} \qquad (5.36a)$$

This could be written as

$$X_s(48\Omega) = \sum_{n=48+m}^{511+48+m} x(n)\, W^{-48(n-m)}$$

$$= W^{48m} \sum_{n=48+m}^{511+48+m} x(n)\, W^{-48n}$$

$$= W^{48m} \left[\sum_{48+m}^{63} \sin 2\pi f_{81} nT\, W^{-48n} + \sum_{64}^{127} \sin 2\pi f_1 nT\, W^{-48n} + \sum_{512}^{512+47+m} \sin 2\pi f_{82} nT\, W^{-48n} \right] \quad (5.36b)$$

where f_{81} = the frequency of the 8th time slot in the preceding signal.

and f_{82} = the frequency of the 8th time slot in the present signal.

These f_{81} and f_{82} frequencies are illustrated in Fig (5.5). As explained in Section (5.2), it can be shown that there is no effect from the other frequencies within the window on the spectral component $X_s(48\Omega)$.

According to our signaling scheme, the frequency of the received signal in the 8th time slot can be either 7750 Hz or 4000 Hz. Therefore, in Equation (5.36b), the frequencies f_{81} and f_{82} can be any of the following combinations:

(a) both f_{81} and f_{82} are 7750 Hz.

(b) both f_{81} and f_{82} are 4000 Hz.

(c) f_{81} = 7750 Hz and f_{82} = 4000 Hz.

(d) f_{81} = 4000 Hz and f_{82} = 7750 Hz.

Hence Equation (5.36b) is analyzed separately for the above four cases.

(a) $f_{81} = f_{82} = 7750$ Hz.

Then Equation (5.36b) reduces to

$$X_s(48\Omega) = W^{48m}\left[\sum_{48+m}^{63}\sin 2\pi f_{81}nT\, W^{-48n} + \sum_{64}^{127}\sin 2\pi f_1 nT\, W^{-48n} + \sum_{0}^{47+m}\sin 2\pi f_{81}nT\, W^{-48n}\right]$$

$$= W^{48m}\left[\sum_{0}^{63}\sin 2\pi f_{81}nT\, W^{-48n} + \sum_{0}^{63}\sin 2\pi f_1 nT\, W^{-48n}\right] \qquad (5.37a)$$

In Section (5.2), it was shown that

$$\sum_{0}^{63}\sin 2\pi f_i nT\, W^{-48n} = 0 \qquad \text{for} \quad i = 2, 3, \cdots, 8$$

Since $f_{81} = f_8 = 7750$ Hz,

$$X_s(48\Omega) = W^{48m}\left[\sum_{0}^{63}\sin 2\pi f_1 nT\, W^{-48n}\right] \qquad (5.37b)$$

$$|\, X_s(48\Omega)\,| = 32 \quad \text{as} \quad |\sum_{0}^{63}\sin 2\pi f_1 nT\, W^{-48n}| = 32 \qquad (5.37c)$$

From Equation (5.10b), $|\, X_s(48\Omega)\,| = 32$ when there is no synchronization error at the receiver. Comparing Equation (5.37c) with Equation (5.10b) it can be concluded that there is no effect from synchronization error on the magnitude of $X_s(48\Omega)$ in this case.

(b) $f_{81} = f_{82} = 4000$ Hz.

Since in this case frequencies f_{81} and f_{82} are equivalent to $\frac{f_s}{2}$, the samples in the time domain are zero. Therefore it is clear that in this case also there is no effect on the magnitude of $X_s(48\Omega)$ due to synchronization error.

(c) $f_{81} = 7750$ Hz and $f_{82} = 4000$ Hz.

In this case, $\sum_{512}^{512+47+m} \sin 2\pi f_{82} nT\, W^{-48n} = 0$, since the samples in the time domain are zero. Hence Equation (5.36b) could be written as

$$X_s(48\Omega) = W^{48m}\left[\sum_{48+m}^{63} \sin 2\pi f_{81} nT\, W^{-48n} + \sum_{0}^{63} \sin 2\pi f_1 nT\, W^{-48n}\right] \qquad (5.38)$$

Comparison of the above expression with Equation (5.37b), shows that due to the summation, $\sum_{48+m}^{63} \sin 2\pi f_{81} nT\, W^{-48n}$, there is an effect on $X_s(48\Omega)$ from synchronization error.

(d) $f_{81} = 4000$ Hz and $f_{82} = 7750$ Hz.

Now, $\sum_{48+m}^{63} \sin 2\pi f_{81} nT\, W^{-48n} = 0$ as the samples in the time domain are zero. Hence Equation (5.36b) reduces to

$$X_s(48\Omega) = W^{48m}\left[\sum_{0}^{63} \sin 2\pi f_1 nT\, W^{-48} + \sum_{0}^{47+m} \sin 2\pi f_{82} nT\, W^{-48n}\right] \qquad (5.39)$$

Comparing Equation (5.39) with Equation (5.37b), Equation (5.39) too indicates an existence of an effect on $X_s(48\Omega)$ from synchronization error, due to the additional summation $\sum_{0}^{47+m} \sin 2\pi f_{82} nT\, W^{-48n}$.

Now considering the case x(n-m) in Equation (5.35a) given by

$$X_s(48\Omega) = \sum_{n=48}^{511+48} x(n-m)\, W^{-48n} \qquad (5.40a)$$

$X_s(48\Omega)$ is evaluated for the above four combinations of frequencies separately. Equation (5.40a) can be expressed as

$$X_s(48\Omega) = \sum_{n=48-m}^{511+48-m} x(n)\, W^{-48(n+m)}$$

$$= W^{-48m} \sum_{n=48-m}^{511+48-m} x(n)\, W^{-48n}$$

$$= W^{-48m} \left[\sum_{48-m}^{63} \sin 2\pi f_{81} nT\, W^{-48n} + \sum_{64}^{127} \sin 2\pi f_1 nT\, W^{-48n} + \sum_{512}^{512+47-m} \sin 2\pi f_{82} nT\, W^{-48n} \right] \quad (5.40b)$$

Now Equation (5.40b) is analyzed for the following cases separately.

(a) $f_{81} = f_{82} = 7750$ Hz

Equation (5.40b) reduces to

$$X_s(48\Omega) = W^{-48m} \left[\sum_{48-m}^{63} \sin 2\pi f_{81} nT\, W^{-48n} + \sum_{64}^{127} \sin 2\pi f_1 nT\, W^{-48n} + \sum_{0}^{47-m} \sin 2\pi f_{81} nT\, W^{-48n} \right]$$

$$= W^{-48m} \left[\sum_{0}^{63} \sin 2\pi f_{81} nT\, W^{-48n} + \sum_{0}^{63} \sin 2\pi f_1 nT\, W^{-48n} \right]$$

As $\sum_{0}^{63} \sin 2\pi f_i nT\, W^{-48n} = 0$ for i=2, 3,...8 and $f_{81} = 7750 = f_8$,

$$\sum_{0}^{63} \sin 2\pi f_{81} nT\, W^{-48n} = 0$$

Hence $X_s(48\Omega) = W^{-48m} \left[\sum_{0}^{63} \sin 2\pi f_1 nT\, W^{-48n} \right]$ (5.41)

Here comparing Equation (5.41) with Equation (5.10b) it can be seen that there is no effect on $X_s(48\Omega)$ due to the synchronization error.

(b) $f_{81} = f_{82} = 4000$ Hz

As the frequencies f_{81} and f_{81} are equal to $f_s/2$, the samples in the time domain are zero. Therefore in this case also, there is no effect on $X_s(48\Omega)$ from synchronization error.

(c) $f_{81} = 7750$ Hz and $f_{82} = 4000$ Hz

In this case $\sum_{512}^{512+47-m} \sin 2\pi f_{82} nT\, W^{-48n} = 0$ as the time domain samples are zero. Therefore, $X_s(48\Omega)$ given in Equation (5.40b) can be written as

$$X_s(48\Omega) = W^{-48m} \left[\sum_{48-m}^{63} \sin 2\pi f_{81} nT\, W^{-48n} + \sum_{0}^{63} \sin 2\pi f_1 nT\, W^{-48n} \right] \quad (5.42)$$

(d) $f_{81} = 4000$ Hz and $f_{82} = 7750$ Hz

Here $\sum_{48-m}^{63} \sin 2\pi f_{81} nT\, W^{-48n} = 0$ as the samples in the time domain are zero. Now Equation (5.40b) reduces to

$$X_s(48\Omega) = W^{-48m} \left[\sum_{0}^{63} \sin 2\pi f_1 nT\, W^{-48n} + \sum_{0}^{47-m} \sin 2\pi f_{82} nT\, W^{-48n} \right] \quad (5.43)$$

By comparing Equations (5.42) and (5.43) with Equation (5.41), it is observed that there is an effect on $X_s(48\Omega)$ by synchronization error, due to the additional summations $\sum_{48-m}^{63} \sin 2\pi f_{81} nT\, W^{-48n}$ and $\sum_{0}^{47-m} \sin 2\pi f_{82} nT\, W^{-48n}$ in cases (c) and (d). The above conclusions are summerized in Table (5.1).

Table (5.1) The effect of synchronization error on $|X_s(48\Omega)|$ with no multipaths

case	$X_s(48\Omega) = \sum_{n=48}^{511+48} x(n+m)\, W^{-48n}$	$X_s(48\Omega) = \sum_{n=48}^{511+48} x(n-m)\, W^{-48n}$
a	$W^{48m} \sum_{n=0}^{63} \sin 2\pi f_1 nT\, W^{-48n}$	$W^{-48m} \sum_{n=0}^{63} \sin 2\pi f_1 nT\, W^{-48n}$
b	$W^{48m} \sum_{n=0}^{63} \sin 2\pi f_1 nT\, W^{-48n}$	$W^{-48m} \sum_{n=0}^{63} \sin 2\pi f_1 nT\, W^{-48n}$
c	$W^{48m}\left[\sum_{n=48+m}^{63} \sin 2\pi f_{s1} nT\, W^{-48n} + \sum_{n=0}^{63} \sin 2\pi f_1 nT\, W^{-48n}\right]$	$W^{-48m}\left[\sum_{n=48-m}^{63} \sin 2\pi f_{s1} nT\, W^{-48n} + \sum_{n=0}^{63} \sin 2\pi f_1 nT\, W^{-48n}\right]$
d	$W^{48m}\left[\sum_{n=0}^{63} \sin 2\pi f_1 nT\, W^{-48n} + \sum_{n=0}^{47+m} \sin 2\pi f_{s2} nT\, W^{-48n}\right]$	$W^{-48m}\left[\sum_{n=0}^{63} \sin 2\pi f_1 nT\, W^{-48n} + \sum_{n=0}^{47-m} \sin 2\pi f_{s2} nT\, W^{-48n}\right]$

5.5.2. Synchronization Error With Multipaths

In this section, the variation of eye opening with DMR in the worst transmitter-receiver configuration is analyzed when a synchronization error is present. According to Section (5.4.1) the minimum eye opening is obtained when $l'_1 = (64a_1+16)$, $l'_2 = (64a_2+32)$ and $a_1 = a_2 = 8$. l'_1 and l'_2 are the number of samples delayed by the first and the second multipaths with respect to the direct path when transmitter is at the surface.

In the above situation, Equation (5.35a) given by

$$X_s(48\Omega) = \sum_{48}^{511+48} x(n \pm m)\, W^{-48n}$$

is first evaluated considering only x(n+m) as follows. Then Equation (5.35a) can be written as

$$X_s(48\Omega) = \sum_{n=48}^{511+48} x(n+m)\, W^{-48n}$$

$$X_s(48\Omega) = W^{48m} \sum_{n=48+m}^{511+48-m} x(n)\, W^{-48n}$$

Assuming that the frequency of the multipath and the direct path is $f_1 = 750$ Hz,

$$\begin{aligned} X_s(48\Omega) = W^{48m} \Bigg[& \sum_{48+m}^{63} \sin 2\pi f_{81} nT\, W^{-48n} + \sum_{64}^{127} \sin 2\pi f_1 nT\, W^{-48n} \\ & + \sum_{512}^{511+(48+m)} \sin 2\pi f_{82} nT\, W^{-48n} - \alpha_1 \sum_{48+m}^{63} \sin 2\pi f_{81}(m_1) nT\, W^{-48n} \\ & - \alpha_1 \sum_{64}^{127} \sin 2\pi f_1 nT\, W^{-48n} - \alpha_1 \sum_{0}^{47+m} \sin 2\pi f_{82}(m_1) nT\, W^{-48n} \\ & - \alpha_2 \sum_{48+m}^{63} \sin 2\pi f_{81}(m_2) nT\, W^{-48n} - \alpha_2 \sum_{64}^{127} \sin 2\pi f_1 nT\, W^{-48n} \\ & - \alpha_2 \sum_{0}^{47+m} \sin 2\pi f_{82}(m_2) nT\, W^{-48n} \Bigg] \end{aligned} \tag{5.44}$$

where α_1 and α_2 are the intensities of two major multipaths with respect to the direct path intensity. As illustrated in Fig (5.6), f_{81} is the frequency of the 8th time slot of the preceding signal and f_{82} is the frequency of the 8th time slot of the present signal. (m_1) and (m_2) represent the first and the second multipaths. Then $f_{81}(m_1)$ and $f_{82}(m_1)$ are the frequencies in the first multipath corresponding to f_{81} and f_{82}. Similarly, $f_{81}(m_2)$ and $f_{82}(m_2)$ are the corresponding frequencies in the second multipath.

According to Section (5.4.1), the direct path signal is overlapped with the two multipaths of the preceding signal. The delays of these two multipaths with respect to the direct path are 66 mSec and 68 mSec respectively. Under these conditions, $f_{81}(m_1) = f_{81}(m_2)$ and $f_{81} = f_{82}(m_1) = f_{82}(m_2)$. Since the frequency of the 8th time slot is selected as either 7750 Hz or 4000 Hz according to the

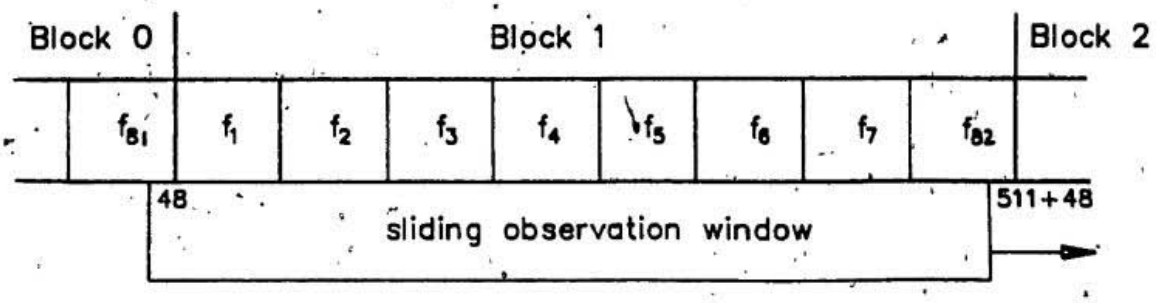

Fig. 5.5 Frequency representation of the received signal with no multipaths.

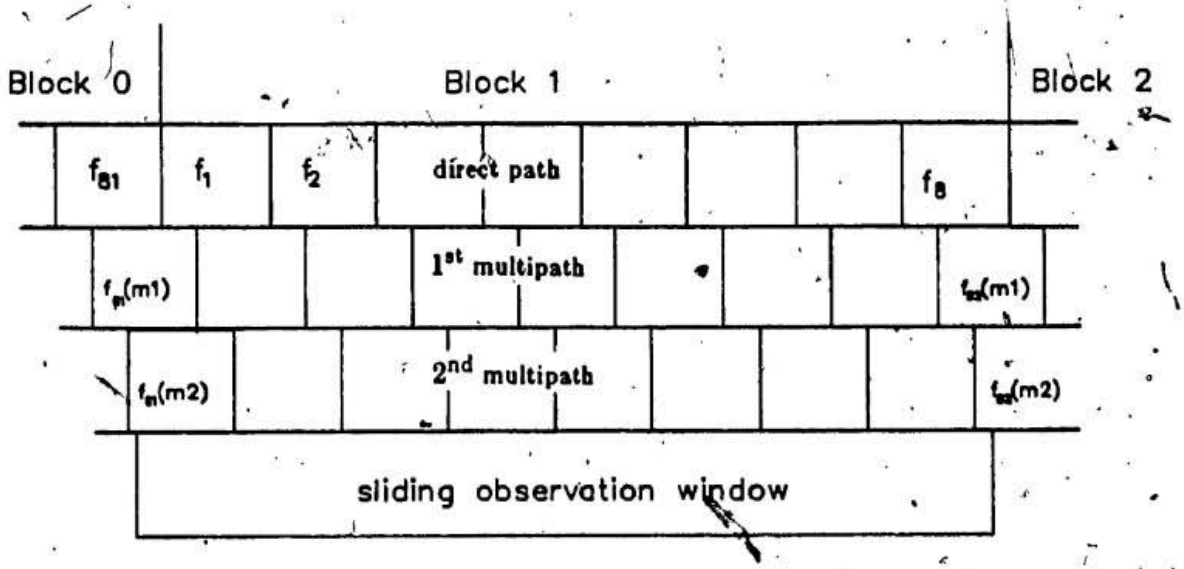

Fig. 5.6 Frequency representation of the received signal with multipaths.

signaling scheme, the only possible frequency combinations for f_{81}, f_{82}, $f_{81}(m_1)$ and $f_{82}(m_1)$ are as follows.

(a) when $f_{81} = f_{82} = f_{81}(m_1) = 7750$ Hz

(b) when $f_{81} = f_{82} = f_{81}(m_1) = 4000$ Hz

(c) when $f_{81} = 7750$ Hz, $f_{81}(m_1) = f_{82} = 4000$ Hz

(d) when $f_{81} = f_{81}(m_1) = 7750$ Hz, $f_{82} = 4000$ Hz

(e) when $f_{81} = f_{82} = 7750$ Hz, $f_{81}(m_1) = 4000$ Hz

(f) when $f_{81} = 4000$ Hz, $f_{81}(m_1) = f_{82} = 7750$ Hz

(g) when $f_{81} = f_{81}(m_1) = 4000$ Hz, $f_{82} = 7750$ Hz

(h) when $f_{81} = f_{82} = 4000$ Hz, $f_{81}(m_1) = 7750$ Hz

Then Equation (5.44) is analyzed separately for the above frequency combinations. In cases (a) and (b), $| X_s(48\Omega) |$ in Equation (5.44) reduces to

$$X_s(48\Omega) = W^{48m}\left[\sum_{0}^{63}\sin 2\pi f_1 nT\, W^{-48n}\right](1-\alpha_1-\alpha_2)$$

as shown in the previous section.

Thus $| X_s(48\Omega) | = 32(1-\alpha_1-\alpha_2)$ as $| \sum_{0}^{63}\sin 2\pi f_1 nT\, W^{-48n} | = 32$ (5.45)

From Equation (5.14), the minimum value of $| X_s(48\Omega) |$ when 'one' is transmitted is $32(1-\alpha_1-\alpha_2)$. Therefore comparing Equation (5.45) with Equation (5.14), we can conclude that there is no effect from synchronization error on $| X_s(48\Omega) |$ in these two cases.

In case (c), Equation (5.44) reduces to

$$X_s(48\Omega) = W^{48m}\left[\sum_{48+m}^{63}\sin 2\pi f_{81}nT\,W^{-48n} + \sum_{64}^{127}\sin 2\pi f_1 nT\,W^{-48n}\right.$$
$$-\alpha_1\sum_{64}^{127}\sin 2\pi f_1 nT\,W^{-48n} - \alpha_1\sum_{0}^{47+m}\sin 2\pi f_{81}nT\,W^{-48n}$$
$$\left.-\alpha_2\sum_{64}^{127}\sin 2\pi f_1 nT\,W^{-48n} - \alpha_2\sum_{0}^{47+m}\sin 2\pi f_{81}nT\,W^{-48n}\right] \quad (5.46a)$$

Since $\sum_{0}^{47+m}\sin 2\pi f_{81}nT\,w^{-48n} + \sum_{48+m}^{63}\sin 2\pi f_{81}nT\,W^{-48n} = 0$,

Equation (5.46a) can be further simplified as

$$X_s(48\Omega) = W^{48m}\left[(1-\alpha_1-\alpha_2)\sum_{0}^{63}\sin 2\pi f_1 nT\,W^{-48n}\right.$$
$$\left.+(1+\alpha_1+\alpha_2)\sum_{48+m}^{63}\sin 2\pi f_{81}nT\,W^{-48n}\right] \quad (5.46b)$$

Assuming $\sum_{48+m}^{63}\sin 2\pi f_{81}nT\cos\frac{3\pi n}{16} = A_1$ and

$$\sum_{48+m}^{63}\sin 2\pi f_{81}nT\sin\frac{3\pi n}{16} = A_2,$$

and using Equation (5.10a) given by

$$\sum_{0}^{63}\sin 2\pi f_1 nT\,W^{-48n} = 0-j32,$$

Equation (5.46a) can be written as

$$X_s(48\Omega) = \left[\cos\frac{3\pi m}{16} + j\sin\frac{3\pi m}{16}\right]\left[(0-j32)(1-\alpha_1-\alpha_2)\right.$$
$$\left.+(A_1-jA_2)(1+\alpha_1+\alpha_2)\right] \quad (5.46c)$$

The real and imaginary parts of Equation (5.46c) can be written as

$$\mathrm{Re}\left\{X_s(48\Omega)\right\} = A_1(1+\alpha_1+\alpha_2)\cos\frac{3\pi m}{16} + A_2(1+\alpha_1+\alpha_2)\sin\frac{3\pi m}{16} + 32(1-\alpha_1-\alpha_2)\sin\frac{3\pi m}{16}$$

$$\text{and } \mathrm{Im}\left\{X_s(48\Omega)\right\} = -32(1-\alpha_1-\alpha_2)\cos\frac{3\pi m}{16} + A_1(1+\alpha_1+\alpha_2)\sin\frac{3\pi m}{16} - A_2(1+\alpha_1+\alpha_2)\cos\frac{3\pi m}{16}$$

Using the real and imaginary parts of $X_s(48\Omega)$, the magnitude of the spectral component $X_s(48\Omega)$, when 'one' is transmitted, is

$$|X_s(48\Omega)| = \left(A_1^2(1+\alpha_1+\alpha_2)^2 + 1024\,(1-\alpha_1-\alpha_2)^2 + A_2^2(1+\alpha_1+\alpha_2)^2 + 64\,A_2\,(1-\alpha_1-\alpha_2)\,(1+\alpha_1+\alpha_2)\right)^{\frac{1}{2}} \qquad (5.46d)$$

Similarly, when 'zero' is transmitted, in the worst situation, the frequency of the two multipaths is f_1=750 Hz. Then Equation (5.46a) can be expressed as

$$\begin{aligned} X_s(48\Omega) &= W^{48m}\left[\sum_{48+m}^{63}\sin 2\pi f_{81}nT\,W^{-48n} + \sum_{64}^{127}\sin 2\pi\frac{f_s}{2}nT\,W^{-48n}\right. \\ &\quad - \alpha_1\sum_{64}^{127}\sin 2\pi f_1 nT\,W^{-48n} - \alpha_1\sum_{0}^{47+m}\sin 2\pi f_{81}nT\,W^{-48n} \\ &\quad \left. - \alpha_2\sum_{64}^{127}\sin 2\pi f_1 nT\,W^{-48n} - \alpha_2\sum_{0}^{47+m}\sin 2\pi f_{81}nT\,W^{-48n}\right] \\ &= W^{48m}\left[(1+\alpha_1+\alpha_2)\sum_{48+m}^{63}\sin 2\pi f_{81}nT\,W^{-48n}\right. \\ &\quad \left. - (\alpha_1+\alpha_2)\sum_{0}^{63}\sin 2\pi f_1 nT\,W^{-48n}\right] \\ &= \left(\cos\frac{3\pi m}{16} + j\sin\frac{3\pi m}{16}\right)\left[(1+\alpha_1+\alpha_2)(A_1-jA_2) - (\alpha_1+\alpha_2)(0-j32)\right] \end{aligned}$$

Considering real and imaginary parts of this expression, the magnitude of $X_s(48\Omega)$ when 'zero' is transmitted can be written as

$$| X_s(48\Omega) | = \left(A_1^2(1+\alpha_1+\alpha_2)^2 + 1024\,(\alpha_1+\alpha_2)^2 + A_2^2(1+\alpha_1+\alpha_2)^2 - 64A_2\,(\alpha_1+\alpha_2)\,(1+\alpha_1+\alpha_2)\right)^{\frac{1}{2}} \quad (5.46e)$$

By subtracting Equation (5.46e) from Equation (5.46d), the eye opening could be obtained. For correct detection eye opening should be greater than zero. Therefore, as explained in Appendix C, it can be shown that

$$\text{DMR} = 10 \log \left(\frac{1}{\alpha_1 + \alpha_2}\right) > 10 \log \left(\frac{32-A_2}{16+A_2}\right) \quad \text{for correct detection.}$$

Similarly in Appendix C, the magnitude of $X_s(48\Omega)$ and the minimum DMR required for correct detection for the remaining cases are obtained as follows.

In case (d),

$$| X_s(48\Omega) | = \left(A_1^2 + A_2^2 + 1024\,(1-\alpha_1-\alpha_2)^2 + 64\,A_2\,(1-\alpha_1-\alpha_2)\right)^{\frac{1}{2}} \quad (5.47a)$$

when 'one' is transmitted and

$$| X_s(48\Omega) | = \left(A_1^2 + A_2^2\ 1024\,(\alpha_1+\alpha_2)^2 - 64\,A_2\,(\alpha_1+\alpha_2)\right)^{\frac{1}{2}} \quad (5.47b)$$

when 'zero' is transmitted. For correct detection

$$\text{DMR} > 10 \log \left(\frac{32}{16+A_2}\right)$$

In case (e),

$$| X_s(48\Omega) | = \left(A_1^2 (\alpha_1+\alpha_2)^2 + A_2^2 (\alpha_1+\alpha_2)^2 + 1024 (1-\alpha_1-\alpha_2)^2 + 64 A_2 (\alpha_1+\alpha_2)(1-\alpha_1-\alpha_2)\right)^{\frac{1}{2}} \quad (5.48a)$$

when 'one' is transmitted and

$$| X_s(48\Omega) | = (\alpha_1+\alpha_2)\left(A_1^2 + A_2^2 + 1024 - 64 A_2\right)^{\frac{1}{2}} \quad (5.48b)$$

when 'zero' is transmitted. For correct detection

$$\text{DMR} > 10 \log \left(\frac{32-A_2}{16}\right)$$

In case (f),

$$| X_s(48\Omega) | = \left(A_1^2 (1+\alpha_1+\alpha_2)^2 + A_2^2 (1+\alpha_1+\alpha_2)^2 + 1024 (1-\alpha_1-\alpha_2)^2 - 64 A_2 (1+\alpha_1+\alpha_2)(1-\alpha_1-\alpha_2)\right)^{\frac{1}{2}} \quad (5.49a)$$

when 'one' is transmitted and

$$| X_s(48\Omega) | = \left(A_1^2 (1+\alpha_1+\alpha_2)^2 + A_2^2 (1+\alpha_1+\alpha_2)^2 + 1024 (\alpha_1+\alpha_2)^2 + 64 A_2 (1+\alpha_1+\alpha_2)(\alpha_1+\alpha_2)\right)^{\frac{1}{2}} \quad (5.49b)$$

when 'zero' is transmitted. For correct detection

$$\text{DMR} > 10 \log \left(\frac{A_2+32}{16-A_2}\right)$$

In case (g),

$$| X_s(48\Omega) | = \left(A_1^2 + A_2^2 + 1024\,(1-\alpha_1-\alpha_2)^2 - 64\,A_2\,(1-\alpha_1-\alpha_2)\right)^{\frac{1}{2}} \quad (5.50a)$$

when 'one' is transmitted and

$$| X_s(48\Omega) | = \left(A_1^2 + A_2^2 + 1024\,(\alpha_1+\alpha_2)^2 + 64\,A_2\,(\alpha_1+\alpha_2)\right)^{\frac{1}{2}} \quad (5.50b)$$

when 'zero' is transmitted. For correct detection

$$\text{DMR} > 10 \log \left(\frac{32}{16-A_2}\right)$$

Finally considering case (h),

$$| X_s(48\Omega) | = \left(A_1^2\,(\alpha_1+\alpha_2)^2 + A_2^2\,(\alpha_1+\alpha_2)^2 + 1024\,(1-\alpha_1-\alpha_2)^2 - 64\,A_2\,(\alpha_1+\alpha_2)\,(1-\alpha_1-\alpha_2)\right)^{\frac{1}{2}} \quad (5.51a)$$

when 'one' is transmitted and

$$| X_s(48\Omega) | = \left(A_1^2\,(\alpha_1+\alpha_2)^2 + A_2^2\,(\alpha_1+\alpha_2)^2 + 1024\,(\alpha_1+\alpha_2)^2 + 64\,A_2\,(\alpha_1+\alpha_2)^2\right)^{\frac{1}{2}} \quad (5.51b)$$

when 'zero' is transmitted. For correct detection

$$\text{DMR} > 10 \log \left(\frac{A_2+32}{16}\right)$$

Similar set of equations are obtained in Appendix C, for all the above cases when

$$X_s(48\Omega) = \sum_{n=48}^{511+48} x(n-m)\,W^{-48n} \quad (5.52)$$

Finally all these equations are evaluated for different m values and the minimum DMR required for correct detection in the presence of a synchronization error is found. The above expressions for $|X_s(48\Omega)|$ when 'one' is transmitted and 'zero' is transmitted and the DMR requirement for correct detection are summerized in Table (5.2). By obtaining the eye opening for all the cases for different m values it is observed that the worst effect on eye opening occurs when m=8. With this synchronization error, DMR is found to be greater than 6.2 dB for correct detection.

5.6 Error Performance of the System in the Presence of Ambient Noise

When Gaussian noise is added to the received signal, the magnitude of the 48^{th} spectral component corresponds to $f_1 = 750$ Hz becomes,

$$|X(48\Omega)| = |X_s(48\Omega) + X_n(48\Omega)| \tag{5.53}$$

where $X_s(48\Omega)$ is the component corresponding to the transmitted signal and $X_n(48\Omega)$ is that corresponding to the noise component. $X_s(48\Omega)$ and $X_n(48\Omega)$ can be written as,

$$X_s(48\Omega) = \sum_{n=48}^{511+48} x(n)\, W^{-48n} \tag{5.54a}$$

$$X_n(48\Omega) = \sum_{n=48}^{511+48} n(n)\, W^{-48n} \tag{5.54b}$$

where n(n) are noise samples.

Since both the signal and noise components are complex, Equation (5.53) can be written as,

$$\begin{aligned} |X(48\Omega)| &= |(X_s + jY_s) + (X_n + jY_n)| \\ &= \left[(X_s + X_n)^2 + (Y_s + Y_n)^2\right]^{\frac{1}{2}} \end{aligned} \tag{5.55}$$

Table (5.2) The effect of synchronization error on $|X_k(48\Omega)|$ and the minimum DMR required for correct detection

case	$\lvert X_k(48\Omega)\rvert_{min}$ when 'one' is transmitted	$\lvert X_k(48\Omega)\rvert_{max}$ when 'zero' is transmitted	Minimum DMR reqd. for correct detection
a	$32B_2$	$32B_3$	3
b	$32B_2$	$32B_3$	3
c	$(A_1^2B_1^2+1024B_2^2+A_2^2B_1^2+64A_2B_1B_2)^{\frac{1}{2}}$	$(A_1^2B_1^2+1024B_3^2+A_2^2B_1^2-64A_2B_1B_3)^{\frac{1}{2}}$	$10\log\left(\frac{32-A_2}{16+A_2}\right)$
d	$(A_1^2+A_2^2+1024B_2^2+64A_2B_2)^{\frac{1}{2}}$	$(A_1^2+A_2^2+1024B_3^2-64A_2B_3)^{\frac{1}{2}}$	$10\log\left(\frac{32}{16+A_2}\right)$
e	$(A_1^2B_2^2+A_2^2B_3^2+1024B_2^2+64A_2B_2B_3)^{\frac{1}{2}}$	$(A_1^2B_3^2+A_2^2B_3^2+1024B_3^2-64A_2B_3^2)^{\frac{1}{2}}$	$10\log\left(\frac{32-A_2}{16}\right)$
f	$(A_1^2B_1^2+A_2^2B_1^2+1024B_2^2-64A_2B_1B_2)^{\frac{1}{2}}$	$(A_1^2B_1^2+A_2^2B_1^2+1024B_3^2+64A_2B_1B_3)^{\frac{1}{2}}$	$10\log\left(\frac{32+A_2}{16-A_2}\right)$
g	$(A_1^2+A_2^2+1024B_2^2-64A_2B_2)^{\frac{1}{2}}$	$(A_1^2+A_2^2+1024B_3^2+64A_2B_3)^{\frac{1}{2}}$	$10\log\left(\frac{32}{16-A_2}\right)$
h	$(A_1^2B_2^2+A_2^2B_3^2+1024B_2^2-64A_2B_2B_3)^{\frac{1}{2}}$	$(A_1^2B_3^2+A_2^2B_3^2+1024B_3^2+64A_2B_3^2)^{\frac{1}{2}}$	$10\log\left(\frac{32+A_2}{16}\right)$

where,

$$B_1 = 1+\alpha_1+\alpha_2$$
$$B_2 = \alpha_1+\alpha_2$$
$$B_3 = 1-\alpha_1-\alpha_2$$

When $X_k(48\Omega) = \sum_{n=-48}^{511+48} x(n+m)\,W^{-48n}$,

$$A_1 = \sum_{n=-48+m}^{48} \sin 2\pi f_{81} nT \cos\frac{3\pi n}{16}$$

and $$A_2 = \sum_{n=-48+m}^{48} \sin 2\pi f_{81} nT \sin\frac{3\pi n}{16}$$

When $X_k(48\Omega) = \sum_{n=-48}^{511+48} x(n-m)\,W^{-48n}$,

$$A_1 = \sum_{n=-48-m}^{48} \sin 2\pi f_{81} nT \cos\frac{3\pi n}{16}$$

and $$A_2 = \sum_{n=-48-m}^{48} \sin 2\pi f_{81} nT \sin\frac{3\pi n}{16}$$

where $X_s = \mathrm{Re}\left\{ \sum_{n=48}^{511+48} x(n)\, W^{-48n} \right\} = \sum_{n=48}^{511+48} x(n) \cos \frac{3\pi n}{16}$ (5.56a)

$Y_s = \mathrm{Im}\left\{ \sum_{n=48}^{511+48} x(n)\, W^{-48n} \right\} = -\sum_{n=48}^{511+48} x(n) \sin \frac{3\pi n}{16}$ (5.56b)

$X_n = \mathrm{Re}\left\{ \sum_{n=48}^{511+48} n(n)\, W^{-48n} \right\} = \sum_{n=48}^{511+48} n(n) \cos \frac{3\pi n}{16}$ (5.56c)

and $Y_n = \mathrm{Im}\left\{ \sum_{n=48}^{511+48} n(n)\, W^{-48n} \right\} = -\sum_{n=48}^{511+48} n(n) \sin \frac{3\pi n}{16}$ (5.56d)

Defining, $(X_s + X_n) = x$ (5.57a)

and $(Y_s + Y_n) = y$ (5.57b)

Equation (5.55) reduces to

$$| X(48\Omega) | = \left[x^2 + y^2 \right]^{\frac{1}{2}} \tag{5.58}$$

Thus, as given in Appendix D, the joint probability density function of the two random variables x and y with means m_1 and m_2, variances $\sigma_x = \sigma_y$ is given by

$$p(x,y) = \frac{1}{2\pi\sigma_x^2} \exp\left[-\frac{\left((x - m_1)^2 + (y - m_2)^2\right)}{2\sigma_x^2} \right] \tag{5.59}$$

Using polar coordinates, $x = R \cos \Phi$, $y = R \sin \Phi$,

Equation (5.58) reduces to

$$| X_s(48\Omega) | = \left[x^2 + y^2 \right]^{\frac{1}{2}} = R \tag{5.60}$$

Then the probability distribution $p(R,\Phi)$ could be obtained using,

$$p(R,\Phi) = p(x,y)\, J\left|\frac{x,y}{R,\Phi}\right| \tag{5.61}$$

$$\text{where} \quad J\left|\frac{x,y}{R,\Phi}\right| = \begin{vmatrix} \frac{\partial x}{\partial R} & \frac{\partial y}{\partial R} \\ \frac{\partial x}{\partial \Phi} & \frac{\partial y}{\partial \Phi} \end{vmatrix} = R \tag{5.62}$$

Now $p(R,\Phi)$ can be written as,

$$p(R,\Phi) = \frac{R}{2\pi\sigma_x^2} \exp\left[-\frac{\left((R\cos\Phi - m_1)^2 + (R\sin\Phi - m_2)^2\right)}{2\sigma_x^2}\right]$$

$$= \frac{R}{2\pi\sigma_x^2} \exp\left[-\frac{\left(R^2 - 2m_1R\cos\Phi - 2m_2R\sin\Phi + m_1^2 + m_2^2\right)}{2\sigma_x^2}\right] \tag{5.63}$$

The distribution of $R = |\, X(48\Omega)\,|$ can be given by,

$$p(R) = \int_0^{2\pi} p(R,\Phi)\, d\Phi \tag{5.64a}$$

$$= \frac{R}{2\pi\sigma_x^2} \exp-\left(\frac{R^2+m_1^2+m_2^2}{2\sigma_x^2}\right) \int_0^{2\pi} \exp\left(\frac{R\,(m_1^2+m_2^2)^{\frac{1}{2}} \cos\left[\Phi - \tan^{-1}\frac{m_2}{m_1}\right]}{\sigma_x^2}\right) d\Phi$$

$$= \frac{R}{2\pi\sigma_x^2} \exp-\left(\frac{R^2+m_1^2+m_2^2}{2\sigma_x^2}\right) \int_0^{2\pi} \exp\left(\frac{R\,(m_1^2+m_2^2)^{\frac{1}{2}} \cos\left[\Phi - \tan^{-1}\frac{m_2}{m_1}\right]}{\sigma_x^2}\right) d\Phi$$

$$= \frac{R}{\sigma_x^2} \exp-\left(\frac{R^2 + m_1^2 + m_2^2}{2\,\sigma_x^2}\right) I_0\left[R\,\frac{(m_1^2 + m_2^2)^{\frac{1}{2}}}{\sigma_x^2}\right] \tag{5.64b}$$

where $I_o = \frac{1}{2\pi}\int_0^{2\pi} \exp\left(x\cos\Phi\right) d\Phi$

Hence the probability of error P_e when detecting a signal in the presence of ambient noise, could be obtained as

$$P_e = \int_0^{\frac{|X_1|}{2}} p(R)\, dR \tag{5.65a}$$

where $X_1 = \sum_0^{63} \sin 2\pi f_1 nT\ W^{-48n}$

In Section (5.2), it was shown that $\frac{|X_1|}{2} = 16$,

$$\text{i.e.}\quad P_e = \frac{R}{\sigma_x^2} \int_0^{\frac{|X_1|}{2}} \exp -\left[\frac{R^2 + a^2}{2\sigma_x^2}\right] I_0\left(\frac{Ra}{\sigma_x^2}\right) dR \tag{5.65b}$$

where $a = \left[m_1^2 + m_2^2\right]^{\frac{1}{2}}$

Defining $\frac{R}{\sigma_x} = R_1$ and $\frac{a}{\sigma_x} = a_1$, Equation (5.65b) becomes

$$P_e = \int_0^{\frac{|X_1|}{2\sigma_x}} R_1 \exp -\left[\frac{R_1^2 + a_1^2}{2}\right] I_0\left(R_1 a_1\right) dR_1 \tag{5.65c}$$

P_e can be evaluated using the method outlined by McGee [28],

$$\int_0^b x \exp -\left[\frac{a^2 + x^2}{2}\right] I_0(a,x)\, dx = \sum_{k=0} f_k h_k \tag{5.66a}$$

where $h_k = h_{k-1} + d_k$ (5.66b)

$$d_k = \frac{a^2}{2} \frac{d_{k-1}}{k} \tag{5.66c}$$

$$f_k = \frac{\frac{(b^2)}{2} f_{k-1}}{k+1} \tag{5.66d}$$

$$d_0 = h_0 = \exp\left(\frac{-a^2}{2}\right) \tag{5.66e}$$

$$\text{and} \quad f_0 = \frac{b^2}{2}\exp\left(\frac{b^2}{2}\right) \tag{5.66f}$$

Then Equation (5.65c) can be written as

$$P_e = \sum_{k=0} f_k h_k \tag{5.67}$$

$$\text{with} \quad a = a_1 = \left(\frac{m_1^2 + m_2^2}{\sigma_x}\right)^{\frac{1}{2}}$$

$$\text{and} \quad b = \frac{|X_1|}{2\sigma_x} = \frac{16}{\sigma_x}$$

Since SNR $= 10 \log \frac{A^2}{2\sigma}$, where A is the strength of the transmitted signal and σ is noise variance, according to Appendix D

$$\sigma_x = 16\,\sigma = 16\frac{A^2}{2}\,10^{-\left(\frac{SNR}{10}\right)}$$

Assuming a unit amplitude signal is transmitted, i.e. A=1, the error probabilities are obtained by varying SNR for different DMR values. Fig (5.6) shows the error probabilities with the variation of SNR for different DMR values when the transmitter is at the surface.

Similarly, in Fig (5.7), the same set of curves are plotted when the transmitter and receiver are in water.

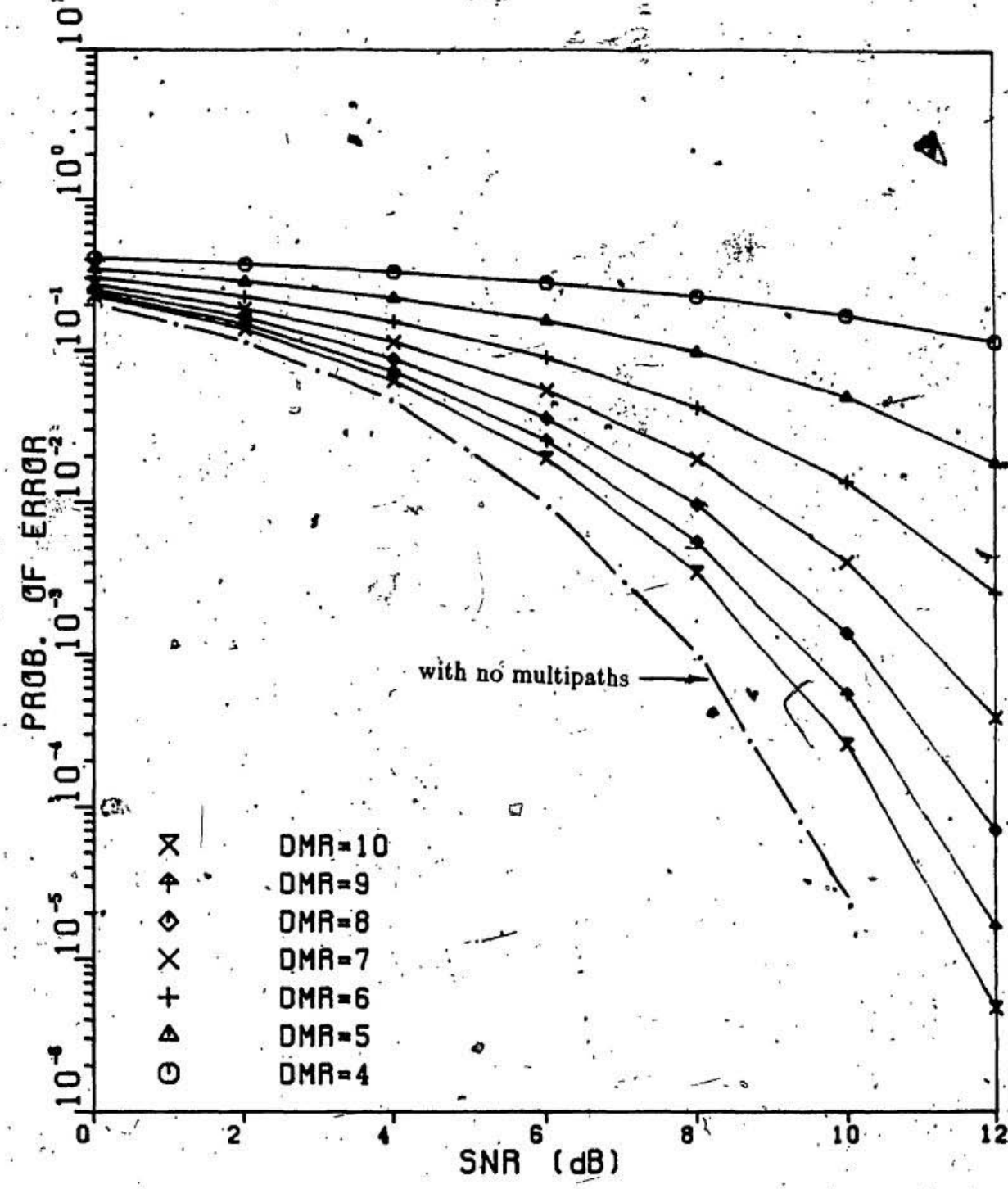

Fig. 5.7 Variation of Probability of error with SNR for Configuration A.

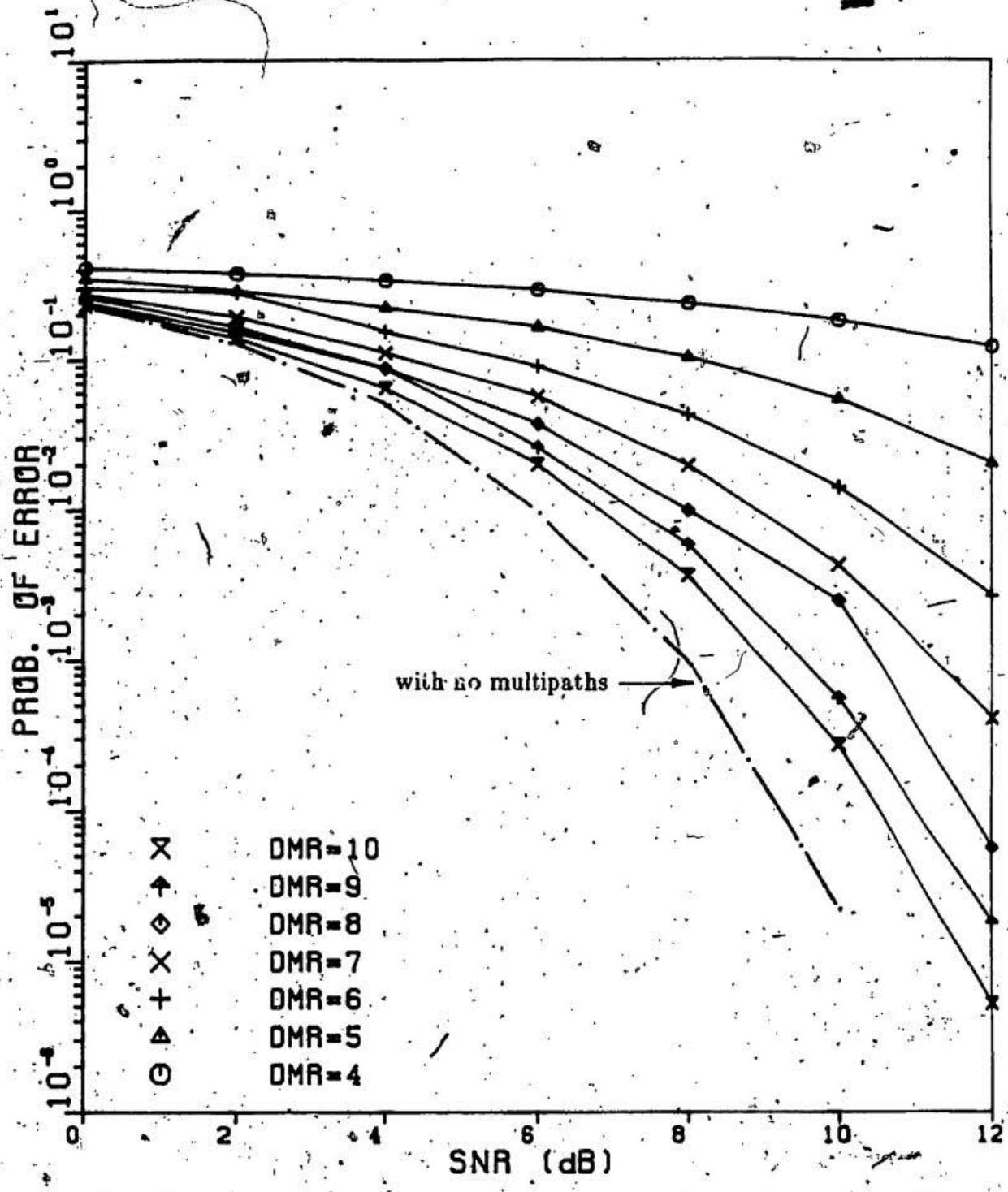

Fig. 5.8 Variation of Probability of error with SNR for Configuration B.

CHAPTER 6

COMPUTER SIMULATION

6.1 Introduction

In this chapter, a computer simulation is carried out to test the transmission scheme described in Chapter 4 using the parameters from the sample design. Since the performance of the system without AGC was analyzed in Chapter 5, the simulation is restricted only to the case with AGC.

The variation of DMR with the distance between transmitter and receiver is obtained for different transmitter-receiver configurations under assumed SRL and BRL values. By generating sequences of random data at the transmitter, a multiple of frequency scans of the received signal are also obtained for two different transmitter-receiver configurations [43,44].

6.2 Simulation Model

Fig (6.1) shows the simulation model being considered. In this model, frequencies are assigned according to the coding scheme explained in Chapter 4 to the random data generated at the transmitter. Then the signal is transmitted through the underwater channel modeled by considering large number of multipaths. The receiver consists of a sampler, an AGC unit, SDFT demodulator and a threshold detector which detects the received signal by threshold comparison of the magnitude of spectral components.

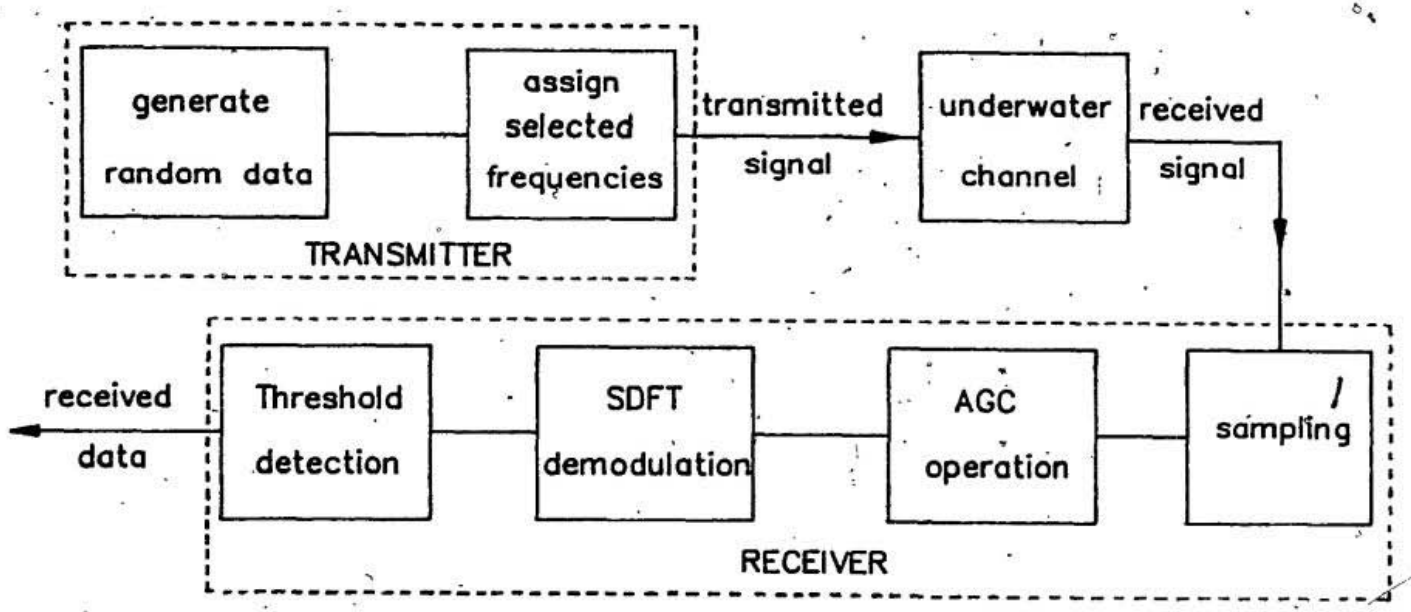

Fig. 6.1 Simulation model.

6.2.1 Transmitter

A long sequence of random numbers is generated and the digits are separated into eight digit words at the transmitter. According to the transmission scheme explained in chapter 4, the frequencies are assigned to these digits. In this process, due to the reason that the sliding observation window is initially positioned as shown in Fig (4.1), the last digit of the preceding word is considered as the first digit of the present signal. Therefore, for example, for a sequence of binary symbols 1, 1, 0, 1, 1, 0, 1, 1, the frequencies assigned are f_8, f_1, $\frac{f_s}{2}$, f_3, f_4, $\frac{f_s}{2}$, f_6, f_7, where

$$f_i = 1000 + (i-1)\,750 \text{ Hz} \qquad \text{for } i = 1, 2, \ldots\ldots, 8$$

Hence the signal at the input of the underwater channel could be written as

$$x(t) = \sum_{j=1}^{m} \sin 2\pi F(j)\,(t-\Delta_j)\,W(t-\Delta_j) \qquad (6.1)$$

where $\Delta_j = j\tau - \frac{\tau}{2}$, $\qquad \tau = 8$ msec

m = the number of binary digits considered

and $F(j)$ is the frequency of the j^{th} digit of the long sequence of digits, which is either one of the values of f_i or $\frac{f_s}{2}$.

6.2.2. Underwater Channel

The channel is modeled by a large number of surface and bottom reflections, each with attendant attenuation and delay as given in Chapter 2. These multipath signals constitute a disturbance for a direct path signal which can be measured by the Direct-to-Multipath intensity Ratio DMR. Figures (6.2), (6.3) and (6.4) show the variation of DMR as a function of distance between transmitter and receiver for various transmitter-receiver configurations and other assumed parameters.

According to the model of the underwater channel explained in Chapter 2, the impulse response of the ocean could be written as

$$h(t) = \sum_{i=0}^{M} \alpha_i \, \delta(t-t_i) \tag{6.2}$$

where α_0 = the intensity of the direct path signal which is normalized to 1.

α_i = the intensity of i^{th} multipath.

t_i = the delay of i^{th} multipath with respect to the direct path signal assuming $t_0 = 0$.

and M = the total number of multipaths which have reasonable intensities compared to the direct path intensity.

Therefore, using Equations (6.1) and (6.2), the signal at the output of the ocean model is

$$y(t) = \sum_{i=0}^{M} \alpha_i \, x(t-t_i) \tag{6.3a}$$

$$= \sum_{i=0}^{M} \alpha_i \sum_{j=1}^{m} \sin 2\pi F(j) \, (t-t_i-\Delta_j) \, W(t-t_i-\Delta_j) \tag{6.3b}$$

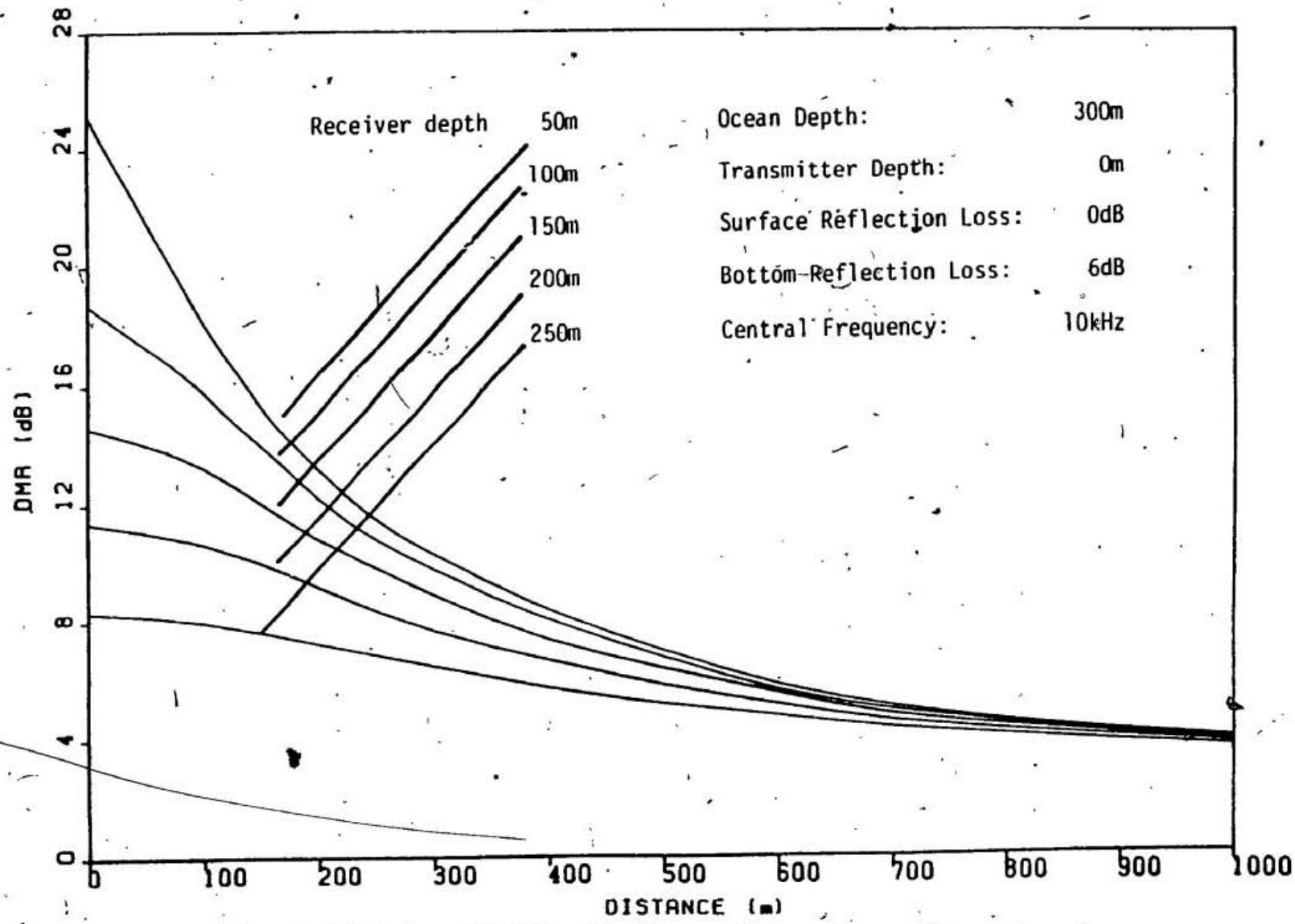

Fig. 6.2 Variation of DMR with distance between transmitter and receiver when the transmitter is at the surface with no surface reflection loss.

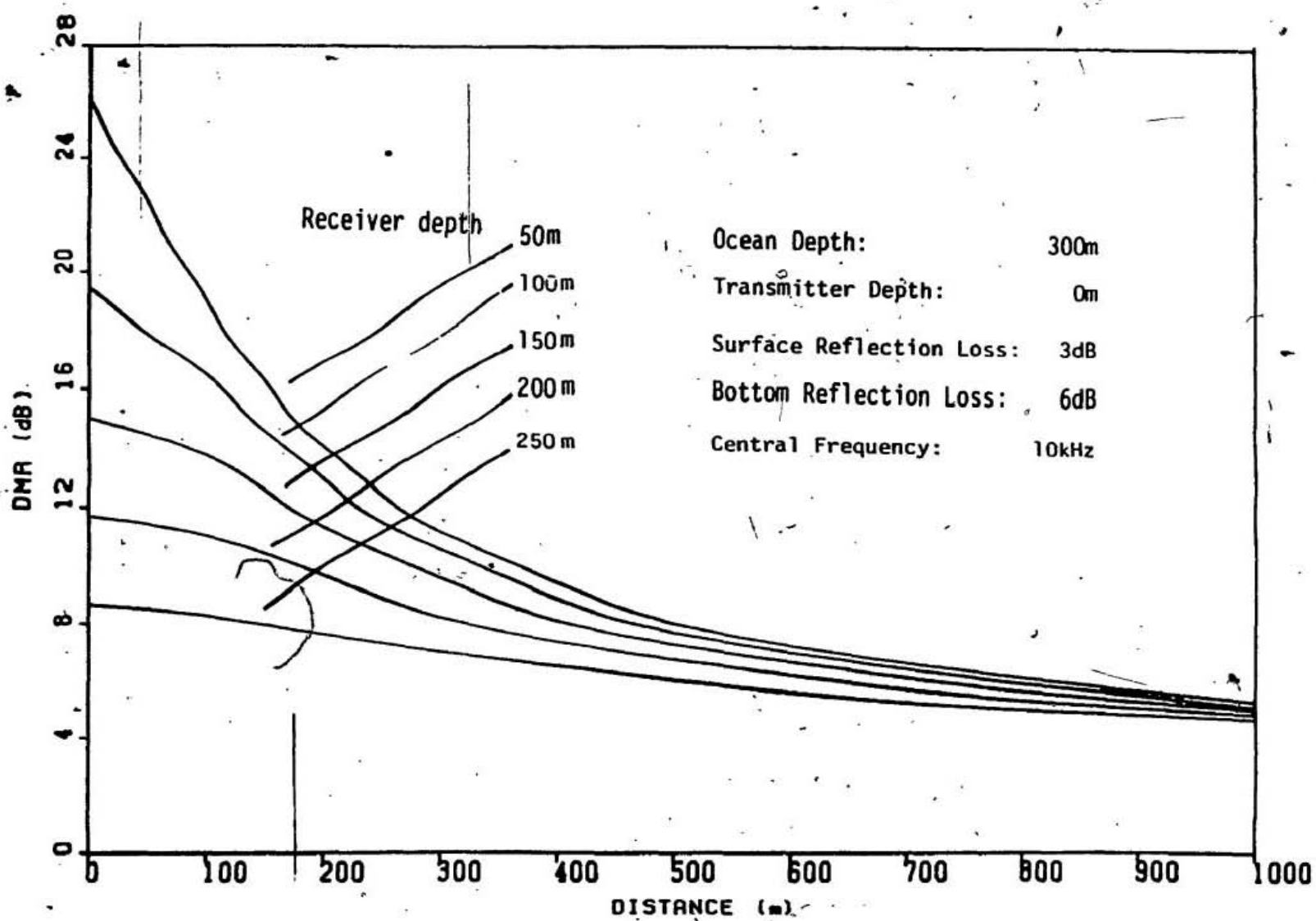

Fig. 6.3 Variation of DMR with distance between transmitter and receiver when the transmitter is at the surface with surface reflection loss = 3 dB.

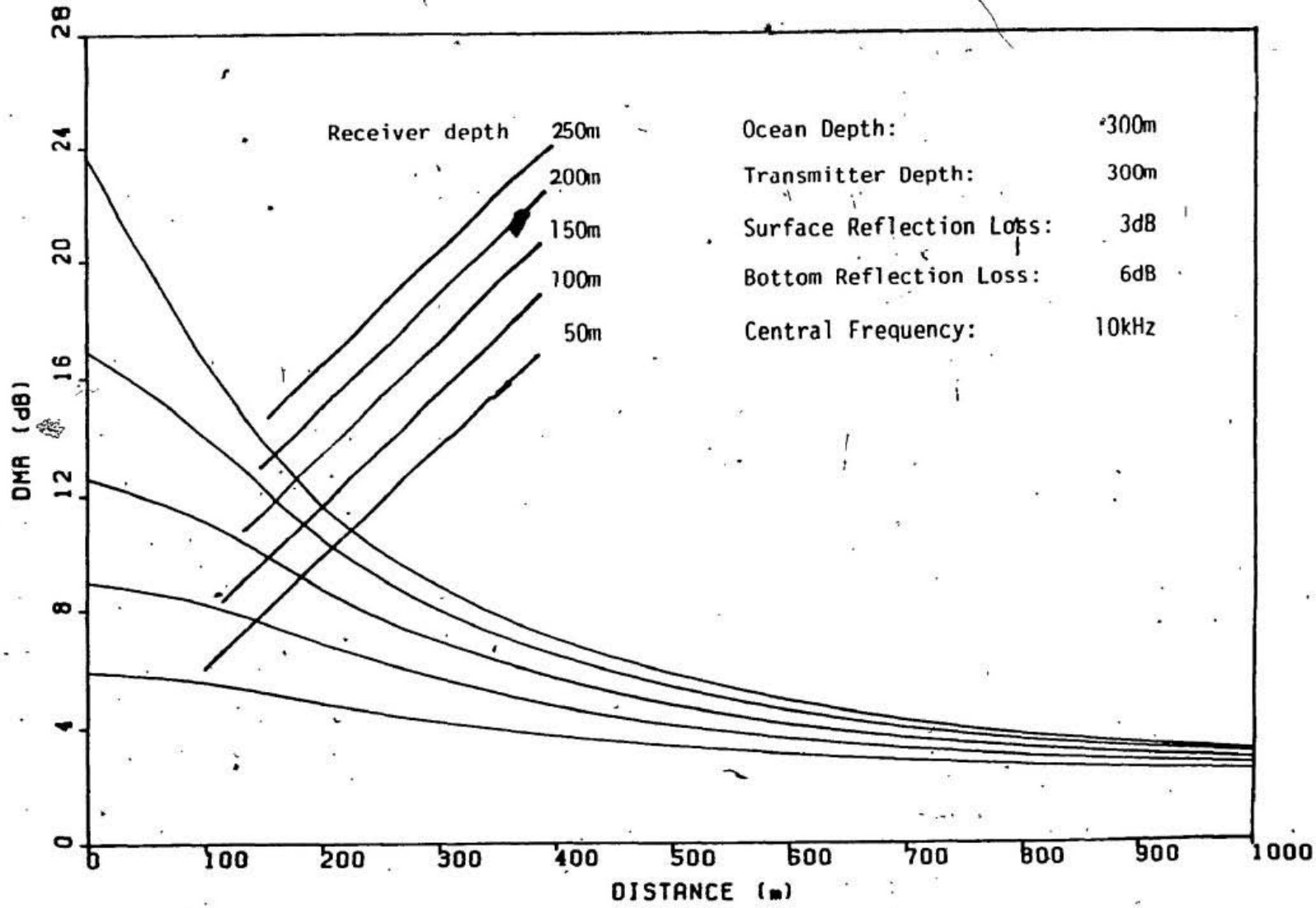

Fig. 6.4 Variation of DMR with distance between transmitter and receiver when the transmitter is at the bottom with surface reflection loss = 3 dB.

For the purpose of analysis all the strong multipaths are assumed to be died out within the interval of three words and hence m has been considered as 24. Therefore any 8 digit word received consists of the direct path signal and multipath signals of the same word and the multipath signals of the preceding two sets of words transmitted.

6.2.3. Receiver

Here the samples y(nT) of the latest 8-bit word received is obtained at the sampling frequency of 8kHz. As the signal is distorted by the multipaths, the received signal is sent through an AGC to stabilize the amplitude before the SDFT is performed.

In the simulation, the AGC operation is achieved by dividing each sample of the received signal by the magnitude of its envelope. If the discrete signal at the input of AGC is y(nT), the constant envelope signal at the output of AGC could be written as

$$Y(nT) = \frac{y(nT)}{\text{Enve. } \{ y(nT) \}} \tag{6.4}$$

Therefore, in modeling the AGC, first of all the envelope of the received signal y(nT) is obtained using the Hilbert Transform of y(nT) as given below.

Recalling Equation (6.3), the samples of the recent 8-bit word are

$$y(nT) = \sum_{i=0}^{M} \alpha_i \sum_{j=1}^{24} \sin 2\pi F(j) \, (T_2 - t_i - \Delta_j) \, W(T_2 - t_i - \Delta_j) \tag{6.5a}$$

where $T_2 = 16\,\tau + nT$, and $T = \frac{1}{f_s}$

the Hilbert Transform of y(nT) in Equation (6.5a) can be written as

$$y(nT) = \sum_{i=0}^{M} \alpha_i \sum_{j=1}^{24} \cos 2\pi F(j) (T_2 - t_i - \Delta_j) \, W(T_2 - t_i - \Delta_j) \qquad (6.5b)$$

Hence the envelope of the received signal could be written as

$$\left([y(nT)]^2 + [y(nT)]^2 \right)^{\frac{1}{2}}$$

Then 512 samples of the received signal Y(nT) are obtained. These 512 samples are then stored in a memory at the position from 0 to 511. Next generating another new set of 8 random numbers, the set of constant envelope samples of the new word are obtained using the same procedure. These samples are also stored in the memory at positions 512 to 1023. Using these 1024 samples, the spectral components of the first 512 samples are then obtained using the SDFT algorithm given in Equation (4.5). Similarly, multitude of frequency scans are obtained generating sequences of random data.

Depending on the magnitude of the spectral components corresponding to the frequencies transmitted, the data transmitted are detected.

6.3 Simulation Results

In this section, the frequency scans obtained by simulation for different random data are presented for the two transmitter-receiver configurations considered in Chapter 5. For comparison of the simulated results with the theoretical results given in Chapter 5, the simulation was carried out using ominidirectional transmitter and receiver with the parameters given in Sections (5.4.1) and (5.4.2).

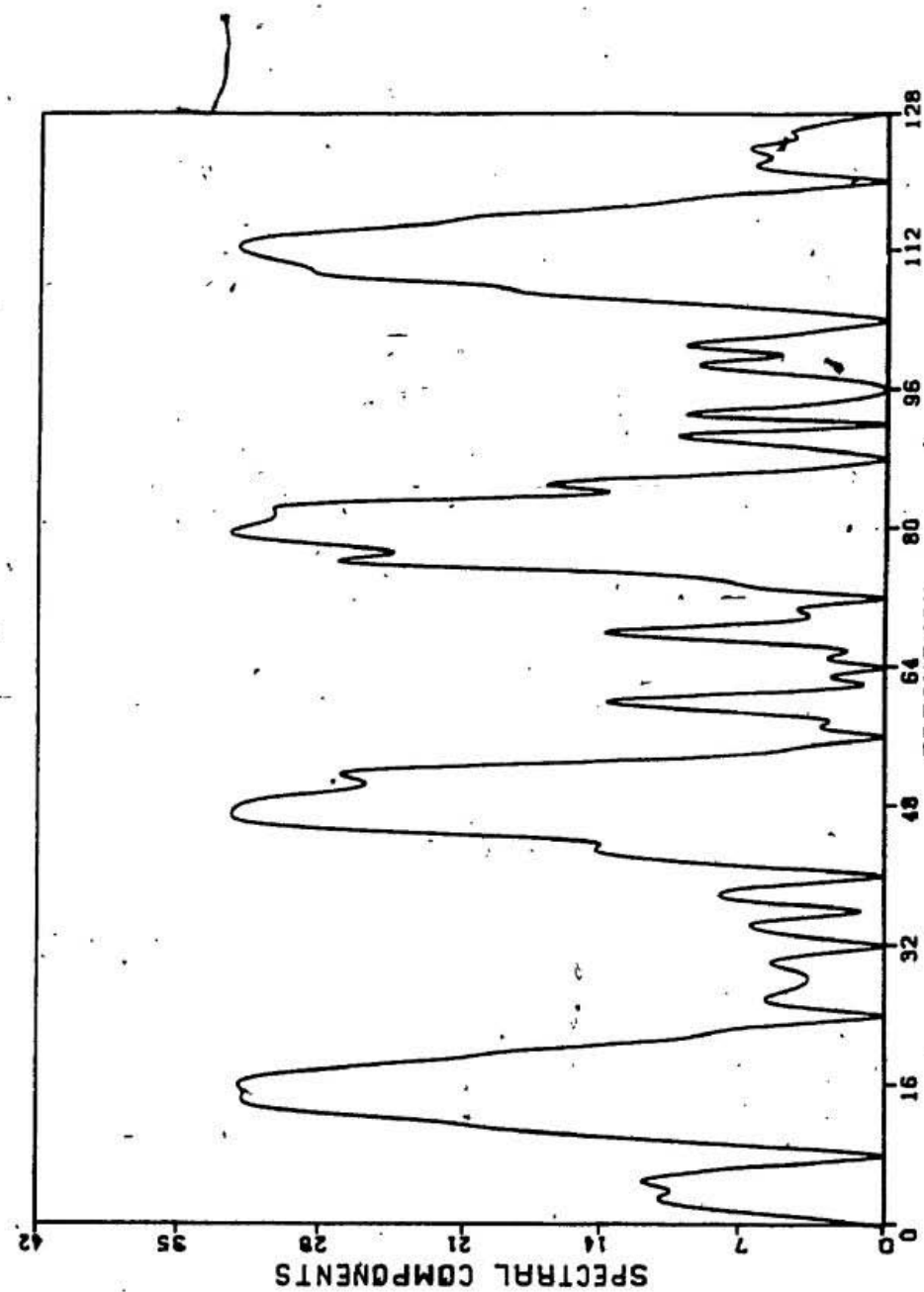

Fig. 6.5 Frequency scan for a selected data sequence.

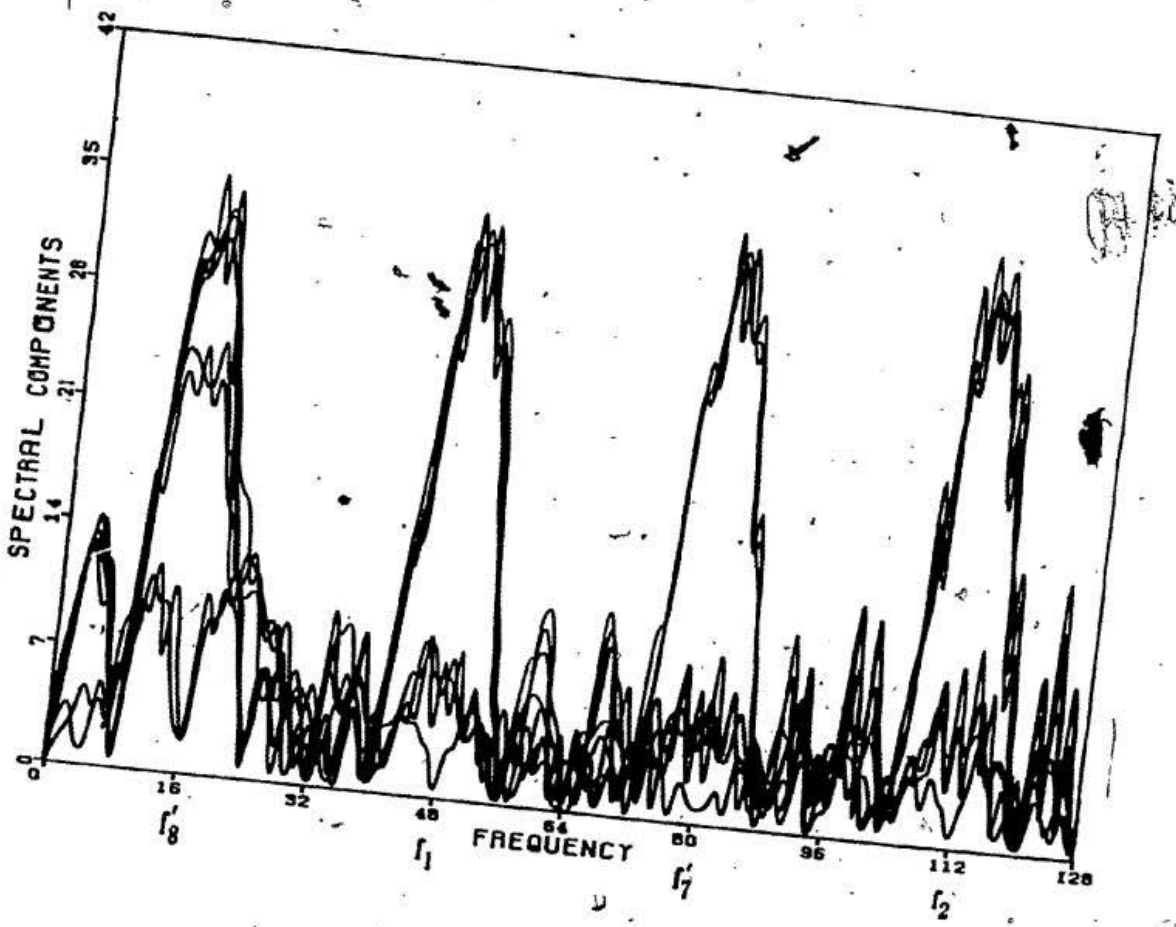

Fig. 6.6 Eye pattern for the SDFT receiver in Configuration A for DMR=4 dB.

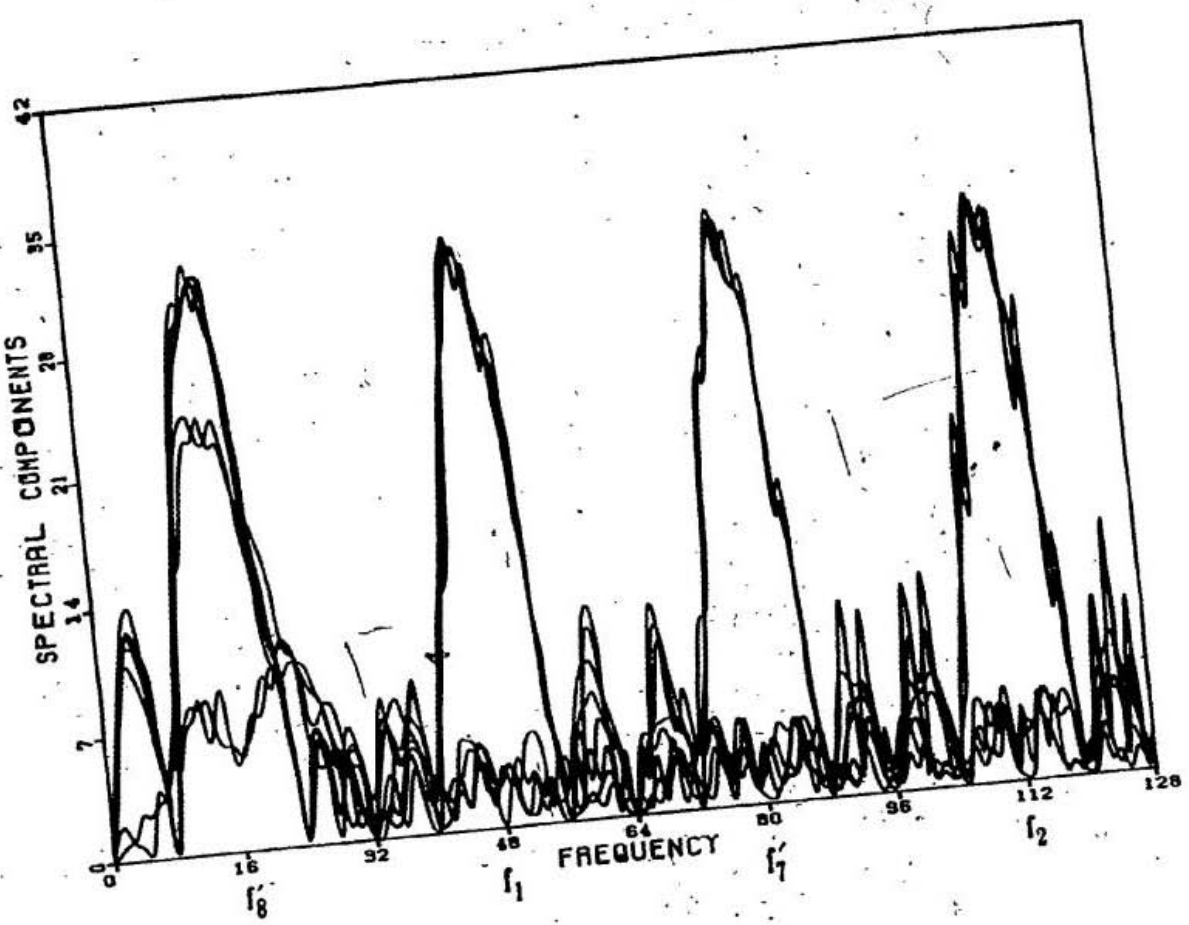

Fig. 6.7 Eye pattern for the SDFT receiver in Configuration A for DMR=9 dB.

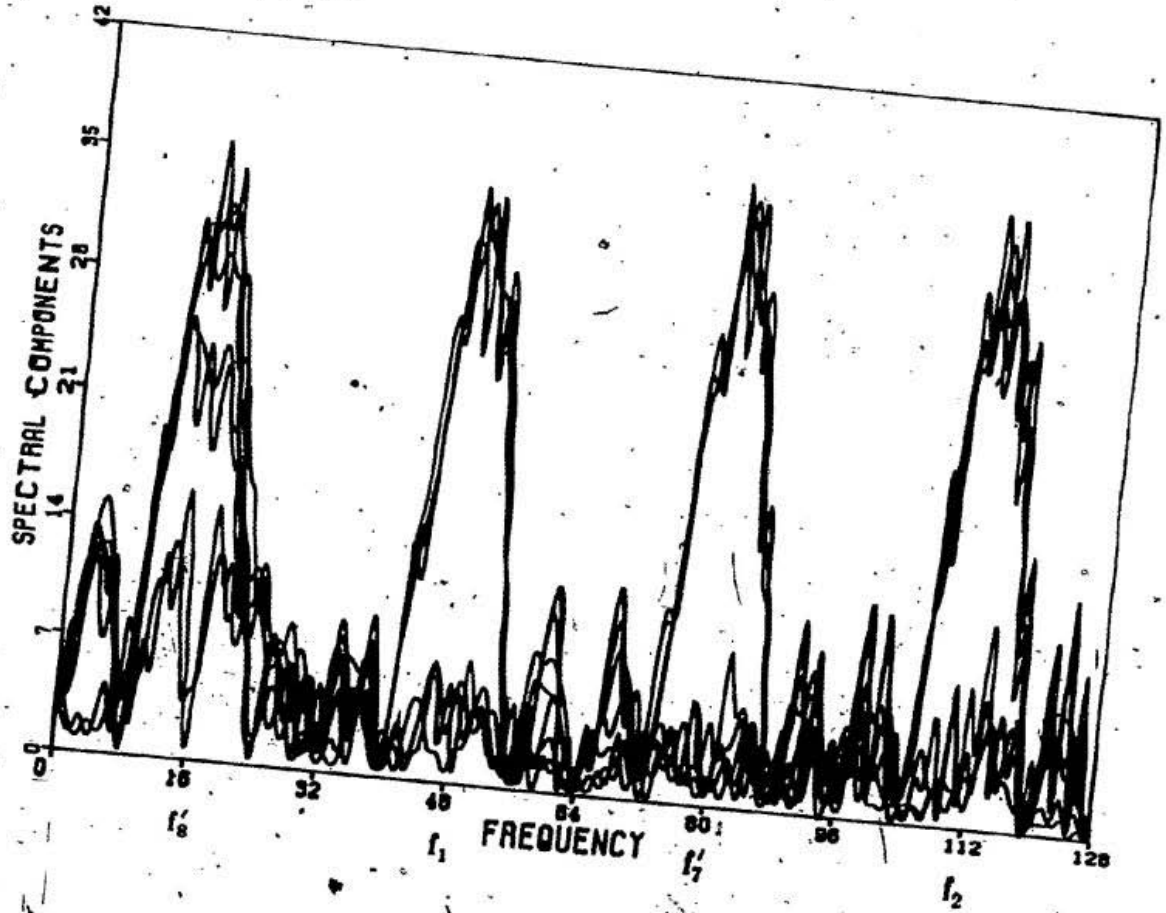

Fig. 6.8 Eye pattern for the SDFT receiver in Configuration B for DMR=4 dB.

Fig (6.5) shows the frequency representation of a transmitted sequence 1, 1, 0, 1, 1, 0, 1, 1 when no multipath is present. For the sake of clarity only the initial portion of the frequency scan is shown.

Figs (6.6), (6.7) and (6.8) show the superimposed frequency scans similar to that shown in Fig (6.5) which form characteristic eye patterns for different DMR values. These patterns demonstrate that the proper detection decisions can be made.

Based on these simulation results obtained, it is clearly seen that the assumptions made in obtaining the transmission scheme is valid and the SDFT detection scheme is a reliable means for communication in underwater multipath channel.

CHAPTER 7

CONCLUSIONS AND DISCUSSION

In this thesis a novel transmission scheme for communication in multipath acoustic channel has been introduced.

Constant envelope multi-frequency signals have been used for digital transmission in the proposed system. The signal design and the frequencies for data transmission were selected so as to avoid Inter Symbol Interference. Demodulation of the received signal is accomplished using the Sliding Discrete Fourier Transform algorithm.

The performance of the proposed transmission scheme has been evaluated analytically. When the direct path signal overlaps with the multipath signals, the envelope of the received signal varies according to the intensities of the direct path and multipath signals. Since the demodulation scheme is designed to operate on constant envelope multi-frequency signals, the received signal needs to be stabilized by an Automatic Gain Controller before carrying out the demodulation. Due to the non-linearity effect of the AGC process, the theoretical analysis was found to be extremely difficult. Owing to this reason theoretical analysis was carried out only for the case with no AGC at the receiver.

In theoretical analysis, first the spectral components were analyzed in the absence of multipaths and it has been concluded that there is no effect on the magnitude of spectral component from the frequencies in the same frame.

The analysis has been extended to the case with multipaths. Here, the variation of minimum eye opening with Direct to Multipath intensity Ratio has been plotted for two transmitter-receiver configurations. It has been observed from these plots that the minimum eye opening increases with the increase of DMR in both the configurations in a similar manner. Also it has been found that for proper detection the DMR should exceed 3 dB.

Next the effect of synchronization error at the receiver on the spectral components has been evaluated. Since it was observed that the effect of synchronization error depends only on the frequencies at the two ends of the window, the variation of minimum eye opening and the minimum DMR required for correct detection have been evaluated for all the possible combinations of frequencies at the two ends of the window. Then by varying the number of samples in error, the minimum DMR required for correct detection has been found out as 6.2 dB in the presence of a synchronization error.

Finally, the error performance of the system has been evaluated in the presence of Gaussian noise. The error rates were plotted with SNR for different DMR values for the two transmitter-receiver configurations considered. It has been observed that in both these configurations, the error rates decrease with the increase of SNR for a given DMR and for a given SNR, the error rates decrease with the increase of DMR. Also, it has been observed that the error performance is poor even at high SNR values when DMR falls below 6 dB.

A computer simulation has been carried out to test the proposed transmis-

sion scheme and the demodulation technique with an AGC at the receiver. By generating sequences of random data at the transmitter a multiple of frequency scans of the received signal were obtained. Based on the eye patterns of the received signal obtained the proposed scheme appears to be a reliable means for communication in multipath underwater channels.

The variation of DMR with the horizontal distance between the transmitter and the receiver for various transmitter-receiver configurations and locations indicates that the DMR decreases and reaches a constant value with the increase of transmitting range.

The analytical and simulation results reveal that the proposed scheme is a reliable means for underwater communications in multipath channels. Even though a comparison of analytical results and simulation results has not been carried out, it may perhaps be useful to compare the analytical results and the simulation results with each other as well as with the results of other available schemes for further improvements of the proposed scheme.

Since the SDFT algorithm can be easily implemented with the use of commercially available integrated circuits, the system is attractive in situations where power and space conservation are of prime importance. The implementation of the proposed scheme will also be an interesting topic for future research.

BIBLIOGRAPHY AND LIST OF REFERENCES

1. Adam, J.A., 'Probing beneath the Sea,' IEEE Spectrum, April 1985, pp. 55-64.

2. Allen, J. and Glasgow, J., 'Limitation of Range and Bandwidth for Acoustic Technology,' Underwater Technology, Vol. **10** , No. 3, 1984, pp. 3-7.

3. Anderson, V.C., 'Acoustic Communication is Better Than None,' IEEE Spectrum, Oct. 1970, pp. 63-68

4. Andrews, R.S. and Turner, L.F., 'On the Performance of Underwater Data Transmission Systems Using ASK Techniques,' IEEE Trans. on Sonics and Ultrasonics, Vol. **SU-23** , No. 1, Jan. 1976, pp. 64-71.

5. Anonymous, 'Acoustics in Control for Balmoral Pipelines,' Offshore Engineer, Feb. 1986.

6. Anonymous, 'Recticon, Data Sheet, Quad Chirped Transversal Filter R5601.'

7. Baggeroer, A.B. et al, 'DATS-A Digital Acoustic Telemetry System for Underwater Communications,' Ocean 81, IEEE-MTS Conference, Boston, Sept. 1981, pp. 55-60.

8. Barbour, R.L., 'Underwater Acoustic Swept Carrier Communications,' M.Eng. Thesis, Memorial Univ. of Newfoundland, St. John's, Newfoundland, Canada, April, 1979.

9. Bohman, C.E. and Jackson, D.E., 'Underwater Acoustic Communications,' Sperry Technology, Vol. **1** , No. 4, 1973, pp. 10-15.

10. Broderson, R.W., Hewes, C.R. and Buss, D.D., 'A 500-Stage CCD Transversal Filter for Spectral Analysis,' IEEE J. of Solid-State Circuits, Vol. **SC-11** , No. 1, Feb. 1976, pp. 75-83.

11. Cattanach, D., 'A 16-Channel Digital Acoustic Telemetry System,' The Radio and Electronic Engineer, Vol. **42** , No. 3, March 1972, pp. 141-151.

12. Chase, J.V., 'A Tracking and Telemetry System for Severe Multipath Acoustic Channels,' Ocean 81, IEEE-MTS Conference, Boston, Sept. 1981, pp. 35-39.

13. De Pinto, V., Kosalos, J.G. and Lapter, S., 'An Acoustic Telemetry System for a Shallow-Water under Ice Arctic Environment,' Offshore Technology Conference, Houston, May 1983, pp. 429-435.

14. Dunbar, R.M., Roberts, S.J., Wells, S.C., 'Communications, Bandwidth Reduction, and System Studies for a Tetherless Unmanned Submersibles,' Ocean 81, IEEE-MTS Conference, Boston, Sept. 1981, pp. 127-131.

15. Fisher, F.H. and Simmons, V.P., 'Sound Absorption in Sea Water', J. Acoust. Soc. of Am., Vol. 62 , 1977, pp. 558-564.

16. Garrood, D.J., 'Applications of the MFSK Acoustical Communication System,' Ocean 81, IEEE-MTS Conference, Boston, Sep. 1981, pp. 67-71.

17. Garrood, D.J. and Miller, N.D., 'Acoustic Telemetry for Underwater Control,' Ocean 82, IEEE-MTS Conference, Washington D.C., Sept. 1982, pp. 111-114.

18. Gradshteyn, I.S. and Ryzhik, I.W., Table of integrals, series and products, New York, San Fransisco, London, Academic Press, 1965, pp. 25-35.

19 Howse, E.D., 'A Digital Acoustic Underwater Communication System,' M. Eng. Thesis, Memorial Univ. of Newfoundland, St. John's, Newfoundland, Canada, Sep. 1981.

20. Howse, E.D., and Zielinski, A., 'Multipath Modeling for Acoustic Communication,' Ocean 82, IEEE-MTS Conference, Washington D.C., Sept. 1982, pp. 217-222.

21. Jacobsen, H.P. et al, 'Acoustic Control System,' Ocean 82, IEEE-MTS Conference, Sept. 1982, pp. 106-110.

22. Kearny, P.O. Jr. and Laufer, C.A., 'Sonarlink-A Deep Ocean High Data Rate, Adaptive Telemetry System,' Ocean 84, IEEE-MTS Conference, Washington D.C., Sept. 1984, pp. 49-53.

23. Kinsler, L.E., Frey, A.R., Coppens, A.B. and Sanders, J.V., Fundamentals of Acoustics, John Willey and Sons, 1982.

24. Leonard, R.W. et al, 'Attenuation of Sound in Synthetic Sea Water,' J. Acoustic Soc. of Am., Vol. 21 , 1949, pp. 63-68.

25. Leroy, C.C., 'Development of Simple Equations for Accurate and more Realistic Calculations of the Speed of Sound in Sea Water,' J. Acoust. Soc. of Am. Vol. **46** , No. 1 (Part 2), 1969, pp. 216-226.

26. Liebermann, L.N., 'Sound Propagation in Chemically Active Media,' Physics Rev., Vol. **76** , 1949, pp. 1520-1524.

27. Lord, G.E. and Plemons, T.D., 'Characterization and Simulation of Underwater Acoustic Signals Reflected from the Sea Surface,' J. Acoust. Soc. of Am., Vol. **63** , No. 2, 1978, pp. 378-385.

28. McGee, W.F., 'Another Recursive Method of Computing the Q Function,' IEEE Trans. on Information Theory, July 1970, pp. 500-501.

29. Miller, C.S. and Bohman, C.E., 'An Experiment in High Rate Underwater Telemetry,' Ocean 72, IEEE-MTS Conference, Newport, Sept. 1972, pp. 34-38.

30. Morgera, S.D., 'Digital Filtering and Prediction for Communications Systems Time Synchronization,' IEEE Journal of Oceanic Engineering, Vol. **OE-7** , No. 3, July 1982, pp. 110-119.

31. Morgera, S.D., 'Multiple Terminal Acoustic Communication System Design,' IEEE Journal on Oceanic Engineering, Vol. **OE-5** , No. 3, July 1980, pp. 199-204.

32. Morgera, S.D. and Reuben, K.A., 'A Microprocessor based Acoustic Telemetry System for Tide Measurement,' IEEE Journal of Oceanic Engineering, Vol. **OE-11** , No. 1, Jan. 1986, pp. 100-108.

33. Quazi, A.H. and Konrad, W.L., 'Underwater Acoustic Communications,' IEEE Communications Magazine, March 1982, pp. 24-30.

34. Rosesmyth, M.C., 'Manned Submersibles :valuable Applications,' Sea Technology, Vol. **27** , No. 4, April 1986, pp. 52-54.

35. Skelhorn, C., 'Acoustic Technology Today,' International Underwater Systems Design, Vol. **8** , No. 1, Jan. 1986, pp. 18-22.

36. Urick, R.J., Principles of Underwater Sound for Engineers, New York, N.Y., McGraw-hill, 1967.

37. Wax, D.W., 'MFSK-The Basis for Robust Acoustical Communications,' Ocean 81, IEEE-MTS Conference, Boston, Sep. 1981, pp. 61-65.

38. Williscroft, R.G. and Macleod, N.C., 'A Non-Acoustic Long Distance Underwater Communications System,' Ocean 78, IEEE-MTS Conference, Sept. 1978, pp. 105-108.

39. Witmer, D.R. and Pearson, R.E., 'Acoustic Telemetry-A Step Toward an Underwater Alternative,' Journal of Petroleum Technology, Oct. 1978, pp. 1403-1406.

40. Annual Report of Woods Hole Oceanographic Institute, 1985.

41. Zielinski, A. and Barbour, R.L., 'The Swept Carrier Underwater Acoustic Communication System,' 5 th International Ocean Development Conference, Tokyo, Japan, Sept. 1978, pp. F2/1-16.

42. Zielinski, A. and Barbour, R.L., 'Swept Carrier Acoustic Underwater Communications,' Ocean 78, IEEE-MTS Conference, Washington D.C., Sept. 1978, pp. 60-65.

43. Zielinski, A. and Caldera, M., 'Underwater Acoustic Communications Using Sliding Discrete Fourier Transform,' Fourth International Symposium on Unmanned Untethered Submersibles Technology, Durham, Newhampshire, June 1985.

44. Zielinski, A. and Caldera, M., 'Digital Acoustic Communications in Multipath Underwater Channels,' Ocean 85, IEEE-MTS Conference, Sandiego, Nov. 1985, pp. 1296-1301.

APPENDIX A

The summation $\sum_{n=48}^{63} \sin 2\pi f_8 nT\, W^{-48n}$ can be simplified as follows:

$$\sum_{n=48}^{63} \sin 2\pi f_8 nT\, W^{-48n} = \sum_{n=0}^{15} \sin 2\pi f_8 (n+48)T\, W^{-48n}$$

$$= \sum_{n=0}^{15} \sin 2\pi f_8 (n+48)T \exp\left(\frac{-j2\pi 48n}{512}\right)$$

$$= \sum_{n=0}^{15} \sin 2\pi f_8 (n+48)T \exp\left(\frac{-j3\pi n}{16}\right)$$

Real and Imaginary parts of this summation can be written as

$$\mathrm{Re}\left\{\sum_{n=48}^{63} \sin 2\pi f_8 nT\, W^{-48n}\right\} = \sum_{n=0}^{15} \sin 2\pi f_8 (n+48)T \cos\frac{3\pi n}{16} \qquad (A.1)$$

$$\text{and } \mathrm{Im}\left\{\sum_{n=48}^{63} \sin 2\pi f_8 nT\, W^{-48n}\right\} = -\sum_{n=0}^{15} \sin 2\pi f_8 (n+48)T \sin\frac{3\pi n}{16} \qquad (A.2)$$

Equation (A.1) can be simplified further using the relationship given by [18],

$$\sum_{k=0}^{n-1} \sin(x + ky) = \sin\left(x + \frac{n-1}{2}y\right) \sin\frac{ny}{2} \operatorname{cosec}\frac{y}{2} \qquad (A.3)$$

Now Equation (A.1) can be simplified as

$$\mathrm{Re}\left\{\sum_{n=48}^{63} \sin 2\pi f_8 nT\, W^{-48n}\right\} = \frac{1}{2}\sum_{n=0}^{15}\left\{\sin\left[2\pi f_8 48T + (2\pi f_8 T + \frac{3\pi}{16})n\right]\right.$$

$$\left. + \sin\left[2\pi f_8 48T + (2\pi f_8 T - \frac{3\pi}{16})n\right]\right\}$$

Using the relationship given in (A.3),

$$\mathrm{Re}\left\{ \sum_{n=48}^{63} \sin 2\pi f_8 nT\, W^{-48n} \right\} = \frac{1}{2} \left\{ \sin\left[2\pi f_8 48T + \frac{15}{2}\left(2\pi f_8 T + \frac{3\pi}{16} \right) \right] \right.$$
$$\sin\frac{16}{2}\left(2\pi f_8 T + \frac{3\pi}{16} \right) \operatorname{cosec}\frac{1}{2}\left(2\pi f_8 T + \frac{3\pi}{16} \right)$$
$$+ \sin\left[2\pi f_8 48T + \frac{15}{2}\left(2\pi f_8 T - \frac{3\pi}{16} \right) \right]$$
$$\left. \sin\frac{16}{2}\left(2\pi f_8 T - \frac{3\pi}{16} \right) \operatorname{cosec}\frac{1}{2}\left(2\pi f_8 T - \frac{3\pi}{16} \right) \right\} \quad \text{(A.4)}$$

When $f_8 = 7750$ Hz and $T = \frac{1}{8}$ msec,

$$\sin\frac{16}{2}\left(2\pi f_8 T \pm \frac{3\pi}{16}\right) = \sin\frac{16}{2}\left[\frac{2\pi \times 7750}{8000} \pm \frac{3\pi}{16} \right]$$
$$= \sin\frac{16}{2}\left[\frac{31\pi \pm 3\pi}{16} \right]$$
$$= 0 \quad \text{(A.5)}$$

Substituting the relationship given in (A.5) in (A.4), it can be shown that

$$\mathrm{Re}\left\{ \sum_{n=48}^{63} \sin 2\pi f_8 nT\, W^{-48n} \right\} = 0 \quad \text{when } f_8 = 7750 \text{ Hz} \quad \text{(A.6)}$$

Similarly, Equation (A.2) can be further simplified using the relationship [18] given below.

$$\sum_{k=0}^{n-1} \cos(x + ky) = \cos\left(x + \frac{n-1}{2}y\right) \sin\frac{ny}{2} \operatorname{cosec}\frac{y}{2} \quad \text{(A.7)}$$

Now Equation (A.2) can be written as

$$\mathrm{Im}\left\{ \sum_{n=48}^{63} \sin 2\pi f_8 nT\, W^{-48n} \right\} = -\frac{1}{2} \sum_{n=0}^{15} \left\{ \cos\left[2\pi f_8 48T + (2\pi f_8 T - \frac{3\pi}{16})\, n \right] - \cos\left[2\pi f_8 48T + (2\pi f_8 T + \frac{3\pi}{16})\, n \right] \right\}$$

Using the relationship given in Equation (A.7),

$$\mathrm{Im}\left\{ \sum_{n=48}^{63} \sin 2\pi f_8 nT\, W^{-48n} \right\} = -\frac{1}{2} \left\{ \cos\left[2\pi f_8 x 48T + \frac{15}{2}\left(2\pi f_8 T - \frac{3\pi}{16} \right) \right] \sin\frac{16}{2}\left(2\pi f_8 T - \frac{3\pi}{16} \right) \mathrm{cosec}\frac{1}{2}(2\pi f_8 T - \frac{3\pi}{16}) - \cos\left[2\pi f_8 x 48T + \frac{15}{2}\left(2\pi f_8 T + \frac{3\pi}{16} \right) \right] \sin\frac{16}{2}\left(2\pi f_8 T + \frac{3\pi}{16} \right) \mathrm{cosec}\frac{1}{2}\left(2\pi f_8 T + \frac{3\pi}{16} \right) \right\}$$

Using the relationship given in Equation (A.5), it can be shown that

$$\mathrm{Im}\left\{ \sum_{n=48}^{63} \sin 2\pi f_8 nT\, W^{-48n} \right\} = 0 \quad \text{when } f_8 = 7750 \text{ Hz} \tag{A.8}$$

When $f_8 = 4000$ Hz, $\sin 2\pi f_8 nT = 0$ for all n. Hence

$$\mathrm{Re}\left\{ \sum_{n=48}^{63} \sin 2\pi f_8 nT\, W^{-48n} \right\} = \mathrm{Im}\left\{ \sum_{n=48}^{63} \sin 2\pi f_8 nT\, W^{-48n} \right\} = 0 \tag{A.9}$$

Using Equations (A.6), (A.8) and (A.9), it can be concluded that

$$\sum_{n=48}^{63} \sin 2\pi f_8 nT\, W^{-48n} = 0, \quad f_8 = 7750 \text{ Hz} \quad \text{or} \quad 4000 \text{ Hz} \tag{A.10}$$

Next the summation $\sum_{n=512}^{512+47} \sin 2\pi f_8 nT\ W^{-48n}$ is simplified as follows:

$$\sum_{n=512}^{512+47} \sin 2\pi f_8 nT\ W^{-48n} = \sum_{n=0}^{47} \sin 2\pi f_8 (n+512)T\ W^{-48(n+512)}$$

$$= W^{-48\times 512} \sum_{n=0}^{47} \sin 2\pi f_8 nT\ W^{-48n}$$

$$= \sum_{n=0}^{47} \sin 2\pi f_8 nT\ W^{-48n}$$

Real and Imaginary parts of the above summation can be written as

$$\mathrm{Re}\left\{ \sum_{n=0}^{47} \sin 2\pi f_8 nT\ W^{-48n} \right\} = \sum_{n=0}^{47} \sin 2\pi f_8\, nT \cos \frac{3\pi n}{16} \qquad \text{(A.11)}$$

$$\text{and } \mathrm{Im}\left\{ \sum_{n=0}^{47} \sin 2\pi f_8 nT\ W^{-48n} \right\} = -\sum_{n=0}^{47} \sin 2\pi f_8\, nT \sin \frac{3\pi n}{16} \qquad \text{(A.12)}$$

Equation (A.11) can be further simplified using the following relationship given by [18],

$$\sum_{n=1}^{N} \sin nx = \sin \frac{N+1}{2} x \sin \frac{Nx}{2} \operatorname{cosec} \frac{x}{2} \qquad \text{(A.13)}$$

Now Equation (A.11) can be written as

$$\mathrm{Re}\left\{ \sum_{n=0}^{47} \sin 2\pi f_8 nT\ W^{-48n} \right\} = \sum_{n=0}^{47} \sin 2\pi f_8\, nT \cos \frac{3\pi n}{16}$$

$$= \frac{1}{2} \sum_{n=0}^{47} \left\{ \sin\left(2\pi f_8 T + \frac{3\pi}{16}\right) n + \sin\left(2\pi f_8 nT - \frac{3\pi}{16}\right) n \right\}$$

$$= \frac{1}{2} \left\{ \sin \frac{48}{2} \left(2\pi f_8 T + \frac{3\pi}{16} \right) n \sin \frac{47}{2} \left(2\pi f_8 T + \frac{3\pi}{16} \right) \right.$$

$$\operatorname{cosec} \frac{1}{2} \left(2\pi f_8 T + \frac{3\pi}{16} \right)$$

$$+ \sin \frac{48}{2} \left(2\pi f_8 T - \frac{3\pi}{16} \right) n \sin \frac{47}{2} \left(2\pi f_8 T - \frac{3\pi}{16} \right)$$

$$\left. \operatorname{cosec} \frac{1}{2} \left(2\pi f_8 T - \frac{3\pi}{16} \right) \right\} \qquad \text{(A.14)}$$

when $f_8 = 7750$ Hz and $T = \frac{1}{8}$ msec,

$$\sin\frac{48}{2}\left(2\pi f_8 T \pm \frac{3\pi}{16}\right) = \sin\frac{48}{2}\left[\frac{2\pi x 7750}{8000} \pm \frac{3\pi}{16}\right]$$

$$= \sin\frac{48}{2}\left[\frac{31\pi \pm 3\pi}{16}\right]$$

$$\equiv 0 \qquad \text{(A.15)}$$

Substituting the above relationship in Equation (A.14), it can be shown that

$$\mathrm{Re}\left\{\sum_{n=0}^{47} \sin 2\pi f_8 nT\, W^{-48n}\right\} = 0 \quad \text{when} \quad f_8 = 7750 \text{ Hz} \qquad \text{(A.16)}$$

Similarly Equation (A.12) can be simplified using the following relationship [18],

$$\sum_{k=0}^{n-1} \cos kx = \cos\frac{nx}{2} \sin\frac{n+1}{2} x \operatorname{cosec}\frac{x}{2} \qquad \text{(A.17)}$$

Now Equation (A.12) simplifies as

$$\mathrm{Im}\left\{\sum_{n=0}^{47} \sin 2\pi f_8 nT\, W^{-48n}\right\} = -\sum_{n=0}^{47} \sin 2\pi f_8 nT \sin\frac{3\pi n}{16}$$

$$= -\frac{1}{2}\sum_{n=0}^{47}\left\{\cos(2\pi f_8 T - \frac{3\pi}{16})\, n - \cos(2\pi f_8 T + \frac{3\pi}{16})\, n\right\}$$

$$= -\frac{1}{2}\left\{\cos\frac{48}{2}\left(2\pi f_8 T - \frac{3\pi}{16}\right) n \sin\frac{49}{2}\left(2\pi f_8 T - \frac{3\pi}{16}\right)\right.$$

$$\operatorname{cosec}\frac{1}{2}\left(2\pi f_8 T - \frac{3\pi}{16}\right)$$

$$- \cos\frac{48}{2}\left(2\pi f_8 T + \frac{3\pi}{16}\right) n \sin\frac{49}{2}\left(2\pi f_8 T + \frac{3\pi}{16}\right)$$

$$\left.\operatorname{cosec}\frac{1}{2}\left(2\pi f_8 T + \frac{3\pi}{16}\right)\right\}$$

$$\mathrm{Im}\left\{\sum_{n=0}^{47} \sin 2\pi f_8 nT\ W^{-48n}\right\} = -\frac{1}{2}\left[\frac{\sin\frac{49}{2}\left(2\pi f_8 - \frac{3\pi}{16}\right)}{\sin\frac{1}{2}\left(2\pi f_8 - \frac{3\pi}{16}\right)} + \frac{\sin\frac{49}{2}\left(2\pi f_8 + \frac{3\pi}{16}\right)}{\sin\frac{1}{2}\left(2\pi f_8 + \frac{3\pi}{16}\right)}\right]$$

When $f_8 = 7750$ Hz, it can be shown that the above expression becomes zero. Hence,

$$\mathrm{Im}\left\{\sum_{n=0}^{47} \sin 2\pi f_8 nT\ W^{-48n}\right\} = 0 \quad \text{when} \quad f_8 = 7750 \text{ Hz} \tag{A.18}$$

As shown before, when $f_8 = 4000$ Hz, $\sin 2\pi f_8 nT = 0$ for all n. Hence,

$$\mathrm{Re}\left\{\sum_{n=0}^{47} \sin 2\pi f_8 nT\ W^{-48n}\right\} = \mathrm{Im}\left\{\sum_{n=0}^{47} \sin 2\pi f_8 nT\ W^{-48n}\right\} = 0 \tag{A.19}$$

Now using Equations (A.16), (A.18) and (A.19), it can be concluded that

$$\sum_{n=512}^{512+47} \sin 2\pi f_8 nT\ W^{-48n} = 0, \quad f_8 = 7750 \text{ Hz or } 4000 \text{ Hz}. \tag{A.20}$$

The Imaginary part of $X_s(48\Omega)$ given in Equation (5.8b) can be written as

$$\mathrm{Im}\left\{X_s(48\Omega)\right\} = -\frac{1}{2}\sum_{i=2}^{7}\sum_{n=0}^{63}\left[\cos\frac{\pi(i-1)n}{4} - \cos\left\{\frac{\pi(i-1)n}{4} + \frac{3\pi n}{8}\right\}\right] - \sum_{n=0}^{63}\sin^2\frac{3\pi n}{16}$$

Using the relationship given in (A.7), the above summation can be simplified as

$$\begin{aligned}\mathrm{Im}\left\{X_s(48\Omega)\right\} &= -\frac{1}{2}\sum_{i=2}^{7}\left\{\cos\frac{64}{2}\left[\frac{\pi(i-1)}{4}\right]\sin\frac{65}{2}\left[\frac{\pi(i-1)}{4}\right]\mathrm{cosec}\frac{1}{2}\frac{\pi(i-1)}{4}\right.\\ &\quad -\cos\frac{64}{2}\left[\frac{\pi(i-1)}{4}+\frac{3\pi}{8}\right]\sin\frac{65}{2}\left[\frac{\pi(i-1)}{4}+\frac{3\pi}{8}\right]\\ &\quad \left.\mathrm{cosec}\frac{1}{2}\left[\frac{\pi(i-1)}{4}+\frac{3\pi}{8}\right]\right\}-\sum_{n=0}^{63}\sin^2\frac{3\pi n}{16}\\ &= -\frac{1}{2}\sum_{n=2}^{7}\left[\frac{\sin\frac{65}{2}\frac{\pi(i-1)}{4}}{\sin\frac{1}{2}\frac{\pi(i-1)}{4}}-\frac{\sin\frac{65}{2}\left[\frac{\pi(i-1)}{4}+\frac{3\pi}{8}\right]}{\sin\frac{1}{2}\left[\frac{\pi(i-1)}{4}+\frac{3\pi}{8}\right]}\right]-\sum_{n=0}^{32}\sin^2\frac{3\pi n}{16}\end{aligned}$$

This can be further simplified and shown that

$$\begin{aligned}\mathrm{Im}\left\{X_s(48\Omega)\right\} &= -\sum_{n=0}^{63}\sin^2\frac{3\pi n}{16} \qquad (A.21)\\ &= \mathrm{Im}\left\{\sum_{n=0}^{63}\sin 2\pi f_1 nT\, W^{-48n}\right\}\end{aligned}$$

Using the following relationship [18]

$$\sum_{n=1}^{N}\sin^2 nx = \frac{N}{2}-\frac{\cos(N+1)x\,\sin Nx}{2\sin x} \qquad (A.22)$$

Equation (A.21) can be written as

$$\begin{aligned}\mathrm{Im}\left\{X_s(48\Omega)\right\} &= -\sum_{n=0}^{63}\sin^2\frac{3\pi n}{16}\\ &= -\sum_{n=1}^{64}\sin^2\frac{3\pi n}{16}\\ &= -\left[\frac{64}{2}-\frac{\cos\frac{65\times 3\pi}{16}\sin\frac{64\times 3\pi}{16}}{2\sin\frac{3\pi}{16}}\right]\end{aligned}$$

$$\mathrm{Im}\left\{X_s(48\Omega)\right\} = -32 \qquad (A.23)$$

$$= \mathrm{Im}\left\{\sum_{n=0}^{63} \sin 2\pi f_1 nT\ W^{-48n}\right\}$$

Hence it can be concluded that there is no contribution on $\mathrm{Im}\left\{X_s(48\Omega)\right\}$ from frequencies f_i where i=2, 3,.....,7.

APPENDIX B

When the direct path and multipath signals have the same frequency $f_1 = 7750$ Hz, $X_s(48\Omega)$ can be approximated as given in Equation (5.18) as follows:

$$X_s(48\Omega) \approx \sum_{n=64}^{127} \sin 2\pi f_1 nT\, W^{-48n} - \alpha_3 \sum_{n=64a_3+l_3}^{63+64a_3+l_3} \sin 2\pi f_1 nT\, W^{-48n}$$
$$+ \alpha_4 \sum_{n=64a_4+l_4}^{63+64a_4+l_4} \sin 2\pi f_1 nT\, W^{-48n} - \alpha_5 \sum_{n=64a_5+l_5}^{63+64a_5+l_5} \sin 2\pi f_1 nT\, W^{-48n}$$
$$- \alpha_6 \sum_{n=64a_6+l_6}^{63+64a_6+l_6} \sin 2\pi f_1 nT\, W^{-48n}$$

$$\approx W^{-48\times 64} \sum_{n=0}^{63} \sin 2\pi f_1 nT\, W^{-48n} - \alpha_3 W^{-48(64a_3+l_3)} \sum_{n=0}^{63} \sin 2\pi f_1 nT\, W^{-48n}$$
$$+ \alpha_4 W^{-48(64a_4+l_4)} \sum_{n=0}^{63} \sin 2\pi f_1 nT\, W^{-48n} - \alpha_5 W^{-48(64a_5+l_5)} \sum_{n=0}^{63} \sin 2\pi f_1 nT\, W^{-48n}$$
$$- \alpha_6 W^{-48(64a_6+l_6)} \sum_{n=0}^{63} \sin 2\pi f_1 nT\, W^{-48n}$$

$$\approx X_1 - \alpha_3 W^{-48l_3} X_1 + \alpha_4 W^{-48l_4} X_1 - \alpha_5 W^{-48l_5} X_1 - \alpha_6 W^{-48l_6} X_1$$

$$\approx X_1 \left[1 - \alpha_3 W^{-48l_3} + \alpha_4 W^{-48l_4} - \alpha_5 W^{-48l_5} - \alpha_6 W^{-48l_6} \right] \qquad \text{(B.1)}$$

where $X_1 = \sum_{n=0}^{63} \sin 2\pi f_1 nT\, W^{-48n}$ and $f_1 = 750$ Hz.

$= 0 - j32$

$W = \exp\left(\frac{j2\pi}{N}\right)$ and $N = 512$

Now substituting for W in (B.1)

$$X_s(48\Omega) \approx (0\text{–}j32)\left\{1 - \alpha_3\left[\cos\frac{3\pi l_3}{16} - j\sin\frac{3\pi l_3}{16}\right] + \alpha_4\left[\cos\frac{3\pi l_4}{16} - j\sin\frac{3\pi l_4}{16}\right] - \alpha_5\left[\cos\frac{3\pi l_5}{16} - j\sin\frac{3\pi l_5}{16}\right] - \alpha_6\left[\cos\frac{3\pi l_6}{16} - j\sin\frac{3\pi l_6}{16}\right]\right\} \quad (B.2)$$

Real and Imaginary parts of $X_s(48\Omega)$ can be written as

$$\mathrm{Re}\left\{X_s(48\Omega)\right\} = 32\left[\alpha_3\sin\frac{3\pi l_3}{16} - \alpha_4\sin\frac{3\pi l_4}{16} + \alpha_5\sin\frac{3\pi l_5}{16} + \alpha_6\sin\frac{3\pi l_6}{16}\right]$$

$$\mathrm{Im}\left\{X_s(48\Omega)\right\} = -32\left[1 - \alpha_3\cos\frac{3\pi l_3}{16} + \alpha_4\cos\frac{3\pi l_4}{16} - \alpha_5\cos\frac{3\pi l_5}{16} - \alpha_6\cos\frac{3\pi l_6}{16}\right]$$

The squared magnitude of $X_s(48\Omega)$ takes the form

$$|X_s(48\Omega)|^2 = |X_1|^2\left[1 + \alpha_3^2 + \alpha_4^2 + \alpha_5^2 + \alpha_6^2 - 2\alpha_3\cos\frac{3\pi l_3}{16} + 2\alpha_4\cos\frac{3\pi l_4}{16} - 2\alpha_5\cos\frac{3\pi l_5}{16} - 2\alpha_6\cos\frac{3\pi l_6}{16} - 2\alpha_3\alpha_4\cos\frac{3\pi(l_3-l_4)}{16} + 2\alpha_3\alpha_5\cos\frac{3\pi(l_3-l_5)}{16} + 2\alpha_3\alpha_6\cos\frac{3\pi(l_3-l_6)}{16} - 2\alpha_4\alpha_5\cos\frac{3\pi(l_4-l_5)}{16} - 2\alpha_4\alpha_6\cos\frac{3\pi(l_4-l_6)}{16} + 2\alpha_5\alpha_6\cos\frac{3\pi(l_5-l_6)}{16}\right] \quad (B.3)$$

Here, the effect of cross terms $\alpha_n\alpha_m$ where n=3,4,5 and m=4,5,6 and m>n on $|X_s(48\Omega)|^2$ is negligible.

Then the minimum value of $|X_s(48\Omega)|$ occurs when

$$\left.\begin{aligned} \cos\frac{3\pi l_3}{16} &= +1 \\ \cos\frac{3\pi l_4}{16} &= -1 \\ \cos\frac{3\pi l_5}{16} &= +1 \\ \cos\frac{3\pi l_6}{16} &= +1 \end{aligned}\right\} \qquad \text{(B.4)}$$

The l_3, l_4, l_5 and l_6 values which satisfy the set of Equations (B.4) are

$$l_3 = \frac{16}{3}2n_3 \qquad l_4 = \frac{16}{3}(2n_4+1)$$

$$l_5 = \frac{16}{3}2n_5 \qquad l_6 = \frac{16}{3}2n_6$$

where n_3, n_4, n_5 and n_6 are integers.

Substituting the conditions given in Equation (B.4) in Equation (B.3), minimum value of $X_s(48\Omega)$ when 'one' is transmitted can be written as

$$|X_s(48\Omega)|_{min} = |X_1| \left[1 - (\alpha_3 + \alpha_4 + \alpha_5 + \alpha_6)\right] \qquad \text{(B.5)}$$

The maximum value of $|X_s(48\Omega)|$ when 'zero' is transmitted occurs when the two multipaths have the same frequency $f_1 = 750$ Hz and the direct path frequency is $f_s/2$. The spectral component $X_s(48\Omega)$ for this case is given as

$$X_s(48\Omega) \approx |X_1| \left[-\alpha_3 W^{-48l_3} + \alpha_4 W^{48l_4} - \alpha_5 W^{-48l_5} - \alpha_6 W^{-48l_6}\right] \qquad \text{(B.6)}$$

Using the conditions given in (B.4), the maximum value of $|X_s(48\Omega)|$ when 'zero' is transmitted can be written as,

$$|X_s(48\Omega)| \approx |X_1| \left[\alpha_3 + \alpha_4 + \alpha_5 + \alpha_6\right] \qquad \text{(B.7)}$$

APPENDIX C

By subtracting Equation (5.46e) from Equation (5.46d), the eye opening (EO) could be written as follows:

$$\begin{aligned} EO = &\Big[A_1^2 (1+\alpha_1+\alpha_2)^2 + 32^2 (1-\alpha_1-\alpha_2)^2 + A_2^2 (1+\alpha_1+\alpha_2)^2 \\ &+ 2x32\, A_2 (1-\alpha_1-\alpha_2)(1-\alpha_1+\alpha_2)\Big]^{\frac{1}{2}} \\ &- \Big[A_1^2 (1+\alpha_1+\alpha_2)^2 + 32^2(\alpha_1+\alpha_2)^2 + A_2^2 (1+\alpha_1+\alpha_2)^2 \\ &- 2x32\, A_2 (\alpha_1+\alpha_2)(1+\alpha_1+\alpha_2)\Big]^{\frac{1}{2}} \end{aligned} \tag{C.1}$$

For correct detection, EO should be greater than zero. Therefore for correct detection

$$\begin{aligned} 32^2 \Big[(1-\alpha_1-\alpha_2)^2 - (\alpha_1+\alpha_2)^2\Big] + 2x32A_2 (1+\alpha_1+\alpha_2) &> 0 \\ 32^2 \Big[1-2(\alpha_1+\alpha_2)\Big] + 2x32A_2 (1+\alpha_1+\alpha_2) &> 0 \\ (\alpha_1+\alpha_2)\Big[64-2A_2\Big] &< 2A_2 + 32 \\ \frac{1}{\alpha_1+\alpha_2} &> \frac{32-A_2}{16+A_2} \end{aligned} \tag{C.2}$$

$$\text{Hence} \quad DMR = 10\log\left(\frac{1}{\alpha_1+\alpha_2}\right) > 10\log\left(\frac{32-A_2}{16+A_2}\right) \tag{C.3}$$

for correct detection.

In case d, Equation (5.44) can be expressed as

$$X_s(48\Omega) = W^{48m}\Bigg[\sum_{n=48+m}^{63}\sin 2\pi f_{81}nT\,W^{-48n} + \sum_{n=64}^{127}\sin 2\pi f_1 nT\,W^{-48n} - \alpha_1\sum_{n=48+m}^{63}\sin 2\pi f_{81}nT\,W^{-48n} - \alpha_1\sum_{n=64}^{127}\sin 2\pi f_1 nT\,W^{-48n} - \alpha_1\sum_{n=0}^{47+m}\sin 2\pi f_{81}nT\,W^{-48n} - \alpha_2\sum_{n=48+m}^{63}\sin 2\pi f_{81}nT\,W^{-48n} - \alpha_2\sum_{n=64}^{127}\sin 2\pi f_1 nT\,W^{-48n} - \alpha_2\sum_{n=0}^{47+m}\sin 2\pi f_{81}nT\,W^{-48n}\Bigg]$$

$$= W^{48m}\left[(1-\alpha_1-\alpha_2)\sum_{0}^{63}\sin 2\pi f_1 nT\,W^{-48n} + \sum_{n=48+m}^{63}\sin 2\pi f_{81}nT\,W^{-48n}\right]$$

$$= \left[\cos\frac{3\pi m}{16}+j\sin\frac{3\pi m}{16}\right]\left[(1-\alpha_1-\alpha_2)\,(0-j32)+(A_1-jA_2)\right] \qquad (C.4)$$

where $A_1 = \sum_{n=48+m}^{63}\sin 2\pi f_{81}nT\cos\frac{3\pi n}{16}$

$$A_2 = \sum_{n=48+m}^{63}\sin 2\pi f_{81}nT\sin\frac{3\pi n}{16} \quad \text{and} \qquad (C.5)$$

$$\sum_{n=0}^{63}\sin 2\pi f_1 nT\,W^{-48n} = (0-j32)$$

Now considering real and imaginary parts of (C.4), the magnitude of $X_s(48\Omega)$ representing 'one' can be written as

$$|X_s(48\Omega)| = \left[A_1^2+A_2^2+32^2(1-\alpha_1-\alpha_2)^2+2x32A_2(1-\alpha_1-\alpha_2)\right]^{\frac{1}{2}} \qquad (C.6)$$

Similarly, when 'zero' is transmitted, assuming the frequency of the two multipaths is $f_1 = 750$ Hz, $X_s(48\Omega)$ can be written as

$$X_s(48\Omega) = W^{48m}\left[\sum_{n=48+m}^{63} \sin 2\pi f_{81} nT\, W^{-48n} + \sum_{64}^{127} \sin 2\pi \frac{f_s}{2} nT\, W^{-48n} - \alpha_1 \sum_{64}^{127} \sin 2\pi f_1 nT\, W^{-48n} - \alpha_2 \sum_{64}^{127} \sin 2\pi f_1 nT\, W^{-48n}\right]$$

$$X_s(48\Omega) = \left(\cos\frac{3\pi m}{16} + j\sin\frac{3\pi m}{16}\right)\left[-(\alpha_1+\alpha_2)(0-j32)+(A_1-jA_2)\right] \quad (C.7)$$

Considering real and imaginary parts of (C.7), the magnitude of $X_s(48\Omega)$ when 'zero' is transmitted can be written as

$$|X_s(48\Omega)| = \left[A_1^2 + A_2^2 + 32^2(\alpha_1+\alpha_2)^2 - 2x32A_2(\alpha_1+\alpha_2)\right]^{\frac{1}{2}} \quad (C.8)$$

By subtracting (C.8) by (C.7), the EO in this case can be obtained as follows:

$$EO = \left[A_1^2 + A_2^2 + 32^2(1-\alpha_1-\alpha_2)^2 + 2x32A_2(1-\alpha_1-\alpha_2)\right]^{\frac{1}{2}} - \left[A_1^2 + A_2^2 + 32^2(\alpha_1+\alpha_2)^2 - 2x32A_2(\alpha_1+\alpha_2)\right]^{\frac{1}{2}} \quad (C.9)$$

for correct detection, EO should be greater than zero. Therefore for correct detection, it can be shown that

$$(\alpha_1+\alpha_2) < \frac{16+A_2}{32} \quad (C.10)$$

$$DMR = 10\log\left(\frac{1}{\alpha_1+\alpha_2}\right) > 10\log\left(\frac{32}{16+A_2}\right) \quad (C.11)$$

for correct detection.

Similarly, the magnitudes of $X_s(48\Omega)$ and the minimum DMR required for correct detection are obtained for the cases (e), (f), (g) and (h) using the same procedure as follows:

In case (e),

$$| X_s(48\Omega) | = \left[A_1^2(\alpha_1+\alpha_2)^2 + A_2^2(\alpha_1+\alpha_2)^2 + 32^2(1-\alpha_1-\alpha_2)^2 + 2x32A_2(\alpha_1+\alpha_2)(1-\alpha_1-\alpha_2)\right]^{\frac{1}{2}} \quad (C.12)$$

when 'one' is transmitted.

$$X_s(48\Omega) = (\alpha_1+\alpha_2)\left[A_1^2 + A_2^2 + 32^2 - 2x32A_2\right]^{\frac{1}{2}} \quad (C.13)$$

when 'zero' is transmitted. Using the Equations (C.12) and (C.13), the minimum DMR required for correct detection can be obtained as

$$DMR > 10\log\left(\frac{32-A_2}{16}\right) \quad (C.14)$$

In case (f),

$$| X_s(48\Omega) | = \left[A_1^2(1+\alpha_1+\alpha_2)^2 + A_2^2(1+\alpha_1+\alpha_2)^2 + 32^2(1-\alpha_1-\alpha_2)^2 - 2x32A_2(1+\alpha_1+\alpha_2)(1-\alpha_1-\alpha_2)\right]^{\frac{1}{2}} \quad (C.15)$$

when 'one' is transmitted.

$$| X_s(48\Omega) | = \left[A_1^2(1+\alpha_1+\alpha_2)^2 + A_2^2(1+\alpha_1+\alpha_2)^2 + 32^2(\alpha_1+\alpha_2)^2 + 2x32A_2(1+\alpha_1+\alpha_2)(\alpha_1+\alpha_2)\right]^{\frac{1}{2}} \quad (C.16)$$

when 'zero' is transmitted. Using Equations (C.15) and (C.16), we can show that

$$DMR > 10\log\left(\frac{32 + A_2}{16 - A_2}\right) \quad \text{for correct detection.} \qquad (C.17)$$

In case (g),

$$|\ X_s(48\Omega)\ | = \left[A_1^2 + A_2^2 + 32^2\,(1 - \alpha_1 - \alpha_2)^2 - 2x32A_2\,(1 - \alpha_1 - \alpha_2)\right]^{\frac{1}{2}} \qquad (C.18)$$

when 'one' is transmitted.

$$|\ X_s(48\Omega)\ | = \left[A_1^2 + A_2^2 + 32^2(\alpha_1 + \alpha_2)^2 + 2x32A_2(\alpha_1 + \alpha_2)\right]^{\frac{1}{2}} \qquad (C.19)$$

when 'zero' is transmitted. From these two equations the requirement for correct detection can be written as

$$DMR > 10\log\left(\frac{32}{16 - A_2}\right) \qquad (C.20)$$

Finally, in case (h),

$$|\ X_s(48\Omega)\ | = \left[A_1^2\,(\alpha_1 + \alpha_2)^2 + A_2^2\,(\alpha_1 + \alpha_2)^2 + 32^2\,(1 - \alpha_1 - \alpha_2)^2 - 2x32A_2\,(\alpha_1 + \alpha_2)\,(1 - \alpha_1 - \alpha_2)\right]^{\frac{1}{2}} \qquad (C.21)$$

when 'one' is transmitted and

$$|\ X_s(48\Omega)\ | = \left[A_1^2\,(\alpha_1 + \alpha_2)^2 + A_2^2\,(\alpha_1 + \alpha_2) + 32^2\,(\alpha_1 + \alpha_2)^2 + 2x32A_2\,(\alpha_1 + \alpha_2)^2\right]^{\frac{1}{2}} \qquad (C.22)$$

when 'zero' is transmitted. From Equations (C.21) and (C.22) for correct detection

$$DMR > 10\log\left(\frac{32 + A_2}{16}\right) \qquad (C.23)$$

Now, when

$$X_s(48\Omega) = \sum_{n=48}^{511+48} x(n-m)\, W^{-48n}$$

the variation of eye opening with DMR in the worst situation was evaluated. As explained in section (5.5.2), in this situation, $X_s(48\Omega)$ can be written as

$$\begin{aligned} X_s(48\Omega) &= \sum_{n=48}^{511+48} x(n-m)\, W^{-48n} \\ &= \sum_{n=48-m}^{511+48-m} x(n)\, W^{-48(n+m)} \\ &= W^{-48m} \sum_{n=48-m}^{511+48-m} x(n)\, W^{-48n} \end{aligned} \tag{C.24}$$

Assuming that the frequency of the multipaths and the direct path is $f_1 = 750$ Hz, $X_s(48\Omega)$ can be written as

$$\begin{aligned} X_s(48\Omega) = W^{-48m} \Bigg[& \sum_{n=48-m}^{63} \sin 2\pi f_{81} nT\, W^{-48n} + \sum_{n=64}^{127} \sin 2\pi f_1 nT\, W^{-48n} \\ & + \sum_{n=512}^{511+48-m} \sin 2\pi f_{82} nT\, W^{-48n} - \alpha_1 \sum_{n=48-m}^{63} \sin 2\pi f_{81}(m_1) nT\, W^{-48n} \\ & - \alpha_1 \sum_{n=64}^{127} \sin 2\pi f_1 nT\, W^{-48n} - \alpha_1 \sum_{n=0}^{47-m} \sin 2\pi f_{82}(m_1) nT\, W^{-48n} \\ & - \alpha_2 \sum_{n=48-m}^{63} \sin 2\pi f_{81}(m_2) nT\, W^{-48n} - \alpha_2 \sum_{n=64}^{127} \sin 2\pi f_1 nT\, W^{-48n} \\ & - \alpha_2 \sum_{n=0}^{47-m} \sin 2\pi f_{82}(m_2) nT\, W^{-48n} \Bigg] \end{aligned} \tag{C.25}$$

As explained in Section (5.5.2), the frequencies $f_{81} = f_{82}(m_1) = f_{82}(m_2)$ and $f_{81}(m_1) = f_{81}(m_2)$. Here also the same frequency combinations were analyzed separately in the same manner and the results are tabulated in Table 5.2.

APPENDIX D

In the presence of Gaussian noise, $|X(48\Omega)|$ can be expressed as given in Equation (5.55) as

$$|X(48\Omega)| = \left[(X_s + X_n)^2 + (Y_s + Y_n) \right]^{\frac{1}{2}}$$

From Equations (5.57a) and (5.57b),

$$X_s + X_n = x \quad \text{and}$$
$$Y_s + Y_n = y$$

As noise is assumed as Gaussian, x and y become random variables.

If $E\{x\} = m_1$ and $E\{y\} = m_2$, then

$$m_1 = E\left\{X_s + X_n\right\}$$

$$m_1 = E\left\{X_s\right\} \qquad \text{(D.1a)}$$

since noise is assumed as zero mean Gaussian.

Similarly, $m_2 = E\left\{Y_s + Y_n\right\}$

$$m_2 = E\left\{Y_s\right\} \qquad \text{(D.1b)}$$

The variances σ_x and σ_y of the random variables x and y can be written as

$$\sigma_x^2 = E\left\{(x - m_1)^2\right\} = E\left\{(x - X_s)^2\right\}$$

$$= E\left\{X_n^2\right\} \qquad \text{(D.2a)}$$

$$\text{and } \sigma_y^2 = E\left\{(y - m_2)^2\right\} = E\left\{(y - Y_n)^2\right\}$$

$$= E\left\{Y_n^2\right\} \tag{D.2b}$$

Now $E\left\{X_n^2\right\}$ can be obtained as follows:

$$E\left\{X_n^2\right\} = E\left[\sum_{n=48}^{511+48} n(n)^2 \cos^2\frac{2\pi x 48n}{N}\right] \tag{D.3}$$

$$\sigma_x^2 = \sigma^2 \sum_{n=48}^{511+48} \cos^2\frac{2\pi x 48n}{512}$$

where σ is the noise variance.

Using

$$\sum_{n=1}^{N} \cos^2 nx = \frac{N}{2} + \frac{\cos(N+1)x \sin Nx}{2 \sin x} \tag{D.4}$$

Equation (D.3) can be simplified as

$$E\left\{X_n^2\right\} = \sigma^2 \sum_{n=0}^{511} \cos^2\frac{2\pi x 48(n+48)}{512}$$

$$\sigma_x^2 = \sigma^2 \sum_{n=0}^{511} \left[\cos\frac{2\pi x 48n}{512} \cos\frac{2\pi 48x48}{512} - \sin\frac{2\pi x 48n}{512} \sin\frac{2\pi 48x48}{512}\right]^2$$

$$= \sigma^2 \sum_{n=0}^{511} \cos^2\frac{2\pi x 48n}{512} = \sigma^2 \sum_{n=1}^{512} \cos^2\frac{2\pi x 48n}{512}$$

$$= \sigma^2 \left[\frac{512}{2} + \frac{\cos\frac{513x2\pi x48}{512} \sin\frac{512x2\pi x48}{512}}{2 \sin\frac{2\pi x48}{512}}\right]$$

$$= 256\,\sigma^2 \tag{D.5}$$

Similarly $E\left\{Y_n^2\right\}$ can be obtained as follows:

$$E\left\{Y_n^2\right\} = E\left[\sum_{n=48}^{511+48} n(n)^2 \sin^2\frac{2\pi x 48n}{N}\right]$$

$$\sigma_y^2 = \sigma^2 \sum_{n=48}^{511+48} \sin^2\frac{2\pi x 48n}{512} \qquad (D.6)$$

Using

$$\sum_{n=1}^{N} \sin^2 nx = \frac{N}{2} - \frac{\cos(N+1)x \sin Nx}{2 \sin x} \qquad (D.7)$$

Equation (D.6) can be simplified as

$$E\left\{Y_n^2\right\} = \sigma^2 \sum_{n=0}^{511} \sin^2\frac{2\pi x 48(n+48)}{512}$$

$$\sigma_y^2 = \sigma^2 \sum_{n=0}^{511} \left[\sin\frac{2\pi x 48n}{512}\cos\frac{2\pi 48x48}{512} + \cos\frac{2\pi x 48n}{512}\sin\frac{2\pi 48x48}{512}\right]^2$$

$$= \sigma^2 \sum_{n=0}^{511} \sin^2\frac{2\pi x 48n}{512} = \sigma^2 \sum_{n=1}^{512} \sin^2\frac{2\pi x 48n}{512}$$

$$= \sigma^2 \left[\frac{512}{2} - \frac{\cos\frac{513x2\pi x48}{512}\sin\frac{512x2\pi x48}{512}}{2\sin\frac{2\pi x48}{512}}\right]$$

$$= 256\,\sigma^2 \qquad (D.8)$$

Hence $\sigma = \sigma_x = \sigma_y = 16\,\sigma$ (D.9)

The covariance of x and y can be written as

$$E\left\{(x - m_1)(y - m_2)\right\} = E\left\{X_n Y_n\right\}$$

$$= \sum_{n=48}^{511+48} \sum_{m=48}^{511+48} \left[n(n)\, n(m)\right] \cos\frac{2\pi x 48n}{512} \sin\frac{2\pi x 48m}{512}$$

Since $E\left\{n(i)\, n(j)\right\} = 0$ for i=j

$$E\left\{X_n Y_n\right\} = \sum_{n=48}^{511+48} E\{n(n)\}^2 \frac{1}{2} \sin\frac{2\pi x 48 x 2n}{512}$$

$$= \frac{\sigma^2}{2} \sum_{n=48}^{511+48} \sin\frac{2\pi x 48 x 2n}{512}$$

$$= \frac{\sigma^2}{2} \sum_{n=0}^{511} \sin\frac{2\pi x 48 x 2n}{512} = \frac{\sigma^2}{2} \sum_{n=1}^{512} \sin\frac{2\pi x 48 x 2n}{512}$$

Using the relationship

$$\sum_{n=1}^{N} \sin nx = \sin\frac{N+1}{2} x \sin\frac{Nx}{2} \operatorname{cosec}\frac{x}{2}$$

$E\left\{X_n Y_n\right\}$ in the above equation can be simplified as

$$E\left\{X_n Y_n\right\} = \frac{\sigma^2}{2}\left[\sin\frac{513 x 2\pi x 48 x 2}{2x512} \sin\frac{512 x 2\pi x 48 x 2}{2x512} \operatorname{cosec}\frac{2\pi x 48}{2x512}\right]$$

$$= 0$$

Hence

$$\text{the covariance} = 0 \qquad \text{(D.10)}$$

Hence the probability density function of x and y can be written as

$$p(x,y) = \frac{1}{2\pi\sigma_x^2} \exp\left[-\frac{\left\{(x-m_1)^2 + (y-m_2)^2\right\}}{2\sigma_x^2}\right] \qquad \text{(D.11)}$$